

THE PROCEEDINGS OF THE PHYSICAL SOCIETY

VOL. 60, PART 2

1 February 1948

No. 338

CONTENTS

	PAGE
(Dr.) H. WILMAN. The structure of photo-sensitive lead sulphide and lead selenide deposits and the effect of sensitization by oxygen	117
(Dr.) W. A. PROWSE. Solid diagrams illustrating resonance phenomena	132
(Dr.) L. R. G. TRELOAR. Stresses and birefringence in rubber subjected to general homogeneous strain	135
C. H. COLLIE, J. B. HASTED and D. M. RITSON. The dielectric properties of water and heavy water	145
(Dr.) KUN HUANG. Quantum mechanical calculation of the heat of solution and residual resistance of gold in silver	161
(Dr.) W. E. DUNCANSON and (Professor) C. A. COULSON. Electron momenta in atoms .	175
(Dr.) MOHAMMED CHAUDHRI and A. G. FENTON. Some experiments with adjustable Geiger-Müller counters	183
N. F. ASTBURY. The calibration of hydrophones and crystal transceivers	193
N. CORCORAN and J. M. HOUGH. A method of computing a vertical section of the combined polar diagram of a radio aerial, a flat earth and a vertical screen	203
Letters to the Editor:	
(Dr.) F. C. FRANK. An isotopic abundance rule and its bearing on the origin of the nuclei	211
Reviews of books	212
Instructions to Authors	insertion

Price to non-members 8s. 4d. net ; 8s. 10d. inclusive of postage
Annual subscription 63s. inclusive of postage, payable in advance

Published by

THE PHYSICAL SOCIETY

1 Lowther Gardens, Prince Consort Road, London S.W.7

Printed by

TAYLOR AND FRANCIS, LTD.,
Red Lion Court, Fleet Street, London E.C.4

PROCEEDINGS OF THE PHYSICAL SOCIETY

Beginning in January 1948 (Volume 69), the *Proceedings* will be published monthly under the guidance of an Advisory Board.

ADVISORY BOARD

Chairman: The President of the Physical Society (G. I. FINCH, M.B.E., D.Sc., F.R.S.).

E. N. da C. ANDRADE, Ph.D., D.Sc., F.R.S.

Sir EDWARD APPLETON, G.B.E., K.C.B., D.Sc., F.R.S.

P. M. S. BLACKETT, M.A., F.R.S.

Sir LAWRENCE BRAGG, O.B.E., M.A., Sc.D., D.Sc., F.R.S.

Sir JAMES CHADWICK, D.Sc., Ph.D., F.R.S.

Lord CHERWELL OF OXFORD, M.A., Ph.D., F.R.S.

Sir John COCKCROFT, C.B.E., M.A., Ph.D., F.R.S.

Sir CHARLES DARWIN, K.B.E., M.C., M.A., Sc.D., F.R.S.

N. FEATHER, Ph.D., F.R.S.

D. R. HARTREE, M.A., Ph.D., F.R.S.

N. F. MOTT, M.A., F.R.S.

M. L. OLIPHANT, Ph.D., D.Sc., F.R.S.

F. E. SIMON, C.B.E., M.A., D.Phil., F.R.S.

Sir GEORGE THOMSON, M.A., D.Sc., F.R.S.

Papers for publication in the *Proceedings* should be addressed to the Secretary-Editor, Miss A. C. STICKLAND, Ph.D., at the Office of the Physical Society, 1 Lowther Gardens, Prince Consort Road, London S.W.7. Telephone: KENSington 0048, 0049.

Detailed Instructions to Authors will be found in this issue of the *Proceedings*; separate copies can be obtained from the Secretary-Editor.

JOURNAL OF APPLIED PHYSICS

ELMER HUTCHISSON, *Editor*, Case Institute of Technology, Cleveland 6, Ohio

PUBLISHED monthly by the American Institute of Physics, this journal is designed particularly for those applying physics in industry and in other sciences.

Subscription price \$9.00 a year

Other physics journals published by the American Institute of Physics are:

	<i>Yearly Subscription Price</i>
THE PHYSICAL REVIEW	\$16.50
REVIEWS OF MODERN PHYSICS	4.40
JOURNAL OF THE OPTICAL SOCIETY OF AMERICA	7.70
THE JOURNAL OF THE ACOUSTICAL SOCIETY OF AMERICA	8.80
AMERICAN JOURNAL OF PHYSICS	5.50
THE REVIEW OF SCIENTIFIC INSTRUMENTS	7.00
THE JOURNAL OF CHEMICAL PHYSICS	11.00

NOTE: All rates quoted are foreign subscription prices and do not apply to Canada and the U.S.

Send orders with remittances to

American Institute of Physics, 57 East 55 Street, New York 22, New York, U.S.A.

THE PHYSICAL SOCIETY

INSTRUCTIONS TO AUTHORS

§ 1. INTRODUCTION

From necessity papers published in any given Journal must conform to certain conventions in order to give uniformity to the style of the Journal ; MSS. submitted for publication have therefore to be scrutinized and amended before being placed in the printer's hands.

The following instructions refer to the main points which have to be considered, and authors offering papers to any of the Physical Society's publications are asked to conform to these recommendations.

In general the author's degrees or honours will not be printed, but the mode of address, e.g., Professor, Dr., Miss, will be inserted.

§ 2. COPY

Manuscripts should be typed in *double* spacing on paper not wider than 8 in. and not longer than 13 in. Only one side of the paper should be used, and a margin of $1-1\frac{1}{2}$ in. should be left. As alterations in the text cannot normally be allowed once the paper is set up in type, authors should aim at absolute clarity of meaning and of typing, and should check the typescript carefully before submission. It is advantageous where possible to have this read also by a colleague before it is communicated.

(i) *Title and Sectional Headings*

The title should be as concise as is compatible with lucidity ; if it is too long for reproduction at the head of right-hand pages, a short title may be given for this purpose.

Papers are usually divided into sections beginning with § 1. INTRODUCTION and ending with § ... CONCLUSION. These sections are numbered serially and their titles printed in small capitals centrally on the page. If required, sub-section headings may be used ; they are printed centrally in italics and if necessary may be numbered in roman numerals (i), (ii), Sub-sub-section headings are printed in italics at the beginning of the paragraph ; these may be designated (a), (b) . . . if desired.

At the end of the paper there are usually two further headings : ACKNOWLEDGMENTS and REFERENCES. Please note that headings are not part of the text, which should thus be complete if headings were omitted.

(ii) *Abstract*

An abstract is printed at the beginning of the paper. It is not part of the paper, and, perhaps because its purpose is not well understood, an author's abstract is often unsatisfactory. The abstract is intended for two classes of readers, those directly concerned with the subject of the paper and those with a general interest in the subject; for the former the abstract should serve as an index, for the latter as a summary. It should therefore be designed to state briefly the general aspects of the subject on which new information is presented and the main conclusions reached and final numerical results obtained. Details of the methods employed, the definition of the field within which the results are true, and all the finer considerations involved in the work are matters for the paper itself and not for the abstract.

The abstract is placed immediately after the title, name(s) of author(s), and place of employment of author(s). It is thus convenient for the first page of the typescript to contain just these items, and for the second page to start with § 1. INTRODUCTION. This simplifies assessment of the length of the final printed paper.

This "title and abstract" page should be submitted in duplicate.

(iii) Footnotes

Footnotes should be used only for brief notes which cannot conveniently be fitted into the text, but should be avoided whenever possible. They should be inserted in the MS., not at the bottom of the page, but *immediately* below the line to which they refer, and must be separated from the rest of the text by horizontal lines across the page above and below.

(iv) Tables

Tabular matter should be avoided as far as possible except where there is a gain in conciseness by its use. Valuable space can usually be saved by arranging tables with more columns than rows. For instance, comparison of monthly values for, say, five years is better tabulated :

	Jan.	Feb.	Mar.	Apr.	May	June	July	Aug.	Sept.	Oct.	Nov.	Dec.
1939												
1940												
1941												
1942												
1943												

than with dates along the top and months down the side, giving twelve rows and five columns. When it enables space to be saved columns should be numbered or lettered and explanations added at the foot of the table. Rules should not be inserted unless special circumstances make them necessary.

Tables are numbered serially and referred to in the text by number, table 1 (lower case t) etc., as the exact position of the table in the text is governed by its position on the printed page.

(v) Mathematics

It is not necessary to give detailed derivations of mathematical expressions and formulae in a published paper when the work is straightforward ; it is quite sufficient to indicate the method of treatment and the final results. When interested readers are likely to find the argument difficult to follow fuller treatment is called for.

Extraordinary care should be taken with mathematical scripts ; especially for expressions in the least complicated, legible longhand is preferable to typing, as most typewriters have no characters suitable for indices and subscripts, for which our printers use smaller type; further, the letter "1" is often used for the figure one, which may lead to ambiguity. For simple fractions, the solidus / should be used instead of a horizontal

line, e.g., $\lambda/2\pi$ rather than $\frac{\lambda}{2\pi}$, care of course being taken to insert brackets where necessary

to avoid ambiguity. Exceptions to this rule are the proper fractions $\frac{1}{2}, \frac{1}{3}, \frac{2}{3}$, etc., which are available as single types and so are better left in this form, though such fractions as $9/17$, $12/25$ are better written with the solidus.

Full formulae or equations should be displayed, i.e. written on a separate line, and equalities numbered serially (1), (2), . . . on the right-hand side. In displayed expressions the solidus should be used with discretion. Short expressions occurring in the text may be incorporated with the text, as in the expression $\lambda/2\pi$ above.

When complicated expressions occur repeatedly in mathematical work they should not be written in full every time. Both the reader and the compositor will be helped if they are represented by a special symbol of which the meaning is defined when the expression occurs first.

Care should also be taken with exponential expressions and with subscripts ; the principle to bear in mind is simply that matter above or below the level of the normal type involves special treatment which leads both to less elegant work and to greater expense : P subscript n is simple, P_n , but a subscript n_2 (P_{n_2}) is not; e^x is simple but e^{x^2} is not, and may on occasion be written $\exp x^2$. $(a^2+b^2)^{\frac{1}{2}}$ and $\sqrt{(a^2+b^2)}$ are preferable to $\sqrt{a^2+b^2}$. As other fractional indices commonly occur the use of the fractional index is recommended.

For the logarithm of x to base 10 write 'log x ' and for that to base e write 'ln x '. Do not write 'log₁₀ x ' or 'log _{e} x '.

An interesting and explanatory document on the setting out of mathematics is the London Mathematical Society's "Notes on the Preparation of Mathematical Papers", obtainable from Messrs. C. F. Hodgson & Son Ltd., 2 Newton Street, Kingsway, Strand, W.C. 2, price 1s.

(vi) References

In the text bibliographical references are made by giving the name of the author and the year of publication in brackets, e.g. (Jones 1942), and details are given in the last section, "REFERENCES". Here the references are arranged in alphabetical order of authors' names and in date order for each author ; the form of reference is : Author, initials, year, journal, volume, page, e.g.

KOEHLER, J. S., 1941, *Phys. Rev.*, 60, 397.

The abbreviations used are those on the World List of Periodicals, with the slight difference that capital letters instead of lower case are used for adjectives. It will probably be most convenient for authors to give all journal names in full ; the appropriate abbreviations will then be made editorially. Books are referred to as follows :—

LOVE, A. E. H., 1944, *Elasticity* (Cambridge : The University Press).

§ 3. DRAWINGS

Drawings should be in Indian ink on tracing cloth, tracing paper or white card, with lettering in soft pencil. The drawings should in general be sufficiently large to allow of reduction in printing and the lines should therefore be bold ; the frame lines of graphs should be slightly finer than those of the plotted curves. Essential photographs can be reproduced as plates, but they should be avoided when possible because of their expense.

If authors are unable to submit drawings in the required form, arrangements can be made for these to be drawn and the cost price charged to the author.

If the drawings are made on tracing cloth or paper, it is advisable to send a set of prints with the MS. so that the originals may not be handled unduly. The pencil lettering will show on the print if it is done in soft (2B or 3B) pencil with a flat "chisel" point.

Figures should be numbered serially in arabic numerals and referred to in the text as figure 1, figure 2, . . . i.e. word in full with lower case f.

§ 4. ABBREVIATIONS AND JOURNAL STYLE

For symbols indicating position or quality, use roman type, e.g. the point A ; k_a , value of k in air, k_g , value of k in glass. In MS. these are left with no comment.

For symbols indicating quantity use italic type ; e.g. current I , voltage V , angles θ_1 , θ_2 . . . θ_n . In MS. these have single underlining, e.g. V.

For vectors use bold face letter (**r**). In MS. these are to be underlined with a wavy line, e.g. r. Italic bold face type (**k**) should be used for universal constants.

Greek letters should be explained by a pencil note in the margin, e.g. 'Greek alpha'.

Units are used in abbreviated form in the singular, e.g. cm. (not cms.), mm., km., kc/s., Mc/s., sec., μ a., ma.

Lower case "a" is used for unit of current to distinguish from Ångström units ; most other units, often derived from names, are rendered in small capitals (indicated by double underlining) ; Ångström units A., volts v., degrees Kelvin °K., degrees centigrade °C., kilo-x-ray units kx. A short list of abbreviations is given in an appendix.

Care should be taken to see that spelling is consistent throughout each paper. The preferred style is -ize in such words as recognize, polarize.

§ 5. LENGTH OF PAPER

Papers should be kept as short as possible. This can often be achieved by attention to mathematics and diagrams. The time taken for publication of a paper increases with its length ; speedy publication can usually be assured for papers of less than 3000 words.

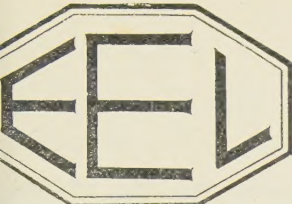
§ 6. CONCLUSION

It is hoped that authors will cooperate by seeing that these recommendations have been adhered to before communicating their papers ; such assistance would go far to remove the difficulties experienced in editing and in setting up type, which are the major problems in the publishing of a paper.

APPENDIX

ABBREVIATIONS AND SYMBOLS

a.	Amp.
A.	Ångström unit.
A.U.	Atomic unit.
A.C.	Alternating current.
D.C.	Direct current.
E.M.F.	Electromotive force.
C., F., K.	Degrees Centigrade, Fahrenheit, Kelvin.
V.	Volt.
X.U.	X-ray unit.
kva.	Kilovolt-amp.
ev.	Electron volt.
mev.	Mega electron volt.
<i>h, m, e, c, k</i>	Universal constants.
\approx	Is approximately equal to



**SELENIUM
PHOTO-CELLS**

The unique standard of performance demanded of every EEL cell before it leaves our laboratories has built a world reputation of which we are proud.

For the research engineer, together with the industrial engineer, it means that instruments incorporating EEL selenium cells are capable of the finest results. They are the

Best in the World

If you would like technical data, or if you require specific information on EEL selenium photo-cells, we shall be pleased to hear from you

A product of

**EVANS ELECTROSELENIUM
Ltd.**

Harlow

Essex



**BASICALLY BETTER
AIR-SPACED**

CO-AX LOWLOSS CABLES
TRANSRADIO LTD. 16 THE HIGHWAY BEACONSFIELD · 9 BUCKS.

REPORTS ON PROGRESS IN PHYSICS

Copies of the following volumes, bound in cloth, are available at 30s. each inclusive of postage.

Volume X (1944-45). 442 pages. General Editor: W. B. MANN.

Cosmic rays, by W. F. G. Swann.—*Seismology*, by H. Jeffreys.—*X-ray diffraction techniques in the industrial laboratory*, by H. P. Rooksby.—*Sound*, by E. G. Richardson.—*Phase separation in aqueous colloidal systems*, by P. Koets.—*Physics and textiles*, by A. B. D. Cassie.—*Some applications of physics to the processing of textiles*, by J. G. Martindale.—*Electron microscopy*, by L. Marton.—*The theory of the elementary particles*, by H. J. Bhabha.—*The mechanical design of physical instruments*, by A. F. C. Pollard.—*The lightning discharge*, by J. M. Meek and F. R. Perry.—*Superconductivity*, by K. Mendelssohn.—*Spectroscopy applied to molecular physics*, by J. Cabannes.—*Lessons of the war for science*, by J. D. Bernal,

Volume IV (1937), reprinted 1946. 389 pages. General Editor: ALLAN FERGUSON.

The measurement of time, by Sir Harold Spencer Jones.—*The adsorption of gases by solids*, by E. K. Rideal.—*Surface tension*, by R. C. Brown.—*Sound*, by E. G. Richardson.—*Supersonics in relation to molecular constitution*, by E. G. Richardson.—*Heat*, by R. W. Powell.—*Thermodynamics*, by J. H. Awbery.—*Refrigeration*, by Ezer Griffiths.—*The beginnings of the new quantum theory*, by H. T. Flint.—*Atomic physics*, by C. H. Collie.—*Slow neutrons*, by P. B. Moon.—*The charge of the electron*, by H. R. Robinson.—*The breakdown of insulating materials: electric strength*, by L. Hartshorn.—*Measurement of current at radio frequencies*, by T. Iorwerth Jones.—*Electrical oscillations and biological materials*, by W. H. Ward.—*Frictional electricity*, by W. H. Ward.—*Electrolytes and electrolysis*, by R. W. Gurney.—*Physical-optical instruments and materials*, by F. Simeon.—*Spectroscopy*, by W. R. S. Garton, A. Hunter, R. W. B. Pearse, E. W. Foster, L. Kellner.—*X-ray analysis and applications of Fourier series methods to molecular structures*, by J. M. Robertson.—*Diamagnetic and paramagnetic anisotropy of crystals*, by K. Lonsdale.

Volumes I-III (1934-36) and V-IX (1938-1943) are out of print, and no copies are available at the office of the Society.

Orders, with remittances, should be sent to the Publishers,

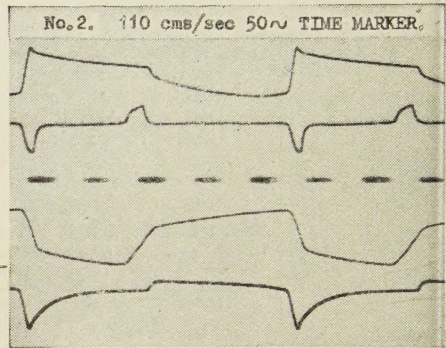
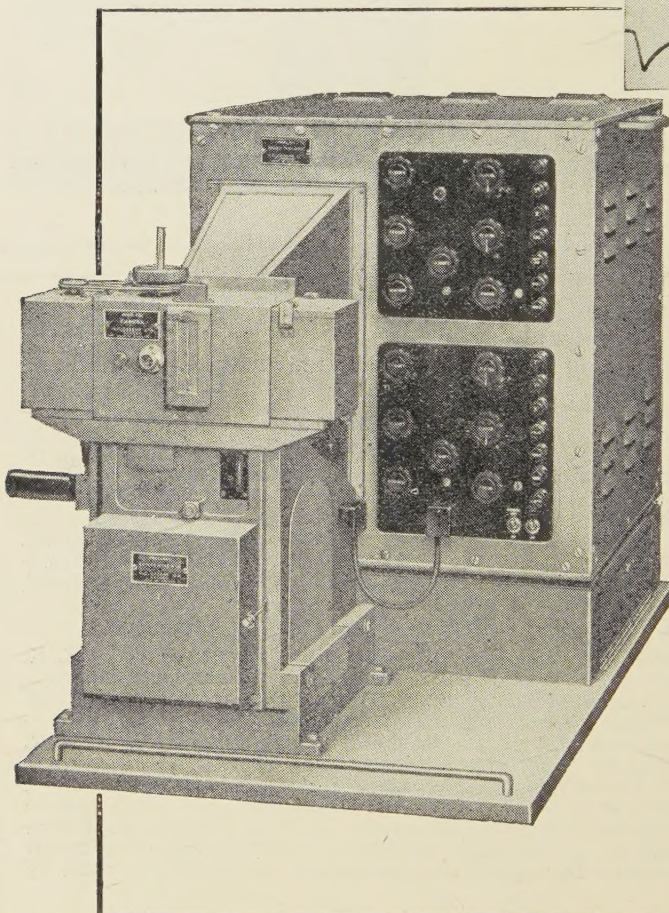
THE PHYSICAL SOCIETY

1 Lowther Gardens, Prince Consort Road, London S.W.7

COSSOR

MULTIPLE RECORDER

**for the Cinematographic
Investigation of Transients
with Two Double-Beam
Cathode Ray Tubes**



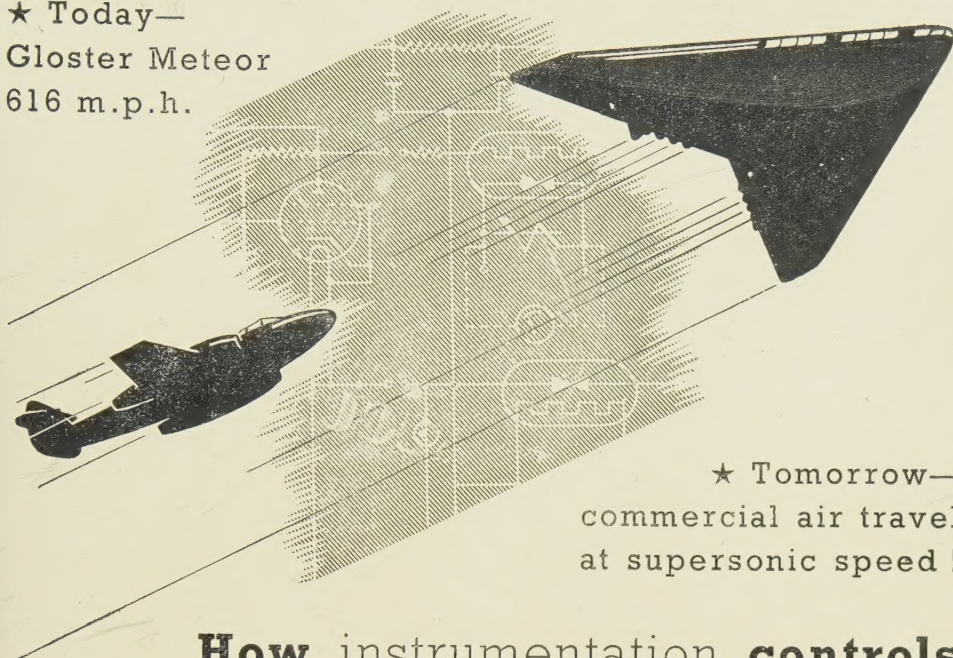
(Actual size 70 mms.)

This equipment is the latest development in the use of sealed-off Cathode Ray Tubes in Multiple Recording technique as pioneered by Cossor. It is designed and precision engineered specifically for field tests, including Traction Recording, Marine and Motor testing and other industrial laboratory investigations. The equipment comprises a Twin Tube unit using two 4½ in. dia. blue screen Double-Beam Tubes and a gear-driven moving film camera mounted complete on a robust plinth including a useful drawer to accommodate accessories. It provides simultaneously four independent and continuous records plus a central electro-optical time marking on 70 mm. unperforated film or paper. By means of interchangeable gears and/or motors, a film speed range of from 0.005 to 250 cms./sec. is obtainable, with a tube spot writing speed up to 2 kms./sec.

Further details on application to :—

A. C. COSSOR LTD., INSTRUMENT DEPT., Highbury, London, N.5.

★ Today—
Gloster Meteor
616 m.p.h.



★ Tomorrow—
commercial air travel
at supersonic speed !

How instrumentation controls today's brilliant technical progress

Engineering advances follow closely on the development of new and better materials. In turn, the manufacture of these calls for ever-increasing refinement in measurement and control—problems solved by SUNVIC specialisation on the latest electronic techniques. Modern aircraft engines, for example, had to await the development of metals which retain their strength at high temperatures. The production of these metals calls for very accurate temperature control—for instance, in the measurement of "creep". Instruments for this purpose are among those developed by SUNVIC and supplied to leading industrial, government and research laboratories at home and abroad.

SUNVIC PRODUCTS INCLUDE Hotwire Vacuum Switches & Units—Glass-sealed Thermostats—Adjustable Stem Thermostats—Electronic Relays—Resistance-Thermometer Controllers—'No-Loss' Energy Regulators—Time-Delay Switches—Moisture Testers, etc., etc.

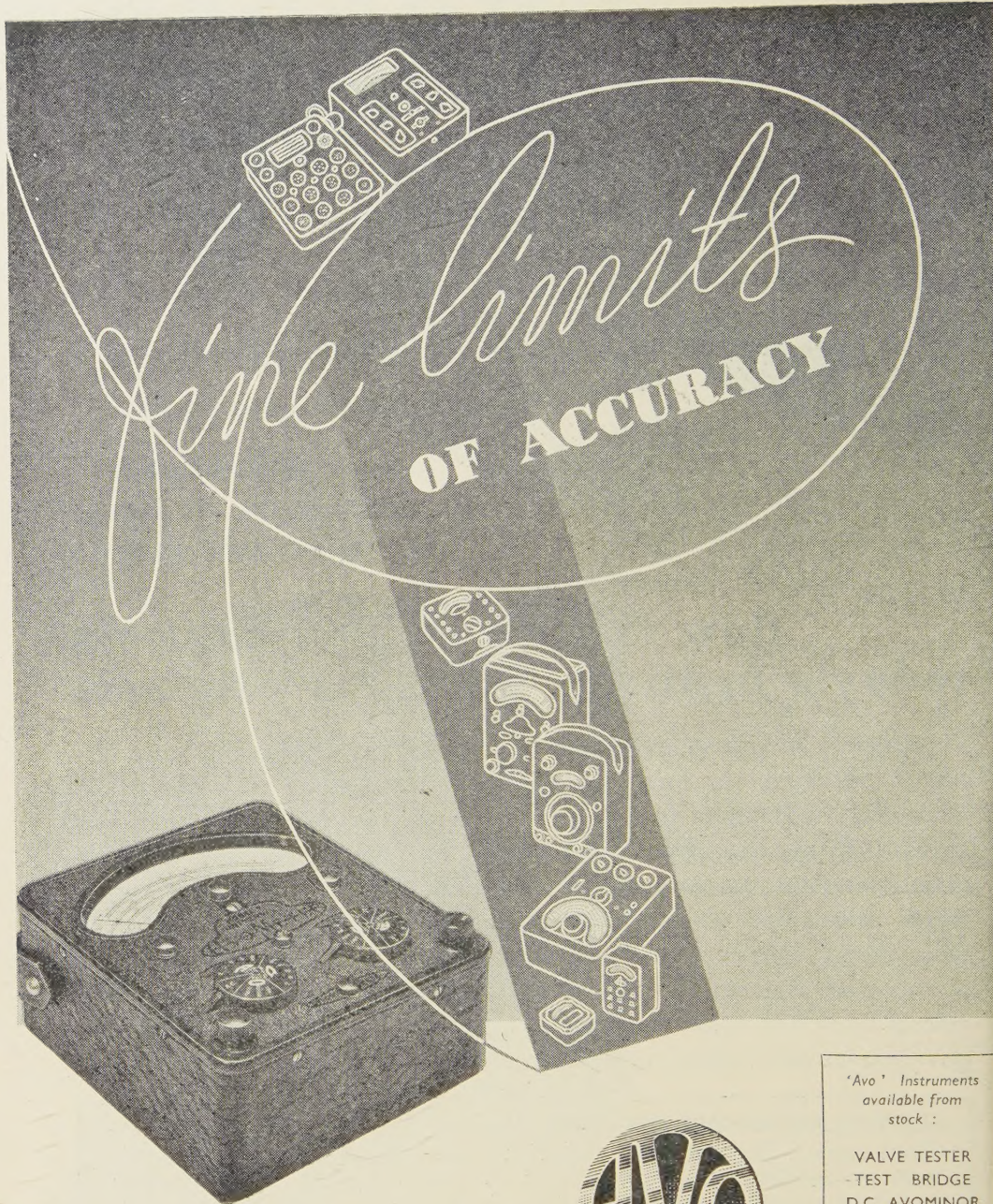
Please write for appropriate Catalogue sections.

Electronic and
thermostatic control
instruments for
science and industry.



SUNVIC CONTROLS LTD.

10, ESSEX STREET,
STRAND, LONDON, W.C.2
Tel: TEMple Bar 7064



The 50 range Model 7 Universal AvoMeter, the pioneer of the comprehensive range of "Avo" precision instruments, is the world's most widely used combination electrical measuring instrument. Fully descriptive pamphlet available on application to the Sole Proprietors and Manufacturers:—



Electrical Measuring Instruments

"Avo" Instruments
available from
stock :

VALVE TESTER
TEST BRIDGE
D.C. AVOMINOR

THE AUTOMATIC COIL WINDER & ELECTRICAL EQUIPMENT CO., LTD.
WINDER HOUSE · DOUGLAS STREET · LONDON S.W.1 · TELEPHONE: VICTORIA 3404/9



THE BALDWIN

FARMER ELECTROMETER FOR RADILOGICAL WORK

A unique electronic instrument for research and routine testing in Hospital Radium and X-ray Therapy Departments.

It has an input resistance of 10^{16} ohms and an input capacity of less than $1 \mu\mu F$. Developed primarily for use in Radiological work, where small condensers of the Sievert type are used extensively for the measurement of gamma and X-ray intensities.

Fully descriptive leaflet supplied on request.

BALDWIN INSTRUMENT COMPANY LTD.

BROOKLANDS WORKS, PRINCES ROAD, DARTFORD, KENT.

Telephone: DARTFORD 2989

VOLTAGE RANGES

- 0 - 50
- 0 - 100
- 0 - 250

DAWE STROBOSCOPES

'FREEZE' MOTION

-thereby enabling high-speed rotating and oscillating mechanism to be viewed as if stationary or in slow motion.

TROBOFLASH. Standard model from our range of Stroboscopes for measuring speed and for observing rotating and oscillating machinery in slow motion. Features: Direct reading over range of 600-14,400 r.p.m., and tending to 100,000 r.p.m. Sharp images at all speeds within range. No contact required with mechanism under measurement. Mains operated. Portable and convenient to use.

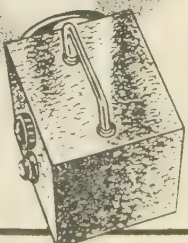
STOL-GRIP LAMP UNIT. For use with Stroboflash in inaccessible locations.

STROBOFLOOD. An accessory unit for the Stroboflash, which provides a greater light output for photographic work or for flood-lighting a large area. Maximum flashing rate 10,000 per minute.

CONTACTOR UNIT. Permits the Stroboflash to be driven in exact synchronism with a spindle of the machine to be viewed. The contactor is fitted with a phasing device enabling the watched part to be held in any desired position.

For technical data write : DAWE INSTRUMENTS LTD.
Quinn Avenue, Great West Road, Brentford, Middx.

Ealing 1850



FOSTER
C.V.
CONSTANT VOLTAGE
TRANSFORMERS

CONSTANT VOLTAGE

means

"C.V."
(TRADE MARK)

CONSTANT EFFICIENCY

FOR METER CALIBRATION — PRECISION PHOTOGRAPHY — X-RAY EQUIPMENT — ELECTRONIC DEVICES and ALL LABORATORY & RESEARCH EQUIPMENT.

Pioneers of constant pressure equipment, we have introduced a range of equipment to meet every demand. 12.5 Va — 5 Va or made to meet specific requirements. We are particularly interested in problems concerning "building-in" "CV's" to your equipment.

FOSTER TRANSFORMERS & SWITCHGEAR LTD.

TELEPHONE LIBERTY 2211 (8 lines) SOUTH WIMBLEDON, LONDON, S.W.19 TELEGRAMS FOSTERACO PHONE LONDON

Write for leaflet F.T.85



PIPE COUPLINGS

ELECTRICALLY HEATED PRESSURE HEADS

FILM ASSESSORS AND SCANNING MICROSCOPES

CONTINUOUS FILM RECORDING CAMERAS AND EQUIPMENT FOR CATHODE RAY OSCILLOGRAPHY, ETC.

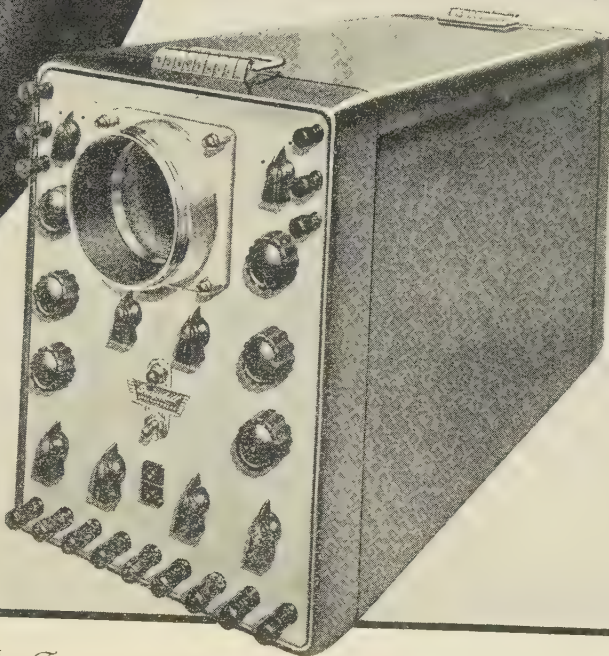


We undertake the Design, Development and Manufacture of any type of Optical — Mechanical — Electrical Instrument. Including Cameras for special purposes.

Avimo Limited, Taunton, England · Telephone Taunton 3634

11790 D

Presenting the New Model D



The Type 1684 series of Oscilloscopes are already well known. The new Model D retains the desirable features of this series—d.c. shifts, response flat to video frequencies, d.c. coupled symmetrical amplifiers on both axes, semi-automatic synchronisation, etc. It incorporates many new features in design, both electrical and mechanical. One such improvement is that the grids of the amplifiers are brought out at Earth potential enabling the instrument to be used more easily for d.c. measurement.



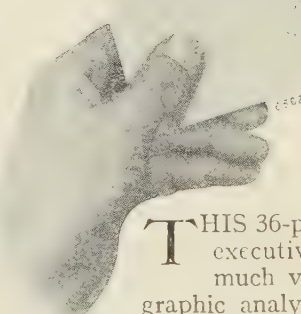
Furzehill LABORATORIES LTD

BOREHAM WOOD, HERTS

CAMBRIDGE POLAROGRAPH

(HEYROVSKY DROPPING MERCURY ELECTRODE METHOD)

CAMBRIDGE POLAROGRAPH



MICRO-ANALYSIS

Some Fields of Application:

- PHYSICAL CHEMISTRY
- METALLURGY
- MINERALOGY
- SUGAR
- EXPLOSIVES
- GASES
- AGRICULTURE
- MEDICINE
- OIL DISTILLING
- DYEING & BLEACHING
- CERAMICS
- WATER PURIFICATION

THIS 36-page publication (109-L) will be sent to responsible executives and research workers on request. It contains much valuable information on the technique of polarographic analysis, with formulæ for base solutions, tables and charts of half-wave potentials, and a bibliography of 168 important references. A special feature is the reproduction of actual records obtained in original experiments in our own laboratory. A supplement describes the new Cambridge Voltamoscope, for routine determinations, which performs the same functions, but is non-recording.

CAMBRIDGE INSTRUMENT COMPANY LTD.
13, GROSVENOR PLACE, LONDON, S.W.1.
WORKS: LONDON & CAMBRIDGE.

THE PROCEEDINGS OF THE PHYSICAL SOCIETY

VOL. 60, PART 2

1 February 1948

No. 338

The Structure of Photo-sensitive Lead Sulphide and Lead Selenide Deposits and the Effect of Sensitization by Oxygen*

By H. WILMAN

Applied Physical Chemistry Laboratory, Imperial College, London

MS. received 2 June 1947

ABSTRACT. An exploration has been made, by electron diffraction and photoconductivity experiments, of the structure of photosensitive lead sulphide and lead selenide deposits prepared by chemical deposition and by sublimation *in vacuo* or in oxygen. In spite of the large variations in photoconductive properties which the deposits show as a result of treatments such as baking in vacuum or oxygen, the PbS and PbSe crystals were found to have a lattice axial dimension which was constant to 0·1% in all samples measured, even in strongly oxidized deposits in which there was estimated to be 10 to 20% of the oxidation product. The oxidation product was identified from its diffraction pattern as PbO·PbSO₄. The photoconductivity measurements, however, indicate that the sensitivity is associated with deviations from the stoichiometric compositions PbS and PbSe, and that oxygen treatments increase the sensitivity of PbS to wavelengths between 1 and 3 μ , but do not do so for PbSe.

§ 1. INTRODUCTION

DURING the war lead sulphide photoconductive cells were manufactured in Germany by Gudden, Kaspar, Kutzscher and others, but the methods of production have not been published. In 1944 methods of manufacture of PbS and PbSe cells were developed at the Admiralty Research Laboratory, Teddington (for details of the vacuum-sublimed deposits see Starkiewicz, Sosnowski and Simpson 1946, Lee and Parker 1946), and a brief account is given below of the structure of the deposits, as revealed by the use of electron-diffraction methods. Electrons of about 60 kv. voltage were used with a camera length of approximately 50 cm. in a Finch type electron-diffraction camera (Finch and Wilman 1937). Early in 1946 further electron-diffraction investigations provided definite information on the amount, chemical nature and form of the oxidation product obtained by heating or subliming (at temperatures above 500° c.) the PbS layers in oxygen at about 0·1 mm. Hg pressure, during their sensitization as photoconductive or photovoltaic cells (Starkiewicz, Sosnowski and Simpson 1946).

The crystal lattice structure and parameters of the PbS and PbSe were practically identical for all the deposits examined; these are stated in § 6. Of the photosensitivity data only a brief outline of some general characteristics is given in § 6.

* This work was carried out in the Applied Physical Chemistry Laboratory, at Imperial College, London, by arrangement with Professor G. I. Finch, M.B.E., D.Sc., F.R.S.

The vacuum-sublimed deposits were all prepared in well degassed pyrex pumping systems (0.5 to 1 hour degassing at 500°c.) evacuated by mercury diffusion pumps to about 10⁻⁶ mm. Hg, with liquid-air trap to avoid mercury contamination.

§ 2. THE STRUCTURE OF LEAD SULPHIDE AND LEAD SELENIDE DEPOSITS FORMED BY CHEMICAL PRECIPITATION

Deposits of lead sulphide with good photoconductivity prepared by Dr. F. Kicinski at A.R.L. were precipitated as mirror-like layers on pyrex substrates from a solution of lead acetate and thiourea by adding sodium hydroxide solution, and after washing with weak ammonium sulphide solution were dried in air at 100°c. Figure 1 shows an example of the electron-diffraction patterns obtained from such mirror-like slightly translucent deposits, which are dark olive-green by transmitted light. The arc positions show that the PbS crystals tended to be orientated with cube faces, i.e. {001}, parallel to the polished pyrex substrate. Similar patterns, but with less distinct arc development, were given by thicker opaque deposits ($\sim 1\mu$ thick) in which the PbS crystals in the surface layers had only to a very slight extent the preferred {001} orientation. The mean crystal size was estimated to be at least 150 Å. and was in some cases of the order of 500 Å.

Translucent olive-brown PbS deposits were also prepared for comparison with the above, by passing H₂S gas over a lead-acetate solution at room temperature, slightly acidified with acetic acid. These floating mirror-like films were picked up on nickel gauze, transferred to the surface of an H₂S water solution to wash them, removed, and a drop of Aquadag graphite added for lattice-constant reference purposes; they were then dried *in vacuo* in the diffraction camera. The ring-patterns obtained at normal transmission, figure 2, became weakly arced on inclining the film, showing that the PbS crystals had their cubic faces, {001}, more or less parallel to the surface of the solution on which they were formed. The mean crystal diameter was about 250 Å.

Similar mirror-like, translucent reddish-brown layers of PbSe were obtained by passing H₂Se over lead-acetate solution acidified with acetic acid, and these gave patterns like figure 13, where the {110} graphite ring is also present for calculation of lattice dimensions. The PbSe crystals had a mean diameter of about 250 Å. and had tended to grow with {001} planes parallel to the surface of the solution. Such PbSe layers showed no change in diffraction pattern after heating for 30 minutes in air at 100° to 130°c. or in steam at 130° to 150°c.

§ 3. THE STRUCTURE OF LEAD SULPHIDE AND LEAD SELENIDE DEPOSITS PREPARED BY VACUUM SUBLIMATION

Some of the early experimental PbS cells made by the vacuum sublimation method were cut open and immediately re-evacuated in the electron-diffraction camera, and an electron beam allowed to graze the inner cylindrical surface of the deposit on the electrode region of the pyrex cell wall. Three types of deposit were examined: (a) PbS volatilized and condensed *in vacuo* then superficially acted upon by sulphur vapour at low pressure and temperature about 500°c. (figure 3); (b) PbS volatilized and condensed in presence of sulphur vapour (figure 4); (c), as for (b), but resublimed in oxygen at 1 mm. Hg pressure.

In all these the mean crystal diameter of the PbS was estimated to be between 150 and 500 Å. or more, and there was usually a marked tendency for the PbS

crystals to grow in a one-degree orientation, either {111}, {110}, {210}, or {311}; in some cases two, or even three, of these were present in the same layer. For example, figure 4 shows that {311} planes in some crystals and {210} in others were parallel to the pyrex substrate. The type of orientation developed presumably depends on the temperature of the surface and the rate of condensation. The one deposit of the third type examined had a larger crystal size than the others, 500 Å. or more, as shown by the incompletely formed spotty rings, cf. figures 5-8. This was to be expected, for the temperature of sublimation of the PbS was higher ($\sim 580^\circ \text{C}$) in oxygen than *in vacuo* ($450^\circ\text{--}500^\circ \text{C}$), and since that of the substrate was also higher, there was more rapid aggregation of the PbS to form larger crystals. Two exceedingly faint unidentified rings were present in this pattern in addition to the PbS rings.

Seven vacuum-sublimed translucent orange-brown PbSe deposits in experimental cells were examined. The PbSe used was prepared by passing H₂Se into lead-acetate solution followed by much repeated washing of the precipitate and drying at about 100° to 130° C. All these deposits yielded clear ring or arc patterns, as in figure 14, due to PbSe crystals either randomly disposed or in strong one-degree {001} orientation on the substrate. The estimated mean crystal size varied between about 150 Å. and 500 Å. or more, increasing with increasing duration and temperature of the vacuum bakes which the layer had undergone after the initial condensation. In one case where a cell had developed a noticeable leak at one of the glass-tungsten seals during formation of the layer, which had become grey in colour, an unidentified diffraction pattern was obtained (figure 16, table 4). This presumably corresponds to one or more of the compounds of Pb, Se and O.

§ 4. THE STRUCTURE OF LEAD SULPHIDE DEPOSITS SENSITIZED BY SUBLIMING AND BAKING IN OXYGEN

(i) *Photoconductive deposits*

Two cells A and B (made by J. Starkiewicz at A.R.L.) which had undergone the normal type of activation treatments by slow sublimation and further baking in oxygen, yielded the electron diffraction patterns, figures 5 and 6; net-plane spacings are given in table 1. In both cells the pumping stem had a narrow constriction impeding escape of SO₂ gas to the liquid air trap, and the final (modulated-light) sensitivity reached the average good high level attained with most cells of this type. Both PbS deposits had a matt grey-black surface and were opaque.

The patterns of spotty arcs (figures 5 and 6) showed that the PbS crystals had relatively large size, probably ~ 1000 Å. diameter, and had grown so that some had {110} planes parallel to the pyrex substrate, others {001}. The lattice dimension was $a = 5.917 \text{ kx}$, relative to graphite $a = 2.456_3 \text{ kx}$. The additional fainter arcs in the patterns showed the presence of an oxidation product (forming about 10-20% of the diffracting layer) which was also crystalline, with mean crystal diameter of the order of 500 Å., and was also (especially in cell A) strongly orientated, the net-plane parallel to the substrate having a spacing of 1.228 kx. This oxidation product was identified from its net-plane spacings as PbO.PbSO₄ (see (iii) below), the crystal habit apparently varying according to the conditions of oxidation and causing some variation in ring intensities, without much change in the lattice dimensions and net-plane spacings.

Table 1. Plane spacings (d) and diffraction intensities for electron diffraction patterns from oxygen-sensitized PbS cells.
Cells A and B—photoconductive cells; C and D—barrier-layer type)

Cell A d (kx.)	Cell B		Cell C		Cell D		PbS ; $a = 5.917$ kx.	
	d (kx.)		PbS	Intensity oxide	d (kx.)	PbS	Intensity oxide	d (kx.)
	PbS	Intensity oxide						Diffraction indices hkl .
6.3	F	—	—	—	—	—	—	—
4.5	F	—	—	—	—	—	—	—
3.45	MS	VF	3.33	MF	3.23	MF	3.42	3.409
3.30	VF	VF	—	—	3.06	3.17	—	111
3.04	S	VF	2.94	MS	2.958	S	3.084	200
2.96	VF	VF	2.72	F	2.85	—	2.954	—
2.78	—	—	2.695	MF	2.68	—	—	—
—	—	—	—	MF	2.38	M(c) MF(D) MF(D)	2.675	—
2.34	MF	MF	2.33	—	—	MF	2.44	—
2.20	VF	VF	2.08	S	—	VF	2.31	—
2.09	V	S	—	—	—	S	—	220
—	—	—	—	—	—	—	—	—
1.845	F(c)	—	—	—	—	—	—	—
1.787	S	—	1.837	VF	1.849	S	1.949	—
—	—	—	1.780	M	1.784	—	—	—
1.704	M	F	1.706	F	(1.71)	M	MF	—
1.655	F	F	1.655	VF	1.644	—	1.846	—
1.603	F	F	1.609	VF	—	S	1.783	311
1.563	F	F	1.555	VF	1.579	—	—	—
—	—	—	1.517	VF	1.525	—	—	—
1.484	M	F	1.478	M	1.481	M	1.720	—
1.425	F	F	—	—	1.424	—	1.704	222
1.414	VF	VF	—	—	—	M	—	—
1.358	M	VF	1.357	M	1.360	—	—	—
1.325	MS	VVF	1.322	S	1.323	—	—	—
1.292	VVF	VVF	1.295	VF	1.298	VVF	1.440	400
1.255	MF(c)	MF(c)	—	—	—	—	1.401	—
1.228	M	MF(c)	1.228	M	1.208	MS	1.363	331
1.208	M	VF	1.208	M	1.168	VVF	1.323	420
1.174	M	—	1.138	M	1.140	M	—	—
1.141	M	—	—	—	—	—	—	—

(c) = central arc, i.e. in plane of incidence. D = strong ; S = medium ; M = faint ; V = very.

(ii) Photovoltaic deposits

Similar patterns, figures 7 and 8, were also obtained from two cells, C and D, which had been activated as photovoltaic or barrier-layer cells by J. Starkiewicz at A.R.I., i.e. after sublimation in oxygen at 0·1 mm. Hg pressure, followed by baking in oxygen, a direct current of 2 ma. was passed through the cell during bakes at 250° to 400° c. (Starkiewicz, Sosnowski and Simpson 1946). Both had about average (modulated-light) photoconductivity. During oxidizing activation of cell C the SO₂ was impeded from reaching the liquid-air trap by constrictions in the pumping stem, while in the case of D no impedance was applied and the SO₂ formed was quickly trapped. The conditions of oxidation were thus appreciably different in the two cases; nevertheless the diffraction patterns showed (table 1) that many of the net-plane spacings of the oxidation product present besides the PbS, were essentially the same within the accuracy of measurement of the radii of the rings or arcs which were often very faint. Moreover, the spacings agreed closely with most of those from cells A and B, and well with many of those found for PbO.PbSO₄, especially from the pattern obtained by heating PbS in air to 350° c. (see (iii) below and table 2). The relative intensities and circumferential positions of the corresponding rings in the two patterns were different, and differed from those of cells A and B, showing that the PbO.PbSO₄ crystals were orientated differently relative to the substrate. In cell C the {001} planes of the PbO.PbSO₄ tended to be parallel to the substrate (cf. tables 1 and 2), while the PbS crystals were mainly in {001} but some in {110} orientation; and in cell D some PbO.PbSO₄ crystals had {111} orientation (as in cells A and B), and in others {102} planes were parallel to the substrate, the PbS being again strongly orientated partly with {001} and partly with {110} planes parallel to the substrate.

(iii) Identification of the oxidation product as PbO.PbSO₄

The net-plane spacings and relative diffraction intensities of the oxidation product from table 1 were compared with the available x-ray data for lead compounds, including that of Hanawalt, Rinn and Frevel (1938) for Pb, PbO (yellow rhombic form), PbO₂, Pb₃O₄, PbSO₄ and PbS₂O₃ (lead thiosulphate), PbCO₃, 2PbCO₃.Pb(OH)₂ and Pb(NO₃)₂, and with electron-diffraction data for the last two of these compounds previously obtained in this laboratory.

Other recent published work on the Pb-O and Pb-O-S compounds was also compared with the data of table 1, but the following gave no agreement: PbO (yellow rhombic)—Halla and Pawlek (1927), Rencker and Bassière (1936), Petersen (1941), Byström (1943); PbO (red, tetragonal)—Dickinson and Friauf (1924), Darbyshire (1932), Clark and Tyler (1939), Clark and Rowan (1941), Moore and Pauling (1941); Pb₃O₄—Clark, Schieltz and Quirke (1937), Gross (1941, 1943), Straumanis (1942), Byström and Westgren (1943); Pb₂O₃—Clark, Schieltz and Quirke (1937), Baroni (1938), Gross (1941); Pb₅O₈—Clark, Schieltz and Quirke (1937), Clark and Rowan (1941), Davidson (1941); PbO₂—van Arkel (1925), Darbyshire (1932); PbO_x—Clark and Rowan (1941); 5PbO.2H₂O—Clark and Tyler (1939); PbSO₄—Basche and Mark (1924), James and Wood (1925); 2PbO.PbSO₄, 3PbO.PbSO₄, 4PbO.PbSO₄—Clark, Mrgudich and Schieltz (1936).

A useful series of x-ray patterns of many of the above is given by Clarke (1940), and x-ray data for the mineral "lanarkite", PbO.PbSO₄, by Richmond and

Table 2

Wolfe (1938). The latter authors give the size of the monoclinic pseudohexagonal unit cell as $a = 13.73 \text{ \AA}$, $b = 5.68 \text{ \AA}$, $c = 7.07 \text{ \AA}$, and $\beta = 116^\circ 13'$. The cell is base-centred, thus only hkl diffractions appear which have $(h+k)$ even. A calculation of the net-plane spacings corresponding to possible diffractions gave the values in table 2, which includes all values above 2 \AA and many below. Relative intensities were obtained by the experiments described in § 5, below.

In the comparison of the lists of spacings and diffraction intensities in tables 1 and 2 the following points must be realized: (i) owing to the orientation of the crystals in the photocell deposits, not all the diffractions in table 2 will be visible above the shadow edge in the reflection patterns; (ii) the relative intensities of the arcs which do appear will be different from those in table 2, owing to the orientation and to absorption which weakens beams emerging near the shadow edge; (iii) planes which are parallel to the surface in most of the crystals give especially strong arcs whose centres lie on the plane of incidence; (iv) there may be a slight difference in the lattice dimensions and the relative diffraction intensities such as that observed in the patterns from PbS heated in air at 350° c. and 550° c. (table 2), although the net-plane spacings are all standardized by comparison with the graphite 110 spacing; (v) strong PbS diffraction arcs may obscure other weaker arcs in their vicinity; (vi) smallness of the radii and of refraction effects decrease the accuracy of measurement of the larger net-plane spacings.

Bearing in mind the above conditions the oxidation product in the photocell deposits was identified from the spacings given in table 1 and from the circumferential positions of the arcs in the patterns, figures 5 to 8, as $\text{PbO} \cdot \text{PbSO}_4$ (or approximating closely to that composition and lattice structure) for the following reasons:

(i) The spacings in the first four lists in table 1 agree well with themselves and with many of those in table 2, notwithstanding the faintness of some of the diffractions. (ii) The lanarkite structure accounts for the large spacings of the two innermost diffractions of figure 8 (cell A). (iii) On the basis of the lanarkite structure, the net-planes which are orientated parallel to the substrate are densely populated planes having small indices, {111} in cells A, B and D, and {111} and {102} together in cell D; the second and third orders of reflection from the {111} planes give as the {111} spacing the value 3.68 \AA . in agreement with the value for lanarkite in table 2. (iv) The circumferential positions of the arcs on the other rings appeared to correspond well with those to be expected from lanarkite crystals in these orientations. (v) The plane spacings of the transmission patterns obtained after complete oxidation of PbS films in air at 350° c. and 550° c. agreed closely with those calculated for lanarkite (table 2).

In order to obtain diffraction patterns from other Pb-O-S compounds several other materials were examined by electron diffraction, and though they did not correspond to that of the oxidation product discussed here, they are of some interest and provide another example of appreciable changes of diffraction intensities associated with only slight changes in lattice dimensions. Figure 11 and table 3 (spacings calibrated by graphite) show the diffraction data obtained by transmission from a floating white surface layer precipitated by passing SO_2 gas over lead-acetate solution. This is certainly not PbSO_4 , but the pattern seems to have some similarities with those of the 2-, 3- and 4- $\text{PbO} \cdot \text{PbSO}_4$ oxysulphates. When this material was heated in air for 5 minutes at 300° c. it gave a pattern (see table 3), in which the ring intensities were appreciably changed though their

relative radii were nearly unaltered; after a further 45 minutes in air at 550° c. it gave figure 12 (table 3), which may possibly be closely related to the x-ray pattern from 2PbO.PbSO₄ though it is not identical with this.

Table 3. (a) and (b) are nearly identical and are closely related to the pattern (b) of table 2; the spacings of (c) correspond with most of those of table 2(c) but the intensities are different.

(a) White pp. from Pb acetate + SO ₂		(b) Pp. of (a) heated 5 min. at 300° c. in air		(c) Spec. of (b) heated 45 min. at 550° c. in air	
d (kx.)*	Intensity	d (kx.)*	Intensity	d (kx.)*	Intensity
8.07	VVF	—	—	—	—
6.75	VF	6.4	VF	—	—
5.182	F	5.14	VF	4.45	F(D)
4.261	M	4.24	MF	4.11	F(D)
3.753	MS	3.73	MS	3.68	MF(D)
3.414	MF	3.40	MF	3.48	F(D)
3.218	MS	3.215	M	3.286	MF
3.122	MS	3.110	M	2.963	VS
2.905	MS	2.905	S	2.849	S
2.723	S	2.719	S	(2.63)	VF
2.576	F	2.575	VF	2.528	M
2.469	MF	2.444	F	2.395	MF
2.341	VF	—	—	—	—
2.248	M	2.246	F	2.263	F
2.136†	MF	2.127†	MF	2.182	F
2.058	MS	2.064	M	2.047	M
2.025‡	MS	2.025‡	M	—	—
1.958	MF	1.960	F	1.954	F(D)
1.903	MF	1.901	F	1.896	F(D)
1.865	F	1.852	F	1.843	F(D)
1.831	F	1.825	VF	—	—
1.760	VF	—	—	1.754	F(D)
1.719	MF	1.715	MF	1.716	F(D)
1.704	F	—	—	—	—
1.659	F	1.657	F	1.669	F(D)
1.644	F	—	—	—	—
1.606	MF	1.613	F	1.615	F(D)
1.571	MF	1.566	F	—	—
1.502	F	1.502	VF	1.520	F(D)
1.457	M	1.454	MF	1.462	M(D)
1.446	M	—	—	1.419	VF
1.393	MF	1.391	VF	1.386	VF
1.368	F	—	—	1.352	VF
1.339	F	—	—	—	—
1.318	VF	—	—	1.311	MF(D)
1.305	VF	—	—	—	—
1.283	VF	—	—	1.289	MF(D)
1.254	M	1.253	MF	1.249	VF(D)
1.205	VF	—	—	1.206	VF(D)
1.189	VF	—	—	1.169	VF(D)

* Relative to graphite, $d_{110} = 1.228$ kx.

† May be entirely the graphite 100 ring.

‡ May be partly but only in small part due to graphite 101 diffraction.

§ 5. THE OXIDATION OF PbS AND PbSe IN AIR AT ATMOSPHERIC PRESSURE

Translucent olive-green films of PbS with strong metallic reflexion were formed by passing H₂S over lead nitrate solution. After washing by floating on distilled water these gave normal PbS diffraction patterns like figure 2. When such layers were heated in air at atmospheric pressure at 350–370° c. for 10 minutes



Figure 1. Chemically deposited PbS layer (good sensitivity).



Figure 2. PbS layer from H_2S over Pb acetate solution.



Figure 3. PbS cell ; layer formed by vacuum sublimation and treatment with S.

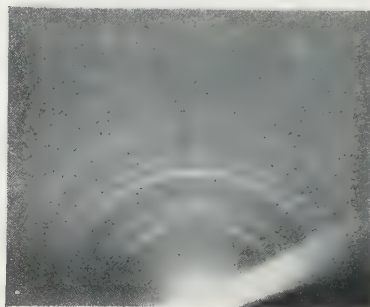


Figure 4. PbS cell ; layer formed by vacuum sublimation in presence of S.



Figure 5. PbS cell "A" ; layer sublimed in O_2 .

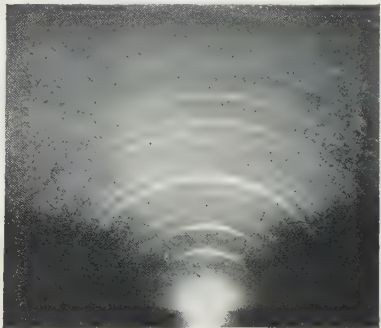


Figure 6. PbS cell "B" ; layer sublimed in O_2 .



Figure 7. PbS cell "C" ; formed in oxygen, but photovoltaic type.



Figure 8. PbS cell "D" ; formed in O_2 , but photovoltaic type.



Figure 9. $\text{PbO} \cdot \text{PbSO}_4$ by heating PbS in air at 350°C . for 10 minutes. (Two outermost rings graphite.)



Figure 10. $\text{PbO} \cdot \text{PbSO}_4$ by heating PbS in air at 550°C . for 5 minutes. (Graphite present as reference.)

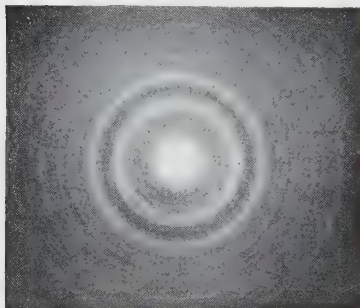


Figure 11. White layer by SO_2 over Pb acetate solution.

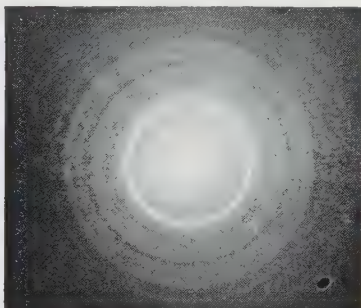


Figure 12. Deposit of figure 11 heated in air at 550°C . for 45 minutes.

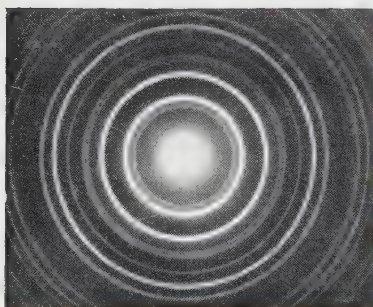


Figure 13. PbSe layer from H_2Se over Pb acetate solution.



Figure 14. PbSe cell; layer formed by vacuum sublimation.

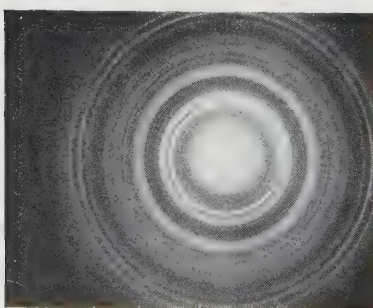


Figure 15. PbSe heated in air at 350°C . for 10 minutes.



Figure 16. PbSe cell after a leak had caused oxidation.

they became transparent yellowish-grey, giving a different pattern, figure 9, which corresponds exactly to $\text{PbO} \cdot \text{PbSO}_4$. Table 2 shows the plane spacings (calibrated by comparison with graphite) and the relative intensities of the diffraction rings, and these are compared there with the data for lanarkite, $\text{PbO} \cdot \text{PbSO}_4$.

A fresh PbS layer, heated in air up to 550°C . for 7 minutes and kept there for 5 minutes, became milky-transparent and gave a pattern, figure 10 and table 2, with spacings nearly identical with those of figure 9, but with a difference in the relative intensities of the corresponding rings, the random disposition of the crystals in both cases was checked by photographs with the specimen inclined to detect any arcing of the rings. This slight change in lattice dimensions may indicate a slightly different degree of oxidation in the two cases with only a small difference in crystal lattice dimensions. The change in relative intensities of the rings may be attributed to a difference in the external shape of the crystals, which would cause different absorption of the various diffracted beams passing through different thicknesses of crystal in different directions (Böhm and Gantner 1928, Fordham 1940, Brandenberger 1945).

Similar PbSe layers formed by passing H_2Se gas over lead-acetate solution acidified with acetic acid gave unchanged ring patterns by transmission electron diffraction after heating the layers at 100° to 130°C . in air for 30 minutes or in steam at 130° to 150°C . for 30 minutes; but heating in air at 350°C . for 10 minutes converted them completely to a transparent yellowish oxidation product (figure 15), the diffraction data for which are given in table 4. Comparison with the pattern data from the PbSe layer oxidized by a leak in a cell during a vacuum bake (see § 3) seems to show some similarities in spacings though differences in ring intensities.

§ 6. SUMMARY AND DISCUSSION OF RESULTS

A. Electron-diffraction results

The following results were obtained by electron diffraction:

1. All the lead sulphide and lead selenide deposits (~ 500 – $10\,000\text{\AA}$. thick) which were examined by electron diffraction were found to be crystalline with no noticeable signs of any amorphous material; diffraction methods would only detect proportions of the order of 1% or more of the material.
2. All the deposits had the face-centred-cubic structure of sodium chloride type, previously found for PbS and PbSe by x-ray diffraction (*Strukturbericht, Z. Kristallogr.*, **1**, 1928).
3. The mean crystal size and the extent and nature of the orientation present in these polycrystalline deposits varied widely from one specimen to another.
4. All the PbS deposits showed an absence of appreciable variation of the lattice dimensions within the crystals of each deposit, and all the deposits examined had the same lattice dimensions within the limits of accuracy of the measurement (to approximately 0.1%), whether the deposits had been prepared by (a) chemical deposition from a lead acetate + thiourea + sodium hydroxide reaction on to pyrex substrates, (b) as a floating mirror-like layer by passing H_2S gas over concentrated slightly acidified lead acetate or lead nitrate solution, the film being washed by floating on an H_2S -water solution and dried in vacuum at room temperature, (c) sublimation of well-washed and dried precipitated PbS, in an evacuated pyrex cell at about 10^{-6} mm. Hg pressure, with or without further short bakes in vacuum.

Table 4.

(a) PbSe ($a=6 \cdot 117$ kx.)*			(b) PbSe heated in air 1 hour at 350° C. (figure 15)			(c) PbSe cell which developed a leak during a vacuum bake (figure 16)		
d (kx.)	Intensity	hkl	d (kx.)*	Intensity		d (kx.)†	Intensity	
3.532	M	111	6.16	MF	—	—	—	
			5.34	F	4.67	F	—	
			4.45	F(D)	4.33	F	—	
			3.92	MF	4.06	F	—	
			3.68	MF	3.69	MF	—	
	M		3.515	M	3.413	F	—	
			3.262	S(B)	3.253	F	—	
			—	—	3.068	MF	—	
			—	—	2.988	VF	—	
			—	—	2.838	MF	—	
3.058	M	200	2.970	MS(B)	2.711	S	—	
			2.845	MF	—	—	—	
			2.763	MS	—	—	—	
			2.578	MF	—	—	—	
			2.506	F	2.468	F	—	
	S		2.404	F	—	—	—	
			2.291	MF	2.309	MS	—	
			2.131‡	M	2.191	M	—	
			2.063	M	2.110	MF	—	
			1.992	MF	2.009	F	—	
2.163	S	220	1.946	MF	1.924	F	—	
			1.906	F	—	—	—	
			1.837	MF	1.841	F	—	
			1.764	MF	1.764	MS	—	
			1.702	MF	1.706	F	—	
	MF	311	1.678	MF	1.667	F	—	
			1.634	M	1.627	F	—	
			1.588	F	1.570	M	—	
			1.529	MF	1.540	MF	—	
			—	—	(1.520)	VF	—	
1.844	MF	331	1.473	M	1.465	F	—	
			1.424	F	1.425	F	—	
			1.327	VF	1.352	MS	—	
			1.304	MF	1.296	MS	—	
			1.287	MF	1.269	VF	—	
1.368	S	420	1.254	F	1.238	M	—	
			—	—	1.172	M	—	
1.248	S	422	—	—	—	—	—	
			—	—	1.149	VF	—	
1.177	F	{ 333 511 }	—	—	1.127	VF	—	
			—	—	1.097	VF	—	
			—	—	1.076	M	—	
			—	—	1.023	M	—	

* Relative to graphite $d_{110}=1 \cdot 228$ kx.

† Not relative to graphite; absolute values as a whole may be a few % in error.

‡ May be entirely due to the graphite 100 diffraction ring.

at between 200° and 400° C., (d) sublimation in oxygen at 0.1 to 0.3 mm. Hg pressure at 500° to 580° C.

A similar constancy (to $\sim 0.1\%$) was also found for PbSe deposits prepared (a) as a floating mirror-like layer by passing H_2Se gas (from either FeSe + dilute HCl, or Al_2Se_3 + boiled distilled water) over concentrated lead acetate solution acidified with acetic acid, (b) by method (a) followed by heating in air at 130° to 150° C. for 30 minutes, (c) by method (a) followed by heating in steam at 150° C. for 30 minutes, (d) by sublimation on to pyrex in a cell evacuated to 10^{-6} mm. Hg, with or without further short bakes (of the order of 10–30 minutes) in vacuum at 200° to 400° C.

The mean lattice constants found for PbS and PbSe were $a = 5.917 \pm 0.005$ kx., and 6.117 ± 0.005 kx. respectively*, relative to $a = 2.456_3$ kx. for graphite (Trzebiatowski 1937, Nelson and Riley 1945, Finch and Fordham 1936, Finch and Wilman 1936, cf. also Wilman 1940), the 110 graphite diffraction ring with $d = 1.228$ kx. being used as the comparison standard.

Previous x-ray measurements, mainly for the more or less impure minerals galena (PbS) and clausthalite (PbSe) have given the following lattice dimensions: for PbS, $a = 5.96_{6 \pm 4}$ Å. (Lehmann 1924), 5.91 Å. (Kolderup 1924–5), for very pure galena from Pribram Bohemia, 5.93 Å. (Ramsdell 1925), 5.95 Å. (Goldschmidt 1927–28), 5.96 Å. (Bravo 1926), 5.91 ± 0.03 Å. (Vlasak and Trousil 1934) 5.935 Å. (von Zeipfel 1935 a, corrected for more accurate value of λ of Al-K α x-rays by S. von Friesen 1935), 5.92334 kx. (von Zeipfel 1935 b), 5.94 Å. (Hanawalt, Rinn and Frevel 1938), 5.92 Å. and 5.93 Å. for galena containing 6% Bi (Goldschmidt 1927–28), for PbSe, $a = 6.14$ Å. (Ramsdell 1925), 6.162 Å. (von Olshausen 1925); and $6.13_{5 \pm 5}$ Å. from Pb>Se melted together in N₂ (Goldschmidt 1927–28).

The constancy of the lattice axial dimension to within 0.1% for PbS and PbSe in the various degrees of oxidation can be taken as showing that the proportion of excess Pb atoms or S defect ("holes"), or of S or Se respectively replaced by O ions in the PbS or PbSe lattice is very small, and probably less than about 1%, even in the strongly oxidized deposits in which up to 10 to 20% of PbO·PbSO₄ has segregated out. For example, if the ionic radii of Pb⁺⁺, S⁻⁻ and O⁻⁻ are 1.32, 1.74 and 1.32 Å. respectively, then replacement of 1% of the S⁻⁻ by O⁻⁻ would be expected to result in a reduction in the lattice dimensions of the PbS by approximately 0.08%. However, presence of excess Pb or of "holes" due to missing S⁻⁻ ions might tend to increase the lattice dimension and counterbalance a reduction due to presence of O⁻⁻ ions. Since the outer diffraction rings are not noticeably less sharp than the inner rings, however, it seems that lattice dimension variations larger than 0.1%, do not occur throughout the PbS crystals of 500 to 1000 Å. diameter, or occur only locally to a very small extent.

5. The fact that well-defined diffraction rings were obtained from the photo-sensitive deposits by the "reflection" method, shows that these deposits were relatively rough even when they appeared to be highly reflecting and optically flat, the height of the "peaks and valleys" being at least 150 Å., and mostly 500 Å. or more in the vacuum-sublimed deposits. Correspondingly the electron-diffraction patterns show the structure of the deposit to this depth below the outer parts of the surface.

6. While the electron-diffraction patterns from the chemically-prepared, and also the vacuum-sublimed, PbS and PbSe deposits showed no trace of any other material present, those from PbS sublimed or baked in oxygen at ~ 0.1 mm.Hg pressure (the SO₂ formed being trapped by liquid air cooling) showed besides the strong PbS rings or arcs a much fainter pattern due to an oxidation product, which was estimated to be present in the surface layers to the extent of about 10–20%. When the oxidation was slight this pattern was represented by only one or two very faint diffuse rings, but in the four typical cells of this type examined, two of photo-conductive and two of photovoltaic type, it consisted mainly of clearly defined rings

* This can be converted to Ångströms by multiplying by 1.00202, the factor recently agreed on by the X-ray Analysis Group of the Institute of Physics and the American Society for X-ray and Electron Diffraction.

or sharp arcs, from the positions of which the oxidation product was identified as lead oxysulphate (lanarkite), $\text{PbO} \cdot \text{PbSO}_4$. Translucent PbS layers heated in atmospheric air at 350°C . for 10 minutes were completely converted to a pale yellow transparent material also identified as $\text{PbO} \cdot \text{PbSO}_4$; and heating at 550°C . in air, followed by cooling to room temperature, caused only very slight changes in the lattice dimensions but distinct changes in the relative intensities of the diffraction rings, probably due to a different crystal shape having been developed, causing greater absorption for some diffracted beams than for others.

Lead selenide deposits, when similarly heated or sublimed in oxygen, were also converted into a greyish-yellow oxidation product; this was not identified owing to lack of diffraction data for the lead oxyseleum compounds. No improvement in photosensitivity was obtained from these oxidizing treatments of PbSe.

B. Photoconductivity results

With regard to the photosensitivity of the PbS and PbSe cells, only the following results will be stated here for consideration with the diffraction results, and a more detailed account of PbS cells will be published shortly by Starkiewicz *et al.*

1. The photoconductivity properties of the deposits varied widely according to the conditions of formation of the deposit (e.g. in vacuum-prepared cells the temperature, rate of condensation, thickness of deposit, pressure of residual gas in the apparatus, nature of substrate etc.), and the further heat treatments in vacuum or in oxygen. No definite relationship was observed between the magnitude or the spectral distribution of the photosensitivity and the crystal size or kind and degree of orientation of the PbS or PbSe as shown by the diffraction electron patterns. Since no full and systematic investigation has yet been made, only brief general indications will be stated here about the photoconductive and other properties of the deposits. It was noticeable, however, that the sensitization of PbS cells by subliming the material (or baking it) in oxygen led to a large increase in the crystal size as shown by the incomplete formation (spottiness) of the sharp diffraction rings due to the small number of crystals in the path of the electron beam. It is well known that crystal growth is much faster in the presence of oxygen than in vacuum, though it is not clear whether such accelerated growth is accompanied by appreciable diffusion of oxygen into the crystal lattice in solid solution. In the present case the sensitization in oxygen was found (Lee and Parker 1946) to be associated with development of a peak in the spectral sensitivity curve at a wavelength near 2.7μ in addition to that at 1.1μ , evidently indicating strong adsorption or absorption of oxygen. The relation of the rise in infrared sensitivity to the observed increase in crystal size and the formation of relatively large crystals of $\text{PbO} \cdot \text{PbSO}_4$ is not yet clear, but the state of over-oxidation evidently corresponds to segregation of a large proportion of $\text{PbO} \cdot \text{PbSO}_4$ among the PbS crystals.

The observed absence of beneficial effects of oxygen treatments on the photosensitivity of PbSe deposits is probably due to the absence of appreciable "reducing" action, i.e. liberation of lead, and to too rapid segregation of the oxidation product. Segregation is accelerated in this case because selenium is not readily removable as SeO_2 , which is a solid at temperatures up to several hundred degrees Centigrade, whereas SO_2 is gaseous and is removed from the layer.

2. As a brief general indication of the electrical properties of the deposits it may be stated here that the resistances of the PbS and PbSe deposits between graphite or platinum electrodes 1 cm. long and 1 mm. apart were in the range 10 to 1000 k Ω and were approximately doubled when the cells were cooled in liquid air. The PbS cells, when illuminated by a broad, roughly collimated beam of unmodulated white light from a 36-watt lamp, showed a decrease of resistance of up to about half the dark resistance and a ratio of signal to noise of unity was observed with the cells exposed to 800 cycles/sec. modulated radiation from a 3 mm. aperture in front of a black body at 200° c., at a distance of the order of 70 cm. Further details of the sensitivity are given by Lee and Parker (1946). The PbSe cells showed only negligible photoconductivity (<2% change in resistance) with continuous illumination, and with the modulated radiation had mainly a sensitivity of the order of 1–2% of that of good PbS cells.

3. In spite of the observed degree of constancy of the lattice dimensions calculated from the electron-diffraction patterns (§ 4) obtained from cells whose properties differed widely, the electrical properties of both the PbS and PbSe deposits, measured at room temperature, varied within a wide range when previously well-outgassed cells were baked (at between 200° and 500° c.) while evacuated to about 10⁻⁶ mm. Hg pressure. In the case of PbSe, for example, the translucent reddish-orange deposits made by vacuum sublimation in presence of excess selenium, had low resistance ($\sim 10\,000\ \Omega$), very small "noise" and also very low signal and signal/noise ratios, when using a small red-hot tungsten filament to give a light beam which was interrupted 800 times/sec. by a rotating slotted disc, the resulting alternating current being amplified. Successive periods of 10 minutes heating in vacuum at about 350° c. (Se begins to vaporize appreciably in vacuum at about 200° c.) then caused progressive increase of the resistance, noise, signal and signal/noise ratio, as in figure 17, until a maximum was reached for all these properties nearly simultaneously. By driving in excess selenium and then again heating *in vacuo* in successive stages, these properties again passed through a maximum and returned to a nearly constant low level again (figure 17). (Note that in figure 17 the periods of baking stated were at the temperatures indicated by the apexes of the triangles in the lower diagram, additional to the 4–5 minute heating-up.) These observations, together with the visible loss of selenium from the cell to form a condensed deposit in the cooler parts of the pumping stem, appear to indicate that the vacuum baking resulted in at least the upper layers of the PbSe deposit losing selenium and passing from a composition having excess Se, through the stoichiometric composition PbSe with no Pb or Se impurity centres which corresponds to the maximum of resistance etc., to one with a defect of Se (i.e. excess Pb). In view of these very wide variations the constancy of the lattice dimensions is remarkable. Wide variations in electrical properties of PbS layers have been described by Hinterburger (1942) and of PbSe layers by Eckart and Raithel (1941). The progressive decrease of the successive maxima in figure 17 may possibly be due to gradual oxidation resulting from the minute trace of residual air in the vacuum system or oxygen evolved from the selenium side tube, or it may be due to some other cause such as loss of selenium from the lower parts of the layer so as to make it tend towards stoichiometric composition (and later recede from it again due to Se defect?), or perhaps a gradual aggregation to form larger more isolated PbSe crystals owing to the energetic diffusion of the selenium in the layer. Figure 18, plotted from these same measurements shows a progressive

increase in resistance of the deposit for a given signal/noise ratio. The initial line 5-6-7-8 passes near the origin, corresponding to a relation of form $(S/N) = Ae^{BR}$. Similar conditions existed for vacuum heat-treatment of PbS cells. Heat treatment of PbS or PbSe in oxygen resulted in more complex variations which will not be described here.

C. General summary

To sum up all the above results, the preliminary electron-diffraction observations have provided a very much more definite knowledge of the nature of the photosensitive PbS and PbSe layers than has hitherto been available. It has identified the composition and defined the form of the crystalline oxidation

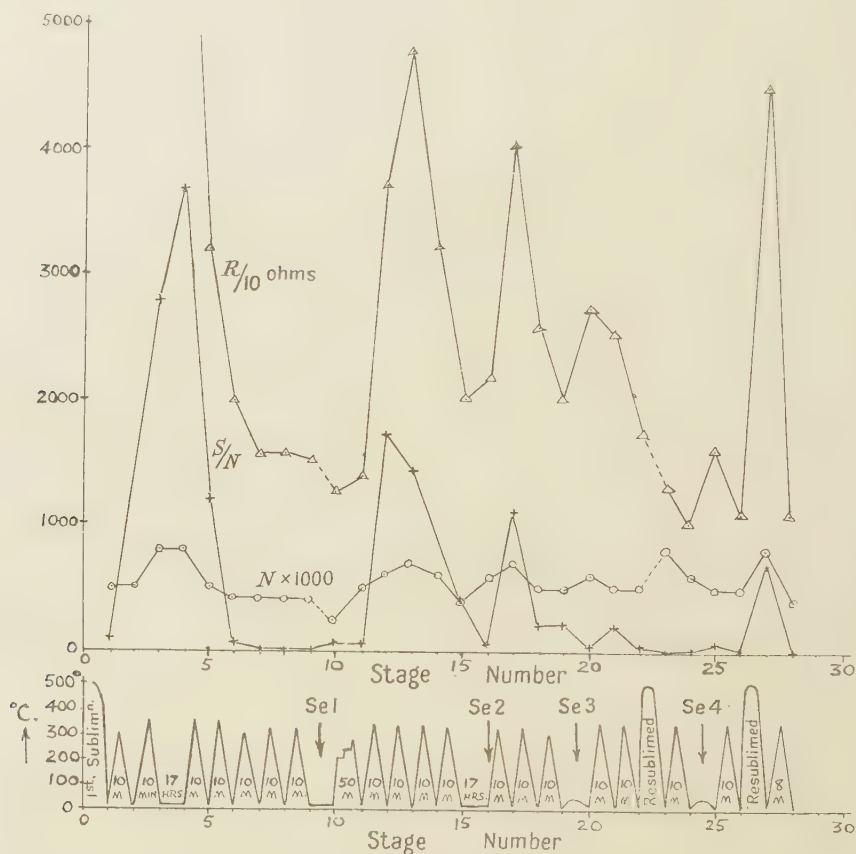
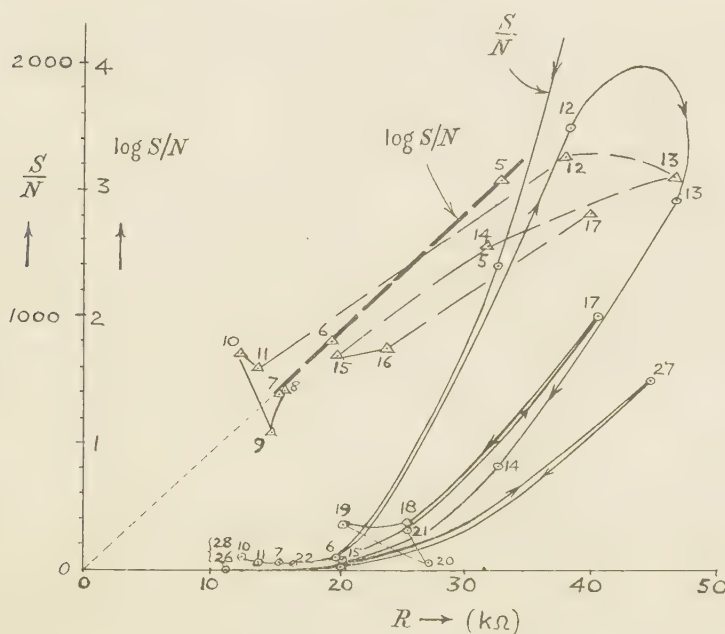


Figure 17.

product formed during sensitization of PbS layers in oxygen, and in conjunction with photoconductivity measurements it has indicated that the crystal orientation has little effect on the photosensitivity compared with other factors such as, especially, very slight deviations from stoichiometric composition, the size of the crystals in the layer, and probably the distribution of the $\text{PbO} \cdot \text{PbSO}_4$ among the PbS crystals. The axial length of the PbS crystals was $a = 5.917 \text{ kx}$, and that of PbSe was 6.117 kx , and no deviation greater than 0.1% occurred whether the PbS contained excess S or excess Pb (as indicated by the photoconductive properties), or whether it was unoxidized or relatively heavily oxidized.



• Figure 18.

ACKNOWLEDGMENTS

The author wishes to thank the Admiralty for permission to publish these results, Captain J. Starkiewicz and Dr. F. Kicinski for making available typical PbS cells for the electron-diffraction examination, and Messrs. R. Jennings and B. W. Soole for their assistance in experiments on the photosensitive properties of PbSe cells.

REFERENCES

- VAN ARKEL, 1925, *Physica*, **5**, 162.
 BARONI, A., 1938, *Gazzetta*, **68**, 387.
 BASCHE, W., and MARK, H., 1924, *Z. Kristallogr.*, **64**, 1.
 BÖHM, J., and GANTNER, F., 1928, *Z. Kristallogr.*, **69**, 17.
 BRANDENBERGER, E., 1945, *Röntgenographisch-analytische Chemie*, p. 130 (Verlag Birkhäuser, Basel).
 BRAVO, F. M., 1926, *Anales Soc. Española Fis. Quim.*, **24**, 611.
 BYSTRÖM, A., 1943, *Arkiv Kemi. Min. Geol.*, **17** B, No. 8.
 BYSTRÖM, A., 1944, *Arkiv Kemi. Min. Geol.*, **18** B, No. 10.
 BYSTRÖM, A., 1945, *Arkiv Kemi. Min. Geol.*, **20** A, No. 11.
 BYSTRÖM, A., and WESTGREN, A., 1943, *Arkiv Kemi. Min. Geol.*, **16**B, No. 14; *Chem. Zentr.*, **2**, 1076.
 CLARK, G. L., 1940, *Applied X-Rays*, p. 31 (McGraw-Hill, New York and London, 3rd ed.).
 CLARK, G. L., MRGUDICH, J. N., and SCHIELTZ, N. C., 1936, *Z. anorg. Chem.*, **229**, 401.
 CLARK, G. L., and ROWAN, R., 1941, *J. Amer. Chem. Soc.*, **63**, 1305 and 1932.
 CLARK, G. L., and TYLER, W. P., 1939, *J. Amer. Chem. Soc.*, **61**, 58.
 CLARK, G. L., SCHIELTZ, N. C., and QUIRKE, T. T., 1937, *J. Amer. Chem. Soc.*, **59**, 2305.
 DARBYSHIRE, J. A., 1932, *J. Chem. Soc.*, 211.
 DAVIDSON, H. R., 1941, *Amer. Mineral.*, **26**, 18.
 DICKINSON, R. G., and FRIAUF, J. B., 1924, *J. Amer. Chem. Soc.*, **46**, 2457.
 ECKART, F., and RAITHEL, K., 1941, *Naturwissenschaften*, **29**, 572.
 FINCH, G. I., and FORDHAM, S., 1936, *Proc. Phys. Soc.*, **48**, 85.
 FINCH, G. I., and WILMAN, H., 1937, *Ergebn. exakt. Naturw.*, **16**, 353.
 FORDHAM, S., 1940, *Nature, Lond.*, **146**, 807.

- VON FRIESEN, S., 1935, *Uppsala Universitets Arsskrift*, p. 14.
- GOLDSCHMIDT, V. M., 1927-8, *Geochem. Verteilungsgesetze der Elemente*, VII and VIII, Skr. Norske Videnskaps-Akad., Oslo, 1. Math-nat. Kl., 1926, No. 2, and 1927, No. 8 (see *Strukturber. Z. Kristallogr.*, 1928, **1**, 131).
- GROSS, S. T., 1941, *J. Amer. Chem. Soc.*, **63**, 1168.
- GROSS, S. T., 1943, *J. Amer. Chem. Soc.*, **65**, 1107.
- HALLA, F., and PAWLEK, F., 1927, *Z. phys. Chem.*, **128**, 49.
- HANAWALT, J. D., RINN, H. W., and FREVEL, L. K., 1938, *Ind. Eng. Chem., Anal. Ed.*, **10**, 457.
- HINTERBERGER, H., 1942, *Z. Phys.*, **119**, 1.
- JAMES, R. W., and WOOD, W. A., 1925, *Proc. Roy. Soc., A*, **109**, 598.
- KOLDERUP, N. H., 1924-5, *Bergens Museum Aarbk. Nat. R.*, No. 2.
- LEE, E., and PARKER, R. C., 1946, *Nature, Lond.*, **158**, 518.
- LEHMANN, W. M., 1924, *Z. Kristallogr.*, **60**, 379.
- MOORE, W., and PAULING, L., 1941, *J. Amer. Chem. Soc.*, **63**, 1392.
- NELSON, J. B., and RILEY, D. P., 1945, *Proc. Phys. Soc.*, **48**, 85.
- VON OLSHAUSEN, S., 1925, *Z. Kristallogr.*, **61**, 463.
- PETERSEN, M., 1941, *J. Amer. Chem. Soc.*, **63**, 2617.
- RAMSDELL, L. S., 1925, *Amer. Mineral.*, **10**, 281.
- RENCKER, E., and BASSIÈRE, M., 1936, *C.R. Acad. Sci., Paris*, **202**, 765.
- RICHMOND, W. E., and WOLFE, C. W., 1938, *Amer. Mineral.*, **23**, 799.
- STARKIEWICZ, J., SOSNOWSKI, L., and SIMPSON, O., 1946, *Nature, Lond.*, **158**, 28.
- STRAUMANIS, M., 1942, *Z. phys. Chem.*, **52**, 127.
- TRZEBIATOWSKI, W., 1937, *Roczn. Chem.*, **17**, 73.
- VLASAK, F., and TROUSIL, Z., 1934, *Věda přírodní.*, **15**, 164 (see *Strukturber.*, **3**, 258).
- WILMAN, H., 1940, *Proc. Phys. Soc.*, **52**, 323.
- VON ZEIPFEL, E., 1935, *Ark. Mat. Astr. Fys.*, **25 A**, No. 8 ; *Chem. Zentr.*, **2**, 1326.

Solid Diagrams Illustrating Resonance Phenomena

By W. A. PROWSE
University of Durham

MS. received 17 April 1947, in amended form 15 July 1947

ABSTRACT. Three dimensional vector loci are used to express the properties of resonant circuits and of the tuned transformer. An indication is given of the application of the method to other problems, including a simple low frequency selector circuit.

§ 1. INTRODUCTION

THE study of the steady state behaviour of systems possessing stiffness, inertia and resistance forms a large part of any treatment of alternating current phenomena, of acoustics and of vibrating systems in general. It is not proposed to add further detail to this type of study, but rather to discuss a method of representing the behaviour of such systems which has been found attractive to students, which presents the solutions in a form which appeals to the imagination, and which is thought to afford a convenient visual summary of the phenomena concerned.

§ 2. SIMPLE RESONANT SYSTEMS

Consider a system whose behaviour is represented by the harmonic equation (figure 1)

$$L \frac{d^2q}{dt^2} + R \frac{dq}{dt} + \frac{1}{C} q = V, \quad \dots \dots (1)$$

where q is the charge on the condenser and V the applied electromotive force.

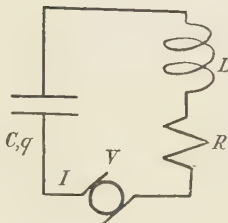


Figure 1.

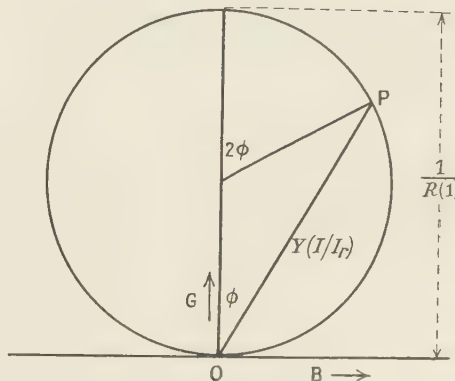


Figure 2. Vector locus of admittance (OP) of circuit of figure 1. Symbols in brackets denote alternative quantities. For the parallel circuit OP represents V/V_r .

The steady state solution may be written in terms of the impedance vector \mathbf{Z} or of the admittance vector \mathbf{Y} . Let these be divided into real and imaginary components; so that

$$\mathbf{Z} = R + jX$$

and

$$\left. \begin{aligned} \mathbf{Y} &= G + jB \\ &= (R - jX)/(R^2 + X^2) \end{aligned} \right\}. \quad \dots\dots (2)$$

For variations of X , the locus of Z is a straight line in the complex plane and that of Y is a circle of radius $1/2R$ (Hague 1945) (figure 2).

The latter result depends only on the relation (2) and not on the means whereby the variation of X is effected. If now a three-dimensional diagram be plotted, with the variable parameter responsible for changes in X along an axis at right angles to the G and B axes, a model of the type shown in figure 3 is obtained. It will be noted that the form of the curve is essentially a single circular turn on a straight line.

In this model the third variable is ω/ω_r , where ω is the angular frequency of V and ω_r the resonant value, $1/\sqrt(LC)$. By suitable illumination the three projections are obtained, showing respectively the variation of B and of G with frequency and the circle diagram, the latter, of course, being the vector locus of the admittance.

When used to illustrate current resonance in a series circuit, it is noted that the current I is related to the current I_r , at resonance, by

$$I/I_r = (1 - jX/R)/(1 + X^2/R^2),$$

so that the circle may be made of unit diameter. Here the chord from the point O (figure 2) to a given point on the circumference represents the vector value of the current, in terms of the current at resonance, for the frequency chosen. It is immediately apparent from the model that (i) the variations of conductance and of susceptance through resonance are simply two aspects of one process, (ii) the total variation of the susceptance is equal to the total variation of the conductance,

(iii) the maxima and minima of the susceptance curve occur on the steep parts of the conductance curve, (iv) the phase change in the neighbourhood of resonance is very rapid, (v) the phase at resonance is zero and (vi) the current is a small quantity in quadrature with the voltage at points well removed from the resonance peak.

§ 3. THE TUNED TRANSFORMER

Let the secondary circuit be of resistance R_2 and reactance X_2 and let it be coupled to the primary circuit by mutual inductance M . The increments of primary resistance ΔR and reactance ΔX , caused by the presence of the secondary are given by

$$\Delta R = \omega^2 M^2 \frac{R_2}{R_2^2 + X_2^2} \quad \dots \dots (3)$$

$$-\Delta X = \omega^2 M^2 \frac{X_2}{R_2^2 + X_2^2} \quad \dots \dots (4)$$

showing an exact correspondence in form with the real and imaginary components of Y (equation (2)).

The increase in impedance of the primary circuit can thus be represented by the same kind of solid diagram; in fact, the projections of the solid curve are perhaps most familiar as representations of the transferred impedance. Here the radius of the circle is $\omega^2 M^2 / 2R_2$, so that the representation is exact for tuning the circuit by varying C_2 or L_2 , but if the applied frequency causes the variation, the diagram is only accurate for sharply tuned circuits.

§ 4. MORE GENERAL METHODS

For purposes of calculation and for more general application (including parallel resonance when the tuning is reasonably sharp) the solution may be expressed in terms of Q and of the ratio of the impressed frequency ω to the resonant frequency ω_r (where ω_r is defined as the frequency for zero phase) (Lee and French 1943).

For the series circuit, since $Q = \omega_r L / R$ and $\omega_r = 1/\sqrt{(LC)}$, we have $R = 1/(Q\omega_r C)$. Substituting these values in equation (1) leads to

$$CV/q = (1 - \omega^2/\omega_r^2) + (j/Q)(\omega/\omega_r),$$

where V and q represent the vector values of the applied voltage and of the charge on the condenser respectively. q_r the charge at the resonant frequency, is given by

$$q_r/q = \omega/\omega_r - jQ(1 - \omega^2/\omega_r^2)$$

and $I/I_r = Y/Y_r = \frac{1}{1 - jQ(\omega_r/\omega - \omega/\omega_r)} \quad \dots \dots (5)$

In the complex plane (5) represents a unit circle in which $\tan \phi = Q(\omega_r/\omega - \omega/\omega_r)$ and, since the angle at the centre is 2ϕ the solid curve may be plotted by means of a piece of graph paper wrapped round a cylinder. This procedure, followed by shaping a piece of wire to fit the curve, was used in making the solid models illustrated.

§ 5. OTHER APPLICATIONS

The method has been found valuable for illustrating the properties of tuned transmission lines and of dielectrics containing charged particles, elastically

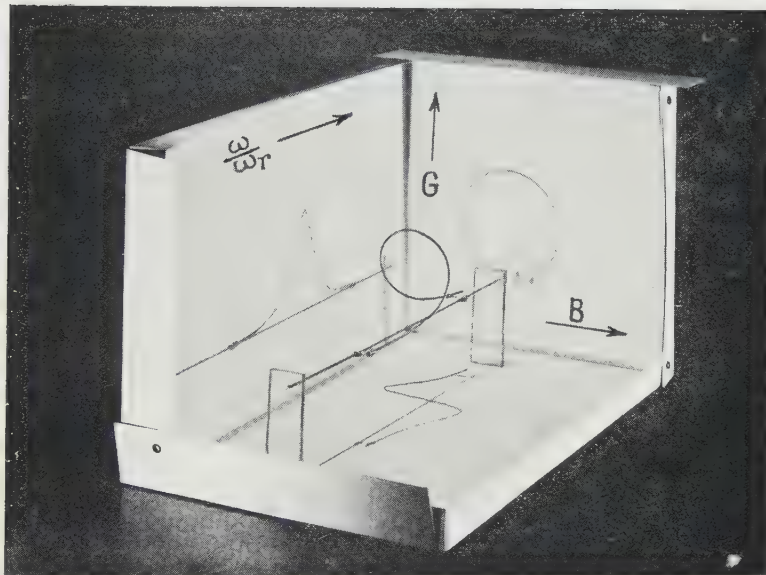


Figure 3.

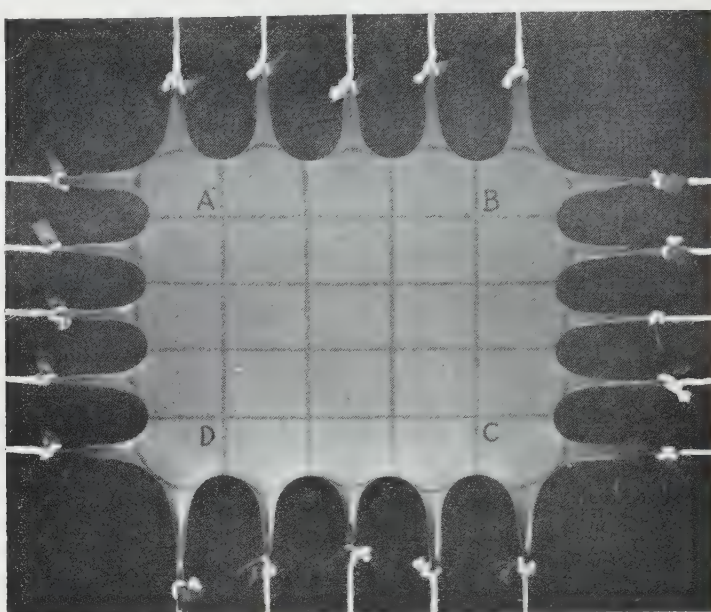


Figure 1. Rubber sheet stretched by factors of 2.5 and 2.0 in two perpendicular directions.

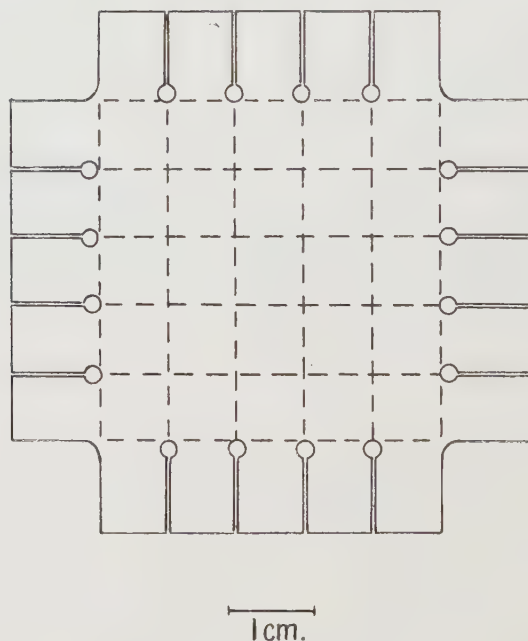


Figure 1 (a). Form of unstrained sample.

bound or aperiodic. In addition, a simple low frequency selector circuit has been developed. This, in effect, is an interstage coupling consisting of two transformers, one tuned slightly above and the other slightly below the required frequency, with the output voltages in opposition. It will be realized that, whereas the output of each transformer separately is represented by a line drawn from the origin to a point on the circumference of the circle (figures 2 and 3), the combined output is the chord joining the ends of two such lines. Thus the maximum output can be the same as that of either component separately, but it drops much more rapidly towards zero on either side of the peak. Satisfactory discrimination against the second harmonic is obtainable at 9 cycles per second.

ACKNOWLEDGMENT

I wish to take this opportunity of thanking the Research Committee of the Durham Colleges for their generous support, particularly in providing the oscillator used.

REFERENCES

- HAGUE, 1945, *A.C. Bridge Methods*, Chap. II (5th Ed., Pitman).
 LEE, A., and FRENCH, W., 1943, *University Radio Conference Proceedings*, p. 67.

Stresses and Birefringence in Rubber subjected to General Homogeneous Strain

BY L. R. G. TRELOAR
 British Rubber Producers' Research Association

MS. received 23 January 1947

ABSTRACT. A method is described by which a sheet of rubber may be subjected to the most general type of homogeneous strain, with simultaneous measurement of the principal stresses and the birefringence. As predicted by the molecular network theory, the birefringence is found to be proportional (*a*) to the difference of the squares of the principal extension ratios, and (*b*) to the difference of the principal stresses in the sheet.

An examination of the stresses shows that these cannot be accurately represented by the equations derived from the network theory. A closer approximation is given by a more general theory of Mooney, the simplest form of which gives a satisfactory account of the behaviour of a swollen rubber. For a dry rubber, on the other hand, the Mooney formula, though better than the network theory, does not adequately represent the experimental data.

§ 1. INTRODUCTION

IN a previous paper (Treloar 1947 a) the author has dealt with the theory of the optical properties of strained rubber on the basis of a model in which the rubber was envisaged as a network of long-chain molecules of randomly-jointed links. These links were assumed to be optically anisotropic, having two different optical polarizabilities, in directions parallel and perpendicular to their length.

The theory was applied to the case of the most general homogeneous deformation of rubber, and it was shown that, for each of the three principal directions of strain, there is an associated optical polarizability, by which the refractive index for light having the corresponding direction of electric vector is determined. If λ_1 , λ_2 and λ_3 are the principal extension ratios, and n_1 , n_2 and n_3 the corresponding refractive indices, the double refraction for light propagated along the direction λ_3 may be represented by the equation

$$n_1 - n_2 = \frac{(\bar{n}^2 + 2)^2}{\bar{n}} \cdot \frac{2\pi}{45} N(\alpha_1 - \alpha_2) v_r^{1/3} (\lambda_1^2 - \lambda_2^2), \quad \dots \dots (1)$$

in which \bar{n} is the mean refractive index, N the number of molecular chains per c.c. and $\alpha_1 - \alpha_2$ the difference of polarizabilities for the link of the chain. The quantity v_r refers to the volume fraction of rubber in the case when the rubber is swollen in an optically inert solvent. Comparison of this result with the corresponding equation for the difference of principal stresses (Treloar 1947 a), i.e.

$$t_1 - t_2 = NkT v_r^{1/3} (\lambda_1^2 - \lambda_2^2), \quad \dots \dots (2)$$

where t_1 , t_2 , t_3 are the principal stresses, k is Boltzmann's constant and T the absolute temperature, leads to a linear relation between the birefringence and the stress-difference, which has already been examined experimentally for the case of a simple elongation in an earlier paper (Treloar 1947 b).

§ 2. EXPERIMENTAL METHOD

In the present paper a study of the stresses and birefringence in the most general type of homogeneous strain is reported. For this purpose a sheet of vulcanized rubber, compounded according to the formula given in the paper referred to (Treloar 1947 b), was stretched in two directions at right angles in such a way that the strain was homogeneous, whilst the two principal extension ratios λ_1 and λ_2 in the plane of the sheet could be varied independently by the application of two sets of forces. The arrangement used permitted the simultaneous measurement of the principal stresses and the double refraction corresponding to any state of strain.

It is not easy to devise a suitable method of applying two unequal strains to rubber in two perpendicular directions. The method here adopted, though not ideal, particularly in that the maximum attainable strain was limited, seemed to provide the simplest means of achieving the desired result. It makes use of the principle of the guard plate to eliminate the effect of the non-uniformity of the strain in the vicinity of the edges of the sheet. The shape of the test piece is shown in figure 1. It was in the form of a square, with five projecting lugs on each side, to which strings were tied for the application of the loads. The surface of the sheet was marked out with a series of lines forming a square lattice, so that the state of strain at all points could be observed. With the sheet placed horizontally, the three middle lugs on one side were loaded by means of three equal weights attached to strings passing over pulleys, whilst the strings attached to the two outermost lugs were secured to a rectangular frame, mounted horizontally. The five strings on the opposite side were connected to the opposite side of the frame. Similarly, the three middle lugs on an adjacent side carried three equal weights, whilst the two

outer lugs, as well as the five on the side opposite to them, were connected to the frame. The 14 strings connected to the frame were provided with tension adjusters, and these strings, as well as the pulleys, could be moved sideways independently, so that each set of strings could be kept parallel and the two sets maintained perpendicular to each other. The appearance of the stretched sheet when the tension on the outer lugs was suitably adjusted is shown in figure 1; in all cases the strain within the rectangle ABCD was sensibly uniform. Under these conditions it was assumed that the stresses acting on the sides of the rectangle ABCD were defined by the loads applied to the three central lugs, and that the non-uniform edge region, though requiring the use of a slightly different tension on the outer lugs *, would be without effect on the stress in this inner, uniformly-strained region.

For the optical measurement a beam of light from a polarizer set at 45° to the directions of principal strain was passed normally through the sheet, the birefringence being measured by means of a Babinet compensator.

The measurements were made at room temperature, which varied between 17 and 22°C .

§ 3. EXPERIMENTAL RESULTS

The data obtained are given in tables 1 and 2. Table 1 refers to the dry rubber, and table 2 to the same rubber swollen in medicinal paraffin to $v_r = 0.525$. Readings were taken in the order given in the tables. Generally about 10 minutes elapsed between the application of a load and the taking of readings. The forces f_1 and f_2 are the loads in grams applied to each of the three middle lugs; the areas of cross-section of the rubber in the unstrained state (A_0), over which these forces act are given in the table. The figures for optical retardation are given in terms of the number of sodium wavelengths phase difference between the two rays, this being the quantity actually measured. To convert this to difference of refractive indices ($n_1 - n_2$) it is only necessary to divide by the thickness of the sheet and multiply by the wavelength. The extension ratio λ_3 , and the corresponding thickness in the strained state, were determined from the measured λ_1 and λ_2 , assuming no change of volume on straining.

In addition to the data represented in tables 1 and 2, figures were obtained for the case of simple elongation, i.e. with $f_2 = 0$, using a parallel strip of rubber cut from the same sheet. These additional data are included in the graphical presentation of the results.

The optical data are presented in figures 2 and 3, omitting points (near the origin) corresponding to the case when $f_1 = f_2$. In the first case (figure 2) the birefringence is plotted against the difference of the squares of the corresponding extension ratios, $\lambda_1^2 - \lambda_2^2$. While the expected linear relationship (equation (1)) is approximately borne out, there are for the dry rubber, slight departures which are probably greater than the errors of measurement. For the swollen rubber, on the other hand, the agreement with the theoretical form is very close. In the second case (figure 3) the birefringence is plotted against $t_1 - t_2$, the difference of the principal stresses. Again, the proportionality is more exact for the swollen than for the dry rubber.

* It was found experimentally that the difference of tension on the outer strings was in fact very slight.

Table 1. Dry rubber. Thickness = 0.082 cm. $A_0 = 0.0648 \text{ cm}^2$

f_1 (gm.)	f_2 (gm.)	λ_1	λ_2	Retardation (sodium wavelengths)
100	100	1.07 ₀	1.08 ₃	-0.02
100	200	0.97 ₈	1.29 ₇	-0.55
200	200	1.16 ₇	1.20 ₉	-0.07
300	200	1.46 ₀	1.09 ₁	+0.54
300	100	1.58 ₂	0.90 ₅	+1.06
300	300	1.35 ₀	1.37 ₀	-0.05
300	400	1.18 ₃	1.88	-0.80
200	400	0.93 ₃	2.04	-1.50
100	400	0.78 ₃	2.14	-2.00
400	400	1.60	1.72 ₅	-0.13
500	400	2.24	1.51 ₃	+0.64
500	300	2.42	1.09 ₆	+1.39
500	200	2.51	0.87 ₅	+2.05
500	100	2.64	0.72 ₅	+2.80
500	500	2.07	2.10	-0.05
600	500	2.68	1.87 ₅	+0.54
400	600	1.25 ₀	2.98	-1.55
300	600	0.98 ₀	3.06	-2.31
200	600	0.79 ₁	3.14	-3.05
100	600	0.67 ₉	3.21	-3.76
600	600	2.34	2.63	-0.18

Table 2. Rubber swollen to $v_r = 0.525$ in paraffin. Thickness
(swollen) = 0.099 cm. $A_0 = 0.0985 \text{ cm}^2$

f_1 (gm.)	f_2 (gm.)	λ_1	λ_2	Retardation (sodium wavelengths)
100	100	1.08 ₈	1.08 ₈	-0.02
100	200	0.99 ₆	1.30 ₅	-0.40
200	200	1.21 ₅	1.19 ₃	+0.01
300	200	1.55	1.06 ₈	+0.51
300	100	1.66	0.88 ₂	+0.93
300	300	1.41	1.36 ₄	+0.03
100	400	0.80	2.04	-1.46
200	400	0.95 ₆	1.95 ₃	-1.02
300	400	1.24	1.83	-0.51
400	400	1.65	1.65 ₄	0.00
400	500	1.50	2.12	-0.46
500	500	1.97	1.94	+0.02
500	300	2.31	1.10	+1.06
500	200	2.43	0.85 ₈	+1.62
500	100	2.48	0.73 ₆	+2.07

Figure 4 represents the difference of the two principal stresses, plotted against $\lambda_1^2 - \lambda_2^2$, for both samples. As with the birefringence, the swollen rubber appears

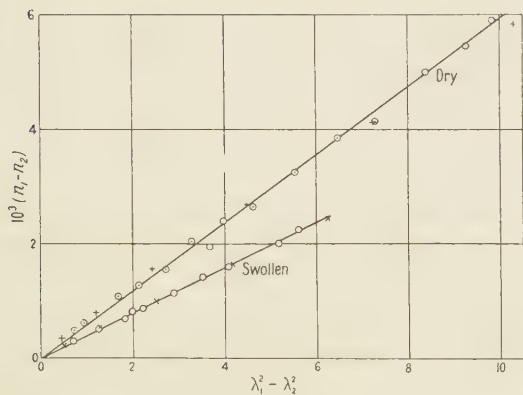


Figure 2. Birefringence plotted against difference of squares of principal extension ratios for dry and swollen rubber. The crosses refer to simple elongation.

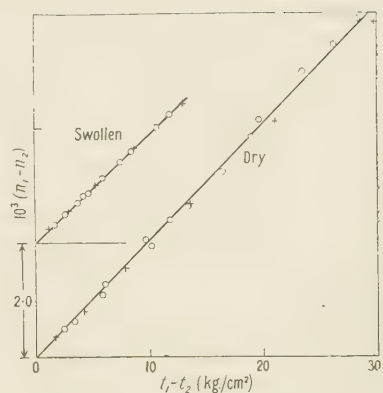


Figure 3. Birefringence plotted against difference of principal stresses for dry and swollen rubber. The crosses refer to simple elongation.

to agree with the theoretical form (2) within the experimental error, but the agreement in the case of the dry rubber is not exact.

§ 4. FURTHER EXAMINATION OF STRESSES

Whilst the evidence presented in figures 2, 3 and 4 suggests that the theoretical expectations regarding the dependence of the birefringence and of the principal stress difference on the two principal extensions in the plane of the sheet are approximately fulfilled, particularly in the case of the swollen rubber, an examination of each of the principal stresses separately reveals consistent deviations from the theoretical form, as will now be shown.

Since the stress t_3 normal to the sheet is zero, we should have, according to the theory previously outlined (Treloar 1947 a),

$$t_1 = G(\lambda_1^2 - \lambda_3^2), \quad \dots \dots (2a)$$

with a corresponding expression for t_2 . According to this equation, a plot of t_1 or t_2 , against $\lambda_1^2 - \lambda_3^2$ or $\lambda_2^2 - \lambda_3^2$ respectively, should yield a straight line. The actual results, shown in figures 5 and 6, present a more complex appearance for both the dry and swollen rubber.

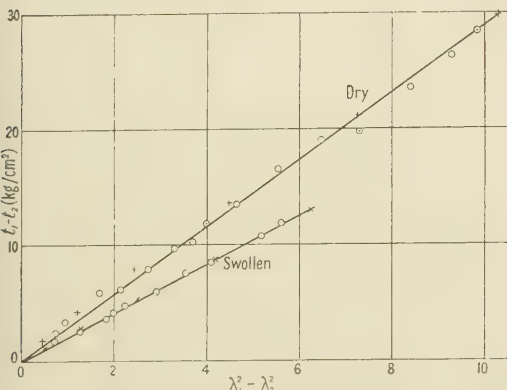


Figure 4. Difference of principal stresses plotted against difference of squares of principal extension ratios. The crosses refer to simple elongation.

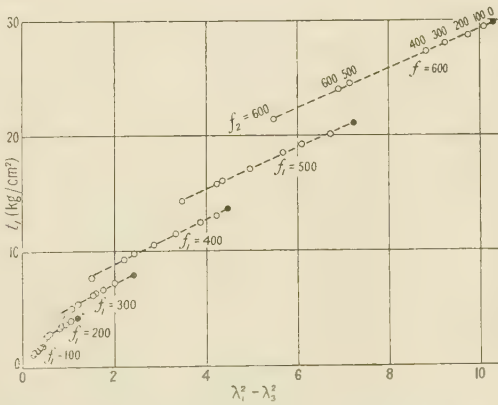


Figure 5. Dry rubber. Stress t_1 plotted against $\lambda_1^2 - \lambda_3^2$. The black circles refer to simple elongation. f_1 and f_2 are expressed in grams.

The method of plotting employed in these diagrams requires a little explanation. Firstly, it must be remembered that the stress (say t_1) is determined by the force (f_1) divided by the area of cross-section, which is itself a function of the strain, i.e. $t_1 = \lambda_1 f_1 / A_0$. Hence, while one of the forces is held constant, the stress corresponding to this force varies with changes in the second force, since such changes alter all the extension ratios. In order to simplify the presentation, the stress plotted is referred to as t_1 , and the corresponding force as f_1 . Thus two points appear on the diagram for each state of strain, one for each of the two principal stresses.

It is seen that the points fall on a set of lines, on any one of which f_1 is constant, while f_2 varies. This clearly means that t_1 is dependent on a more complicated function of the extension ratios λ_1, λ_2 and λ_3 than the one represented by equation (2).

This important departure from the theoretical form exhibited when the principal stresses are plotted separately is rather surprising in view of the fair agreement obtained when only their difference is considered. Before discussing its significance, it seems desirable to examine very carefully the nature of the evidence, in order to make sure that it is not due to some spurious effect introduced by the experimental technique. Three possible sources of trouble will be discussed, namely (a) relaxation, (b) anisotropy in the original sheet, and (c) non-uniform strain round the edges.

(a) Relaxation

It is true that the attainment of equilibrium values of the stresses in strained rubber is a matter of considerable difficulty, requiring the breaking-down of temporary intermolecular "cross-links" by the use of higher temperatures or other means. No attempt was made to obtain genuine equilibrium values in the present experiments, and it is therefore necessary to consider whether the discontinuous array of figures 5 and 6 might arise from this cause.

There are two reasons for rejecting this hypothesis. Firstly, although it was observed that the values of the strain parameters obtained under the application of a given pair of forces depended to some extent on the order of application of the forces and on the previous history of the sample, nevertheless, the stresses, when plotted as in figure 5, invariably fall precisely on the appropriate discontinuous arrays. Secondly, it is clear that swelling should favour the approach to equilibrium, but the discontinuities are no less marked for a rubber swollen with nearly 100% of solvent than for the dry rubber.

(b) Anisotropy in the original sheet

It is conceivable that the departures from the theoretical form might arise from a difference of properties in different directions in the original sheet of rubber, introduced by the rolling process prior to vulcanization. Such an effect would arise from non-equilibrium or secondary linkages rather than from primary linkages, since the form of the stress-strain relations derived from the molecular theory is in no way dependent on the detailed structure of the molecular network (James and Guth 1943). If such anisotropy were present, it would be expected to reveal itself in a non-uniform swelling in different directions; but no such non-uniformity in swelling was observed. Furthermore, a latex rubber sheet,

prepared by a quite different process not involving rolling or pressing, gave a precisely similar type of diagram to that of figure 5. It is therefore concluded that an initial anisotropy cannot be responsible for the essential features of this diagram.

(c) *Non-uniformity of strain*

It has already been suggested that the guard-plate principle used in these experiments should eliminate any effect of non-uniformity of strain in the neighbourhood of the edges of the sheet.

In order to check this point, experiments were made by two independent methods. The first was by the use of parallel strips in simple elongation, using values of force per unit area of the unstrained section equal to the values of f_1 and f_2 in the tables. The points derived from these experiments, separately marked in figures 5 and 6, will be seen to fall exactly on the previously obtained arrays. The second check was obtained from measurements on a circular sheet clamped round its circumference and inflated. Details of the method have been described elsewhere (Treloar 1944 a, 1944 b). This corresponds to the special case where $\lambda_1 = \lambda_2$. The experiment was made on the actual sheet of swollen rubber used to obtain the data of figure 6. The results cannot conveniently be shown on this diagram, because the force could not simply be chosen to correspond to the values of f_1 and f_2 previously used. A plot of t_1 against $\lambda_1^2 - \lambda_3^2$, however, agreed to within 3% with the data in figure 6 for the case $f_1 = f_2$.

These independent experiments relating to the two extreme cases of simple elongation and 2-dimensional extension with $\lambda_1 = \lambda_2$ prove conclusively that the unexpected form of the results is not due to some defect in the technique of measurement. All the evidence suggests that the observed phenomenon represents a fundamental property of the rubber.

§ 5. THEORETICAL INTERPRETATION OF DATA

Mooney (1940) has discussed the form of the general stress-strain relations for a rubber on the basis of an assumed stress-strain relation in simple shear. For the particular case of a linear stress-strain relation in shear, he obtains, for the work of deformation

$$W_2 = C_1(\lambda_1^2 + \lambda_2^2 + \lambda_3^2 - 3) + C_2\left(\frac{1}{\lambda_1^2} + \frac{1}{\lambda_2^2} + \frac{1}{\lambda_3^2} - 3\right), \quad \dots \dots (3)$$

where C_1 and C_2 are physical constants of the material. The more general case of a non-linear shear relation may be resolved by adding further terms to equation (3). Thus the next term in the series would be of the type (Mooney, *loc. cit.* equation (40))

$$W_4 = A_4(\lambda_1^4 + \lambda_2^4 + \lambda_3^4 - 3) + B_4\left(\frac{1}{\lambda_1^4} + \frac{1}{\lambda_2^4} + \frac{1}{\lambda_3^4} - 3\right), \quad \dots \dots (4)$$

and the work of deformation would then be

$$W = W_2 + W_4.$$

From a rather more general standpoint, Rivlin (unpublished work) has argued that the work of deformation, or stored-energy function, must be a function of certain "strain invariants", which are themselves symmetrical functions of the

even powers of the extension ratios λ_1 , λ_2 and λ_3 . The simplest functions which may be chosen for the stored energy are

$$W_1 = G(\lambda_1^2 + \lambda_2^2 + \lambda_3^2 - 3), \quad \dots \dots \dots (5)$$

and

$$W_2 = K\left(\frac{1}{\lambda_1^2} + \frac{1}{\lambda_2^2} + \frac{1}{\lambda_3^2} - 3\right). \quad \dots \dots \dots (6)$$

Next in order of complexity are

$$W_3 = L(\lambda_1^4 + \lambda_2^4 + \lambda_3^4 - 3), \quad \dots \dots \dots (7)$$

and

$$W_4 = M\left(\frac{1}{\lambda_1^4} + \frac{1}{\lambda_2^4} + \frac{1}{\lambda_3^4} - 3\right). \quad \dots \dots \dots (8)$$

Rivlin's approach is perhaps simpler, and avoids the assumption that the form of the stress-strain relation for shear in an isotropic plane is independent of a stretch in the direction normal to that plane. However, the resultant stress-strain relations are the same whichever theory is adopted.

The stored-energy function derived from the molecular theory (Treloar 1947 a), from which equations (2) and (2a) are obtained, is

$$W = G(\lambda_1^2 + \lambda_2^2 + \lambda_3^2 - 3), \quad \dots \dots \dots (9)$$

and is therefore equivalent to Mooney's equation (3) with the constant C_2 put equal to zero.

Let us now examine the stress-strain relations resulting from the first equation of Mooney (equation (3)). Corresponding to this stored-energy function, the principal stresses are given by equation (25) in his paper, which may be written in the form *

$$t_1 - t_3 = (G + K\lambda_2^2)(\lambda_1^2 - \lambda_3^2), \quad \dots \dots \dots (10)$$

which, as will be seen, is a rather more complicated expression than equation (2) derived from the molecular theory, using the stored-energy function (9). In this expression G and K are physical constants expressible in terms of C_1 and C_2 in equation (3). In the case when the forces per unit area of the unstrained rubber, F_1 and F_2 are given, and $F_3 = 0$, we have the following equations relating the strains with the forces (or stresses)

$$\begin{aligned} t_1 &= \lambda_1 F_1 = (G + K\lambda_2^2)(\lambda_1^2 - \lambda_3^2), \\ t_2 &= \lambda_2 F_2 = (G + K\lambda_1^2)(\lambda_2^2 - \lambda_3^2). \end{aligned} \quad \dots \dots \dots (10a)$$

These simultaneous equations enable the extension ratios to be determined when the applied forces F_1 and F_2 are given. Their solution has been obtained graphically, using the particular values $G = 1.0$, $K = 0.1$, for six values of F_1 combined in all possible ways with the same values of F_2 . This solution is represented in figure 7 in terms of the stress t_1 plotted against $\lambda_1^2 - \lambda_3^2$. Detailed comparison with figure 6 shows a very close quantitative correspondence between the theoretical and experimental points.

Another method of comparing the experimental data with the theoretical equation (10) is by plotting the experimental stress t_1 against $(1 + K\lambda_2^2/G)(\lambda_1^2 - \lambda_3^2)$,

* The constant G is not the same as Mooney's G .

choosing a suitable value of K/G . This type of plot is shown in figure 8, in which curve (b) relates to the swollen rubber. With $K/G = 0.1$, the points fall very nearly on a straight line.

Thus Mooney's equation (3) gives a completely satisfactory representation of the behaviour of this particular rubber in the swollen state.

It is interesting to examine some further properties of Mooney's equation. Firstly, for a pure shear, we have one dimension (say λ_2) unchanged, and equation (10) reduces to

$$t_1 = (G + K)(\lambda_1^2 - \lambda_3^2).$$

In this case, therefore, the behaviour is indistinguishable from that given by the simple equation (2a). Secondly, for the difference of the two principal stresses, in the general homogeneous strain, we have

$$t_1 - t_2 = (G + K\lambda_3^2)(\lambda_1^2 - \lambda_2^2). \quad \dots \dots \dots (10b)$$

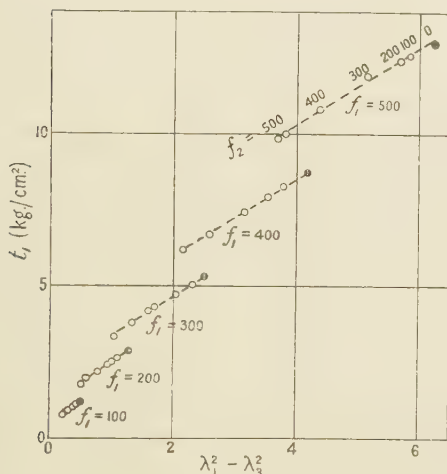


Figure 6. Swollen rubber. Stress t_1 plotted against $\lambda_1^2 - \lambda_3^2$. The black circles refer to simple elongation.

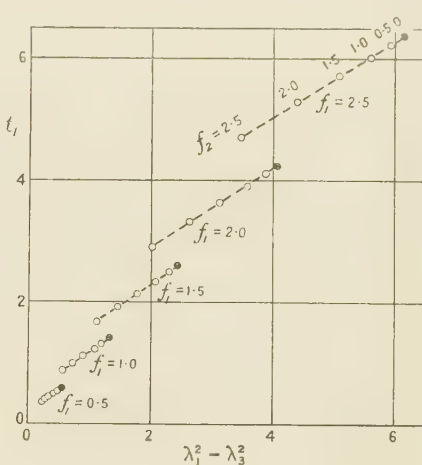


Figure 7. Stress calculated from Mooney's equation, using $G=1.0$, $K=0.1$.

If the forces are applied in the directions λ_1 and λ_2 , the extension ratio corresponding to the thickness direction is always less than unity, and λ_3^2 is generally quite small. If, therefore, K is also small compared with G , the term $K\lambda_3^2$ may be neglected, except at very small strains, i.e. equation (10b) reduces to the simpler form (2). This accounts for the observed linear relation between $t_1 - t_2$ and $\lambda_1^2 - \lambda_3^2$.

Turning now to the dry rubber, we find rather a more complicated picture. By a suitable choice of K/G it is possible to represent the stress t_1 as a continuous function of $(1 + K\lambda_2^2/G)(\lambda_1^2 - \lambda_3^2)$, but this function is not linear (figure 8 (a)). From this observation it is concluded that Mooney's equation represents a part, but not all of the deviation from the molecular theory (equation 2a). To account for the whole discrepancy it would probably be necessary to add further terms to the stored-energy function, such as those represented by equations (7) or (8). Since Mooney's equation (3) is based on a linear stress-strain relation in simple shear, it follows that the dry rubber is non-linear in shear. This fact may also

be deduced by direct interpolation from the experimental data. In other rubbers examined by the author, a non-linear shear relation has been obtained (Treloar 1944), but Mooney (1940) has reported a linear relation up to 200% shear.

§ 6. CONCLUSION

The conclusion to be drawn from the preceding analysis of the stress-strain relations may be summarized in the following way. As a first approximation the equations derived from the statistical treatment of a molecular model provide a basis for the interpretation of the elastic properties of rubber. A closer approximation is obtained by including an additional term in the stored-energy function, i.e. by the use of Mooney's equation (3). This appears to give an accurate representation of the properties of a swollen rubber, but is still inadequate when applied to a dry rubber, for which a third approximation, including at least one more general term, is likely to be required.

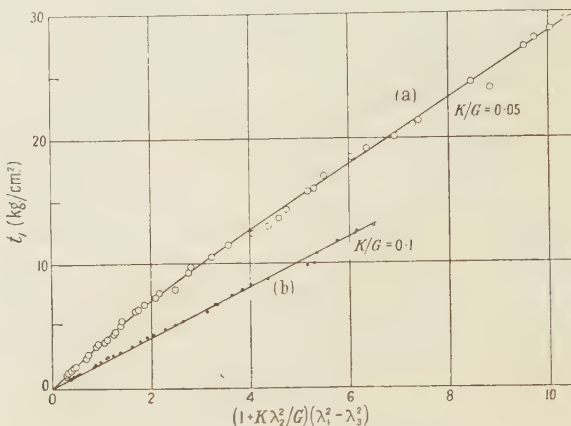


Figure 8. Data from figures 5 and 6 plotted with $(1 + K\lambda_2^2/G)(\lambda_1^2 - \lambda_3^2)$ as abscissae.
(a) Dry rubber, $K/G = 0.05$. (b) Swollen rubber, $K/G = 0.1$.

It is necessary to emphasize that the use of the second or higher approximations does not in itself throw any light on the physical mechanism responsible for the observed behaviour. It is, in fact, the 3-dimensional analogue of simple curve-fitting. It must also be borne in mind that any physical model that might be postulated must necessarily lead to results which may be represented by some combination of the stored-energy functions discussed in § 5.

ACKNOWLEDGMENTS

The author desires to express his thanks to his colleagues Dr. G. Gee and Mr. R. S. Rivlin, for helpful discussions in the course of this work, which forms part of the programme of fundamental research on rubber undertaken by the Board of the British Rubber Producers' Research Association.

REFERENCES

- JAMES and GUTH, 1943, *J. Chem. Phys.*, **11**, 455.
- MOONEY, 1940, *J. Appl. Phys.*, **11**, 582.
- RIVLIN. Unpublished work.
- TRELOAR, 1944 (a), *Inst. Rubber Industry Trans.*, **19**, 201.
- TRELOAR, 1944 (b), *Trans. Faraday Soc.*, **40**, 59.
- TRELOAR, 1947 (a), *Trans. Faraday Soc.*, **43**, 277.
- TRELOAR, 1947 (b), *Trans. Faraday Soc.*, **43**, 284.

The Dielectric Properties of Water and Heavy Water

By C. H. COLLIE, J. B. HASTED AND D. M. RITSON
Clarendon Laboratory, Oxford

MS. received 26 March 1947

ABSTRACT. Measurements by a number of different methods of the dielectric constant and loss angle of water and heavy water at three widely separated wavelengths in the region of anomalous dispersion, $\lambda=10$ cm., 3 cm., 1.25 cm., are described. Results show that the Debye equations are exactly obeyed, there being a single time of relaxation varying with the temperature; the ratios of the relaxation times of water and heavy water are found to be in quantitative agreement with the ratios of the viscosity over a temperature range, suggesting that the re-orientation mechanism in these liquids is the same as that of viscosity. The value of 5.5 found for the optical dielectric constant gives a reasonable result for the dielectric constant of water on the Onsager theory. This theory is discussed and shown to give a relaxation equation of the Debye type for alternating fields.

§ 1. INTRODUCTION

SINCE 1900 the anomalous dielectric dispersion of water at very short wavelengths has been widely investigated, and has been summarized by Dorsey (1940). The main qualitative features of the phenomenon are no longer in doubt, but quantitatively the results of different workers show wide divergencies. The significance of the problem lies in its theoretical bearing on the structure of water, which is not only of fundamental importance but also of technical and biological interest. In addition, a knowledge of the dielectric properties of water is needed in calculations on the transmission of microwaves.

It therefore seemed important to apply the recently developed high-frequency techniques to obtain an accurate measurement of the refractive index n and absorption coefficient κ of water. It was also felt that parallel measurements on heavy water would provide comparative data of theoretical value. In this paper measurements are described at three widely separated wavelengths, namely 10.0 cm., 3 cm., and 1.25 cm., in the temperature range 0°–75°C.

The theory of an ideal polar dielectric in an alternating field was first given by Debye in terms of a single relaxation time. It can be shown that the relation below holds generally for linear dielectrics, as is discussed later in this paper:

$$\epsilon - \epsilon_0 = \frac{\epsilon_s - \epsilon_0}{1 + j\omega\tau}, \quad \dots \dots (1)$$

in which τ is a time of relaxation, and ϵ is the complex dielectric constant at the angular frequency ω ; ϵ_0 is that part of the dielectric constant which is due to the atomic and electronic polarization, and is assumed to be real and independent of ω . The static dielectric constant is ϵ_s . This expression may be expressed in terms of the optical constants as follows:

$$\begin{aligned} n^2 - \kappa^2 &= \epsilon' = \frac{\epsilon_s - \epsilon_0}{1 + \omega^2\tau^2} + \epsilon_0 = \frac{\epsilon_s - \epsilon_0}{1 + [\lambda_s/\lambda]^2} + \epsilon_0, \\ 2n\kappa &= \epsilon'' = \frac{(\epsilon_s - \epsilon_0)\omega\tau}{1 + \omega^2\tau^2} = \frac{(\epsilon_s - \epsilon_0)\lambda_s/\lambda}{1 + [\lambda_s/\lambda]^2}, \end{aligned}$$

where n is the real part of the refractive index, κ the absorption coefficient, ϵ' and ϵ'' the real and imaginary parts of the complex ϵ , λ the wavelength corresponding to a frequency ω , and λ_s the wavelength which corresponds to frequency $1/\tau$ (the so-called "Sprungwellenlänge").

These equations represent the fall of the dielectric constant from its static value ϵ_s to its optical value ϵ_o , the fall being accompanied by a single broad absorption band in the neighbourhood of the characteristic wavelength λ_s . The present measurements were made with the object of finding out whether the simple expression with a single relaxation time does adequately represent the change in optical constants with frequency at a fixed temperature. As will be seen, this is in fact the case, so that one can also investigate:

- (1) the variation of λ_s with temperature. This can then be compared with other physical properties, such as the viscosity, whose temperature dependence is known.
- (2) the ratio of λ_s for water and heavy water.

§ 2. METHODS OF MEASUREMENT

The optical constants vary so rapidly with wavelength and temperature that no universal method is available.

The following methods, some of which have been described in previous publications, have been used:—

- (1) The change of the resonant frequency and damping of an E_{010} resonator, when an axial capillary tube filled with water is inserted, is measured (Willis Jackson 1946, Collie, Ritson and Hasted 1946).
- (2) A similar measurement using an H_{01} resonator (Penrose 1946, Collie Hasted and Ritson 1948).
- (3) Measurements of the absorption coefficient are made by direct transmission in a waveguide filled with the liquid under examination (figure 1, B). If two measurements are made of the absorption coefficient, one, κ_1 , in a rectangular guide of width a_1 , and a second, κ_2 , in a guide of width a_2 near cut-off, then it is easily shown (*loc. cit.*) that

$$\epsilon' = \frac{(c^2/\omega^2)(k_1^2\kappa_1^2 - k_2^2\kappa_2^2)}{\kappa_1^2 - \kappa_2^2} - (\kappa_1^2 + \kappa_2^2),$$

$$\epsilon'' = 2\kappa_1[\epsilon' - k_1^2 c^2 / \omega^2 + \kappa_1^2]^{1/2},$$

in which $k_1 = \pi/a_1$ and $k_2 = \pi/a_2$ for the H_{10} wave in a rectangular waveguide.

This method affords a satisfactory way of measuring both n and κ . As can be seen from the form of the equation the method is a practicable adaptation of the ideal method of determining κ by determining the attenuation in free space, and n by measuring the critical wavelengths of propagation down a guide. The quantities which have to be measured accurately are the width of the guide and the wavelength. These are the two quantities which can be measured with the greatest precision, and the latitude in the choice of a_1 and a_2 is sufficient to allow the two measurements of the attenuation in the guide to be approximately independent measurements of n and κ the optical constants in free space. This method is not limited to rectangular waveguides, and some of the later measurements

have with advantage been made using an H_{11} wave in cylindrical waveguides of radii r_1 and r_2 , in which case $k_1 = 1.841/r_1$, and $k_2 = 1.841/r_2$.

- (4) Direct measurements of the absorption in a sufficiently wide waveguide yield κ directly (figure 1 A).

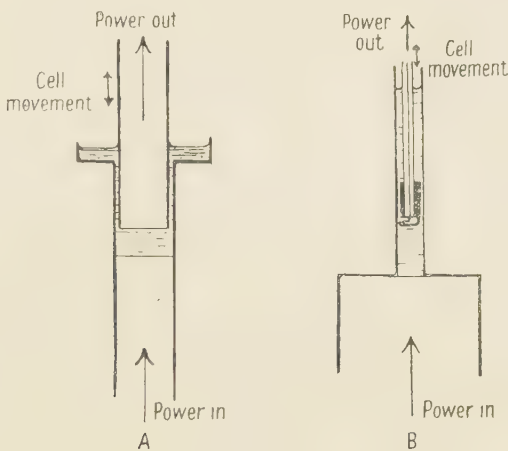


Figure 1. Principle of absorption measurement at 1 cm. and 10 cm.

The methods which have been used are shown in table 1.

Table 1. Methods of determination of n and κ

	H_2O		D_2O	
Wavelength (cm.)	n	κ	n	κ
10	E_{010} resonator. Absorption in two rectangular guides. Absorption in two circular guides.	Absorption in two rectangular guides. Absorption in two circular guides.	Absorption in two rectangular guides.	Absorption in two rectangular guides.
3.2	Absorption in two circular guides.	Absorption in wide rectangu- lar guide. Absorption in two circular guides.	Absorption in two circular guides.	Absorption in two circular guides.
1.25	H_{01} resonator.	Absorption in wide rectangu- lar guide.	H_{01} resonator.	Absorption in wide rectangu- lar guide.

§ 3. MEASUREMENT OF n AND κ AT 10 CM.

These measurements are relatively easy to make using radar receiving equipment whose main features were standardized during the war.

Power from a well screened reflex klystron (type CV 35) is led through a coaxial lead to a coaxial socket of the type first used by the General Electric Company in their research laboratories at Wembley. Commercial pyrotenax cable (type 147/1) is very suitable for the coaxial transmission line since the continuous outer coating facilitates the very high degree of screening needed if the fullest use is to be made of the high sensitivity obtainable (10^{-11} watt) with a superheterodyne receiver.

From the coaxial plug the power reaches the receiver, either through the absorption cell or through an H_{11} piston attenuator.

The construction of these absorption cells is shown diagrammatically in figure 1 B and the absorption cell using circular guides is shown in detail in figure 2.

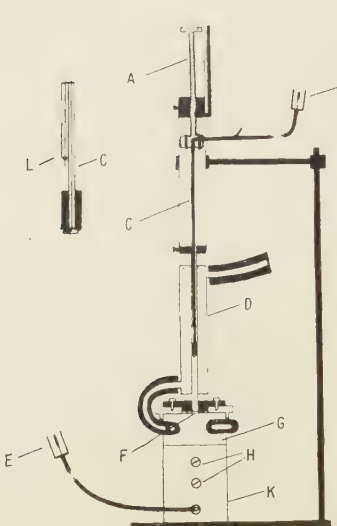


Figure 2.
10-cm. absorption cell.

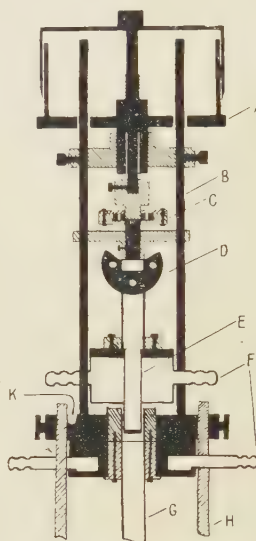


Figure 3.
1-cm. absorption cell.

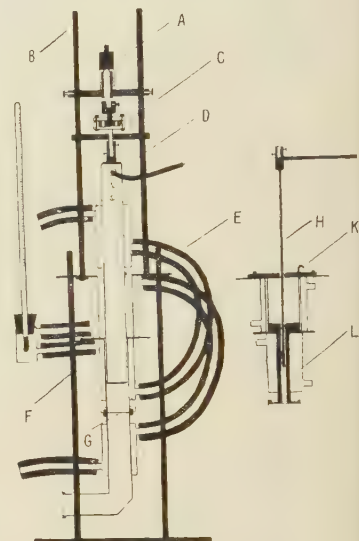


Figure 4.
3-cm. absorption cell.

Power from the coaxial line E is fed into the rectangular wave guide K by means of a probe; a match is obtained with two stubs 3.75 cm. apart at H. A small fixed loop in this section enables the power level to be monitored on a crystal detector. From the top of the guide the power passes through a $\frac{1}{2}$ mm. mica window into a circular guide filled with water. The window is held in position by a plate secured by three countersunk screws. The joint is rendered watertight with Dow-Corning silicone stop-cock grease which provides an effective seal even at 100°C .

The interchangeable circular guide is made from copper tube straightened on a silver steel mandrel. The two diameters used were 1.261 cm. and 0.576 cm. As far as could be judged by measurement of the open ends and the fit of a steel plug the guides were uniform to 1 part in 200, and this is confirmed by the absence of systematic variations of the measured absorption coefficient.

After transmission through the water the power is again picked up by a loop at the end of a movable pyrotenax coaxial cable C. The loop can be withdrawn and its position read by means of a 12 cm. screw movement A.

The loop is held central in the guide by means of a loosely fitting plunger (see inset). The loop extends about $1\frac{1}{4}$ mm. into the liquid and is nearly the same diameter as the tube C. Spacers can be inserted into the movement to allow different portions of the wave guide to be explored by the loop.

A subsidiary electrode L protruding from the cable C enables the conductivity of the water to be measured during the course of measurement. The absolute conductivity is obtained by calibrating the apparatus with N/50 KCl. The true value of ϵ'' is obtained from its apparent value ϵ_a'' by the relationship $\epsilon_a'' = \epsilon'' + 4\pi\sigma/\omega$ in which σ is the D.C. conductivity in E.S.U. If conductivity water is used and the joints are made so that as little solder as possible is in contact with the water the conductivity correction can be kept below 2% of ϵ'' at 80°C. The magnesium oxide filling of the pyrotenax must be prevented from coming into contact with the water by a well baked layer of shellac varnish.

For measurements at 3·2 and 1·25 cm. this correction is sufficiently small to justify the omission of a continuous measurement of the conductivity. This was, however, always measured at the end of a run to verify that excessive corrosion had not occurred.

At all frequencies freshly boiled water must be used to prevent the formation of bubbles. For the same reason the temperature should be progressively lowered during a series of measurements. The heavy water used throughout was of 99·5% purity.

All the relevant parts of the apparatus were water jacketed, and water from a thermostat was circulated through the jackets through lagged pipes.

The temperature was measured in the water stream by a thermometer which had been compared with a set of thermometers by Anschütz, which had themselves been compared with thermometers carrying an N.P.L. certificate.

The measurement of the absorption coefficients is made in two parts. First the receiver responses R_1, R_2, \dots, R_n are measured for a series of positions of the loop in the absorption cell. The piston attenuator is then substituted for the cell and a measurement made of the position of the attenuator loop at which the receiver responses are the same as one of the previously noted values R_1, R_2, \dots, R_n . To verify that the power output of the transmitter and the sensitivity of the receiver have not changed during the measurement, the response R_1 is checked after every reading of R_n . In this way it is possible to plot a curve whose ordinate is the displacement of the loop in the absorption cell and whose abscissa is the displacement of the loop in the H_{11} attenuator which produces the same change in receiver response. This curve should be a straight line whether the receiver response is linear or not.

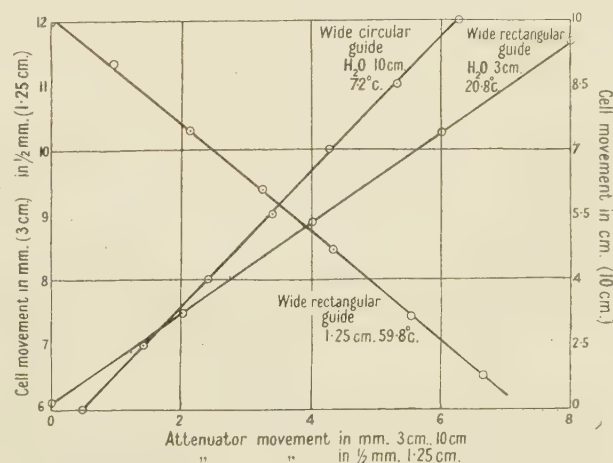


Figure 5. Typical absorption plots.

This offers a valuable check and enables errors in the experimental arrangements to be detected and eliminated. The two most obvious sources of error are pick-up and the production of unwanted modes in the absorption cell. Since the former is most troublesome at low signal strengths and the latter when the path in the water is small and the signal consequently strong, it is very improbable that these sources of error will compensate each other. Typical straight lines are shown in figure 5. The slope of these lines was evaluated by the method of least squares and the absorption coefficient calculated from the theoretical attenuation of the attenuator.

§ 4. THE RECEIVER

An Admiralty receiver type P 50 was used in these measurements. The band width of 3 Mc s. was sufficient to embrace the small frequency wanderings of the transmitter and local oscillator klystrons. Although more complicated than a simple crystal rectifier and sensitive galvanometer it has so many advantages that its use is almost essential if an overall accuracy of 1% is aimed at.

The main advantages are:—

- (a) A constancy of calibration lasting for several hours, and in favourable circumstances over a period of days.
- (b) A factor of at least 10^4 in the usable sensitivity.

The increased sensitivity is of great importance in the type of work being described because:—

- (i) It enables all coaxial leads to be of sufficient length (about 2 m. of pyrotenax) to damp out the standing waves due to inevitable mismatches at plugs and junctions.
- (ii) It enables power levels to be measured with a piston attenuator; otherwise the use of these admirable instruments is precluded by their large insertion loss.

The use of an attenuator allows the receiver to be used as a monitor so that it is sufficient to read the second detector current on a 0-100 microammeter. A suitable resistance net work allows a 40 db. range to be covered without changing the gain of the I.F. stages.

§ 5. MEASUREMENTS AT 1.274 CM.

Accurate measurements at this wavelength offer some difficulty since the degree of frequency stability required is relatively much greater if an I.F. amplifier of 3 Mc/s. bandwidth is to be used, while the valves are inherently less frequency stable than klystrons operating on a longer wavelength, owing to the very small clearances and high power dissipation involved. Satisfactory measurements were made possible by modulating the frequency of the output klystron by means of a 10-40 volt saw-tooth voltage of recurrence 500 c.p.s. applied to the reflector. The output of the receiver is then to a first approximation independent of the absolute frequency, since the I.F. frequency now sweeps through the whole effective spectrum of the I.F. receiver. Satisfactory results were obtained provided outside conditions were kept as constant as possible. This was done by enclosing both the output and local oscillator klystrons in copper screening boxes cooled by

constant stream of compressed air; in addition the voltage control was improved by replacing the neon stabilizers in the power pack by dry batteries. Some attempts were made to use the "two waveguide" method which had proved so convenient at 10 cm. It was not very satisfactory owing to the difficulty of matching into and out of a waveguide only 0·9 mm. in diameter, and the method was abandoned. The refractive index n was measured by the resonator method previously described (Collie, Hasted and Ritson 1948), and κ was determined by direct measurement of the attenuation in the absorption cell, shown in figure 3, and diagrammatically in figure 1B. The water is contained in the upper part of the vertical rectangular guide G of internal cross section 10·75 mm. \times 4·5 mm., supported on a thin (0·15 mm.) mica window firmly clamped and greased in position. After traversing the water the wave is picked up by a movable guide (internal cross section 8·75 mm. \times 3·5 mm.) fitted with a distrene or rubber window about 2 mm. thick. This type of pick-up is very satisfactory and is much easier to match into the water than the loop and coaxial line used at longer wavelengths. The wave is led to the mixer by the right-angle bend at D and a length of flexible waveguide. A pair of stubs provides sufficient matching. In view of the rather open design of the cell it was thought worth while to measure the difference in temperature between the water in the cell and the water circulating in the water jackets. Measurement with a thermocouple showed that after ten minutes at any fixed temperature the difference in temperature between the water in the cell and the thermometer chamber was less than 0·1°C. The attenuation produced by a known thickness of water was measured as before by direct comparison with a piston attenuator.

The greatest source of error in absorption measurements of this sort lies in the possibility that new modes are created when the wave passes through the window into the water-filled guide. Each mode will be differently attenuated so that little precise information can be obtained from the measured attenuation curves, which are not exponential. In these experiments the production of unwanted modes was minimized by using a thin window whose flatness could be investigated by reflected light after it had been mounted in the cell. Distortion due to differential expansion was avoided by greasing, but not sticking, the window to the copper flange. A watertight joint up to 80° was ensured by using non-melting silicone grease. The freedom from unwanted modes, and overall accuracy of measurement, is shown by the achievement of straight-line plots for cell movement against piston attenuator movement. Typical plots at all wavelengths are shown in figure 5.

At this wavelength good straight lines through more than 3 mm. of water were obtained with this design of cell. There is, however, disagreement between these results and those we reported in an earlier paper, which is due to two facts:—

- (i) The design of the earlier cell did not permit the propagation of pure modes, so that curved logarithmic absorption plots were obtained; this curvature was erroneously described as geometrical in origin.
- (ii) In order to eliminate this effect measurements were taken with a large dead space of liquid, but through small thicknesses, with very high receiver sensitivity. Repetition showed that these measurements were vitiated by pick-up.

In the revised method both these sources of error have been eliminated beyond reasonable doubt, and the new results are taken as accurate to $\pm 1\%$.

§ 6. MEASUREMENTS AT 3·213 CM.

Measurement of κ at this wavelength was carried out with a rectangular wave guide cell similar to that described for use at 1·274 cm. It is shown in figure 4.

A type CV 87 reflex klystron was used as the source of power; this valve has a coaxial line output and is connected to a waveguide system by a probe. After passing through a unidirectional feed and a flap attenuator the power is matched by stubs through a thin mica window G into the water-filled cell. The small amount of power (about 1%) led off by the one way feed is coupled into a high-Q resonator, the output of which is fed to a crystal rectifier and a high sensitivity galvanometer. In this way both the power level and the frequency stability of the wave entering the cell are continuously monitored throughout a series of readings.

The method of measurement was similar to that used at 1·274 cm. The cell was so designed that a number of fine cylindrical waveguides could be substituted for the rectangular guide, and a concentric line and pick-up loop for the output guide. These parts are shown in figure 4, and when they are in use the apparatus is similar to that used at 10 cm. for the measurement of both n and κ . The diameters of tube used were 2·51 mm. and 3·77 mm. As can be seen from figure 7, excellent agreement was obtained between values of κ obtained by the two methods, and the fine cylindrical wave guide has been used throughout for κ measurements on heavy water, since less liquid is required. The cylindrical tubes were used throughout for measurement of n .

§ 7. MEASUREMENT OF WAVELENGTH AND ATTENUATION

The wavelengths used were 1·27₄ cm., 3·21₃ cm., and 10·00 cm. respectively. The two former were measured with a simple absorption wave-meter using an H_{11} mode. The absolute accuracy depends upon the diameter of the reamed hole. They are uncorrected for the dielectric constant of air, and probably accurate to better than $\frac{1}{2}\%$. The 10 cm. wavelength was measured with a high precision resonant cavity wavemeter (Admiralty type G 93), which could be calibrated against a crystal-controlled oscillator.

Three inductive piston attenuators using an H_{11} mode were used in these measurements. Their attenuation constants are given below:—

Wavelength (cm.)	Attenuator, diameter (mm.)	<i>A</i>
1·274	4·00	1·575
3·213	9·525	1·70
10·00	12·74	4·48

The attenuation constant κ is calculated from the relationship

$$\kappa = \frac{\text{displacement of the attenuator}}{\text{displacement through the water}} \times A.$$

The attenuation constant A is calculated from the relationship

$$-4\pi^2 A^2/\lambda^2 + (1.841)^2/r^2 = \omega^2/c^2.$$

An account of the theory and construction of these instruments has been given *inter alia* by Clayton, Houldin, Lamont and Willshaw (1946).

§ 8. RESULTS

Values of n and κ have been obtained at a sufficiently large number of temperatures to enable smooth curves to be drawn through the points and values at ten degree intervals from 0° to 75° c. for water and from 5° to 60° c. for heavy water to be given at each frequency. These values, which are estimated as accurate to $\pm 1\%$ (10:1 probability) and $\pm 0.4^\circ\text{c}$. in temperature, are given in tables 2 and 3, together with the values calculated from a single value of λ_s , which is also tabulated at each temperature. Some measured values at 3 cm. and the smooth curves through them are shown in figure 7. It will be seen that except for a very few values there is

Table 2. Dielectric properties of water

$$\epsilon_0 = 5.5$$

T (° c.)	ϵ_s	λ_s	$\lambda = 1.27$ cm.		$\lambda = 3.21$ cm.		$\lambda = 10.0$ cm.	
			n	κ	n	κ	n	κ
0	88.2	3.34	4.94	2.86	7.28	2.86	9.03	1.37 exp.
			4.92	2.81	7.31	2.83	9.04	1.37 calc.
			5.55	2.91	7.73	2.43	8.89	0.982 exp.
10	84.2	2.39	5.60	2.92	7.88	2.39	9.00	0.989 calc.
			6.25	2.86	8.08	1.97	8.83	0.739 exp.
20	80.36	1.80	6.20	2.83	8.16	1.96	8.87	0.737 calc.
			6.75	2.67	8.11	1.57	8.78	0.558 exp.
30	76.7	1.39	6.71	2.64	8.25	1.58	8.70	0.559 calc.
			7.0	2.40	8.20	1.29	8.53	0.442 exp.
40	73.1	1.12	7.02	2.39	8.21	1.28	8.51	0.440 calc.
			7.26	2.11	8.15	1.05	8.28	0.350 exp.
50	69.8	0.912	7.23	2.10	8.12	1.04	8.33	0.348 calc.
			7.30	1.87	7.99	0.865	8.09	0.281 exp.
60	66.6	0.760	7.34	1.83	8.01	0.856	8.14	0.283 calc.
			7.35	1.52	7.82	0.672	7.78	0.212 exp.
75	62.1	0.608	7.34	1.50	7.80	0.663	7.87	0.218 calc.

Table 3. Dielectric properties of heavy water
 $\epsilon_0 = 5.5$

T ($^{\circ}$ C.)	ϵ	λ_s	$\lambda = 1.27$ cm.		$\lambda = 3.213$ cm.		$\lambda = 10.0$ cm.	
			n	κ	n	κ	n	κ
			4.75	2.66	6.82	2.84	—	1.52 exp.
5	85.8	3.84	4.54	2.66	6.84	2.89	—	1.52 calc.
			5.1	2.76	7.24	2.66	—	1.27 exp.
10	83.8	3.12	4.91	2.78	7.27	2.69	—	1.26 calc.
			5.65	2.84	7.78	2.26	—	0.94 exp.
20	80.1	2.31	5.56	2.83	7.72	2.29	—	0.93 calc.
			6.25	2.70	7.98	1.85	—	0.71 exp.
30	76.5	1.76	6.09	2.77	7.97	1.88	—	0.70 calc.
			6.7	2.54	7.98	1.47	—	0.54 exp.
40	73.1	1.36	6.60	2.56	8.04	1.49	—	0.53 calc.
			—	—	7.98	1.23	—	0.43 exp.
50	69.8	1.11	—	—	8.02	1.24	—	0.425 calc.
			—	—	8.00	1.035	—	0.34 exp.
60	66.7	0.923	—	—	7.94	1.025	—	0.343 calc.

agreement to $\pm 1\%$ with the values calculated assuming a single time of relaxation. The results were analysed using the value of κ at 10 cm. and 1.274 cm. as a basis for finding λ_s , the best fit being subsequently obtained by trial and error. At low temperatures it is useful to plot $1/[1 + \lambda_s^2/\lambda^2]$ against ϵ' for different frequencies, to obtain straight lines passing through ϵ_s and ϵ_0 when $1/[1 + \lambda_s^2/\lambda^2] = 1$ and 0. In this way ϵ_0 is found to be 5.5 ± 1 , and the single time of relaxation is conveniently displayed; figure 6 shows straight lines obtained at 0° and 20° C. for water. The value of 5.5 may seem at first to be high, but is in agreement with the recent results of Saxton and Lane (1945), and with measurements of the refractive index in the far infra-red which show a value of $n = 2$, rising as the frequency decreases (Rubens 1915, Cartwright 1936).

§ 9. PREVIOUS MEASUREMENTS

There is a wide field of literature on the dielectric properties of water at high frequencies. Although the measurements of individual workers are in many cases self-consistent there are wide discrepancies between the results of different authors. The early results with damped sources being generally regarded as

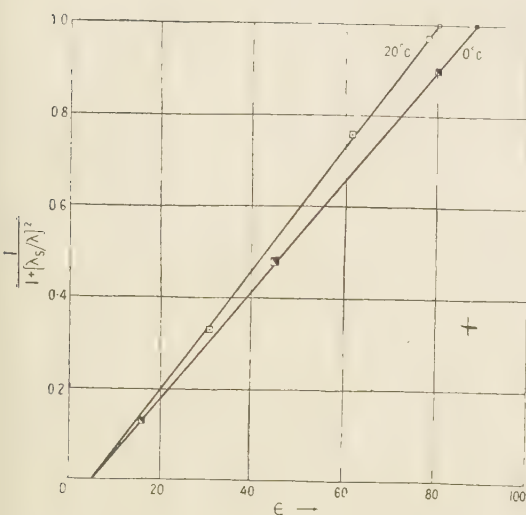
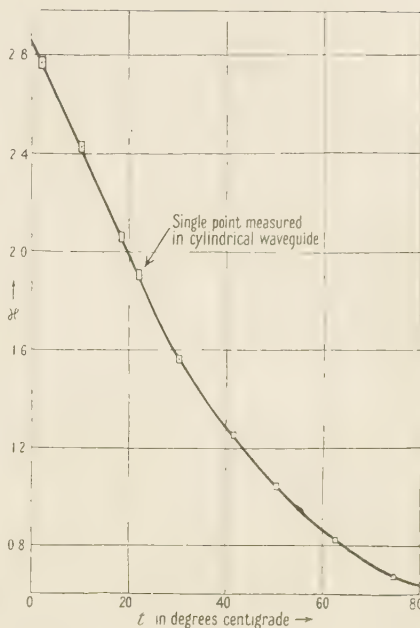


Figure 6. Relaxation-time analysis.

Figure 7. Absorption coefficient H of water at $3\cdot213$ cm., measured directly in rectangular waveguide, plotted against temperature. Squares indicate accuracy claimed, $\pm 1\%$ and $\pm 0\cdot4^\circ$ C.

unreliable, only those obtained with continuous wave sources are shown in table 4.

Table 4. Values of λ_s for water at 20° C.

Date	Authors	Method	Approx. value of λ_s (cm.)
1937	A. Esau and G. Bäß	Free wave	1.85
1937	H. W. Knerr	Wire wave	1.6-1.8
1937	W. Hackel and M. Wien	Thermometric at metric wavelengths	1.60
1939	Slevogt	Wire wave	1.8
1939	W. Kebbel	Free wave	1.85
1940	Divilkowsky and Masch	Thermometric method	1.56
1943	C. P. Connor and W. P. Smyth	Wire wave	2.00
1947	J. A. Saxton and J. Lane	Free wave	1.53
1946	P. Abadie and J. Girard	Wire wave	1.50
1947	Present authors	Waveguides and resonators	1.80

For bibliographical references see end of paper.

These results show that measurements in this field are peculiarly susceptible to concealed systematic errors. The following may be cited as typical:—

- (i) The assumption of a square law voltage current law for crystals,

- (ii) Physically attractive but mathematically invalid approximations. The so called "wire wave" methods are open to such approximations as can be seen from the rigorous treatment which has been given by Slevogt.
- (iii) The relationship

$$R = \frac{n^2 + \kappa^2 + 1 - 2n}{n^2 + \kappa^2 + 1 + 2n}$$

between the reflection coefficient R and the optical constants, shows R to be insensitive to changes in n and methods based on the measurement of R are correspondingly uncertain.

- (iv) Owing to lack of power, experimenters using the optical or free wave method have sometimes had to make measurements before the region of steady exponential attenuation had been reached.

The authors hope that they have avoided or overcome most of these difficulties. As has been already mentioned all power measurements have been made with a piston attenuator, so that the receiver acts only as a monitor. Where possible independent methods have been used to cross-check some of the results.

The most extensive series of independent measurements was made at $\lambda = 10$ cm. at which wavelength the E_{010} resonator method was compared with both versions of the two-waveguide method over a large temperature range. The results given in table 5 show satisfactory agreement. At $\lambda = 3.2$ cm. κ was measured using both cylindrical and rectangular guides. Reference to figure 7 shows that the two methods agree. Up to the present no method of cross-checking the 1.25 cm. results has been possible apart from doubtful tests of self-consistency and consistency with the results at other wavelengths.

Table 5. 10 cm. results showing agreement between various methods

T (° C.)	n Resonator	n Rectangular waveguide	n Cylindrical waveguide	κ Rectangular waveguide	κ Cylindrical waveguide
0	8.99 ± 0.09	9.03 ± 0.05	9.03 ± 0.05	1.37 ± 0.01	1.37 ± 0.01
10	—	8.89	8.89	0.98	0.982
20	8.86	8.83	8.83	0.74	0.739
30	8.68	8.78	8.78	0.56	0.558
40	8.50	8.53	8.53	0.435	0.442
50	8.28	—	8.28	0.345	0.350
60	8.09	—	8.09	0.28	0.281
70	7.87	—	7.78	0.23	—
80	7.71	—	—	0.20	—
90	7.55	—	—	0.17	—
100	7.38	—	—	0.15	—

§ 10. THEORETICAL

It is significant, though not unexpected, that water and heavy water, in common with many other chemically pure liquids, obey the Debye equations exactly and have a single time of relaxation. From these data the values of dielectric constant and loss angle can be calculated for any frequency. For completion of the work, measurements at wavelengths of 0.5 cm. and 1 mm. would be desirable, but technique is not yet advanced sufficiently for these wavelengths to be available.

By such measurements, greater accuracy than ± 1 in the value of ϵ_0 would be obtained.

It is also significant that the single time of relaxation should hold at all temperatures, indicating that the change between the various structures suggested by Bernal and Fowler (1933) is continuous. It would be difficult to imagine dipoles in two different crystalline structures simultaneously present at any given temperature taking the same time of relaxation. It is apparent that the absorption lines shown by water vapour in this region have no effect on the dielectric constant of the liquid.

The expression $\epsilon - \epsilon_0 = (\epsilon_s - \epsilon_0)/(1 + j\omega\tau)$ which reproduces the experimental results was originally obtained by considering a dielectric in which the internal field was a linear function of the polarization. It is well known that this assumption over-estimates the interaction between the dipoles so that the dielectric model becomes spontaneously polarized except at very high temperatures. This difficulty is considerably enhanced by increasing the value of ϵ_0 . Moreover, there is a discrepancy between Debye's τ and the experimental τ which arises from the assumption of the Lorentz internal field (see *Polar Molecules*, p. 92). It is therefore important to consider how the dielectric constant would depend upon frequency on theories such as those of Onsager or Böttcher (1942), which avoid these difficulties by making the interaction between the dipoles depend on the dielectric constant. The following treatment of Onsager's theory follows closely that of Fowler and Guggenheim (*Statistical Thermodynamics*, 1939) except that an alternating field and a relaxation time are introduced.

Consider first a molecule radius a , with a polarizability γ , reduced to a refractive index n by the Lorentz-Lorenz formula as follows:—

$$\gamma = a^3(n^2 - 1)/(n^2 + 2). \quad \dots \dots (1)$$

If the electric moment of the molecule is μ , and it is immersed in a continuous medium of dielectric constant ϵ_s , then by Onsager's theory there will be a "reaction" field R given by

$$R = \mu \cdot 2(\epsilon_s - 1)/(2\epsilon_s + 1)a^3. \quad \dots \dots (2)$$

Where by definition $\mu = \mu_0 \mathbf{u} + \gamma \mathbf{R}$ and \mathbf{u} is the unit vector in the direction of the moment. Therefore

$$\mu = \mu_0 \mathbf{u} + \gamma \mathbf{u} \cdot 2(\epsilon_s - 1)/(2\epsilon_s + 1)a^3. \quad \dots \dots (3)$$

Combining (3) with (1) and re-arranging,

$$\mu = \mu_0 \mathbf{u}(n^2 + 2)(2\epsilon_s + 1)/3(2\epsilon_s + n^2), \quad \dots \dots (4)$$

and combining (4) with (2)

$$\mathbf{R} = 2(n^2 + 2)(\epsilon_s - 1)\mu_0 \mathbf{u}/3(2\epsilon_s + n^2)a^3. \quad \dots \dots (5)$$

Now consider the application of an alternating field \mathbf{E} of frequency ω , and let the dielectric constant corresponding to this frequency be ϵ . Let the additional field this causes at the cavity be \mathbf{E}' .

Then by the Onsager theory

$$\mathbf{E}' = \frac{\mathbf{E} \cdot 3\epsilon}{2\epsilon + 1} + \frac{\mathbf{E}' \cdot \gamma \cdot 2(\epsilon - 1)}{(2\epsilon + 1)a^3}, \quad \dots \dots (6)$$

and by a similar argument as was used for equation (4)

$$\mathbf{E}' = \mathbf{E}(n^2 + 2)\epsilon/(2\epsilon + n^2). \quad \dots \dots (7)$$

The total electric force \mathbf{F} acting on the molecule is given by

$$\mathbf{F} = \mathbf{E}' + \mathbf{R}, \quad \dots \dots (8)$$

so that

$$\mathbf{F} = \frac{\mathbf{E}(n^2 + 2)\epsilon}{2\epsilon + n^2} + \frac{2(n^2 + 2)(\epsilon_s - 1)}{3(2\epsilon_s + n^2)a^3} \mu_0 \mathbf{u}. \quad \dots \dots (9)$$

One may now follow the conventional treatment as given, for example, in Fowler and Guggenheim. In evaluating the mean polarization, the effect of the relaxation time can be introduced as in Debye's original treatment by writing $\mu_0/3kT(1+j\omega\tau)$ instead of the expression $\mu_0/3kT$ appropriate to the static case. With this modification one obtains after some reduction the result that

$$\epsilon - n^2 = \frac{A}{1+j\omega\tau} \cdot \frac{\epsilon}{\epsilon + \frac{1}{2}},$$

in which A is written for the expression

$$\frac{(n^2 + 2)^2 \cdot (2\epsilon_s + 1)}{(2\epsilon_s + n^2) \cdot 6kT} \cdot \mu_0^2.$$

Since $1/2\epsilon$ is small compared with unity no great error will be involved by substituting

$$\epsilon = \epsilon_s/(1+j\omega\tau).$$

Thus

$$\epsilon - n^2 \doteq A/(1+j\omega\tau) - A/2\epsilon_s.$$

As $\omega \rightarrow \infty$, $\epsilon_s - (n^2 - A/2\epsilon_s) \rightarrow A$. If ϵ_0 is defined so that $A = \epsilon_s - \epsilon_0$, then $n^2 - \frac{1}{2} = \epsilon_0$. We have, therefore, $\epsilon - \epsilon_0 = (\epsilon_s - \epsilon_0)/(1+j\omega\tau)$, with $\epsilon_0 + \frac{1}{2} = n^2$. The effective deviation is of the order of $1/4\epsilon^2$ and will therefore be vanishingly small.

We can therefore say that it is impossible to differentiate experimentally between a linear internal field and an Onsager field.

The above calculation also shows that the dielectric constant differs from the value calculated from the relaxation time curve by $\frac{1}{2}$ as $\omega \rightarrow \infty$ on the Onsager model.

It is just possible this might be found experimentally, but small deviations of this order could be attributed to many factors.

It can definitely be stated that the experimental value of ϵ_0 for water is higher than the currently accepted value of 2.0. It is interesting to note that if we substitute $\epsilon_0 = 5.5$ in Onsager's equation instead of $\epsilon_0 = 2.0$, the calculated value of the dipole moment is found by to be 1.5 Debye units.

The accepted value of μ_0 is 1.87 in the vapour phase, and it is therefore apparent that if the high value for ϵ_0 is accepted, Onsager's formula gives, unexpectedly, a value of $\epsilon_s = 130$ which is greater than that found experimentally.

However, this large value for ϵ_0 is not without its own difficulties; the value of ϵ_0 for ice is 3, so that one might expect a considerable decrease in dielectric constant when water freezes. Also, if one substitutes the high value of ϵ_0 in equations (3) and (9), one finds a ratio $\mu/\mu_0 = 2.6$. Since μ_0 is already 1.87 Debye units this would mean so great an electronic polarization that γ could no longer be regarded as constant.

The only possibility is to leave μ throughout the equations, which would finally give

$$\epsilon - n^2 = \frac{4\pi}{V} \cdot \frac{3(2\epsilon_s + n^2)}{2\epsilon_s + 1} \cdot \frac{\mu^2}{3kT(1+j\omega\tau)} \cdot \frac{\epsilon}{2\epsilon + 1}.$$

It is possible that the anomalous dielectric properties of "associated" liquids are due to the fact that the atomic and electronic polarizations are very much higher than is generally assumed. It can be seen qualitatively that association might produce high polarizabilities.

It is of interest to test the Debye relation $\tau = 8\pi\eta a^3/2kT$ experimentally. We find for water and heavy water a fair approximation to the proportionality of τ and η/T , which is shown in figure 8. It appears that a power law slightly different

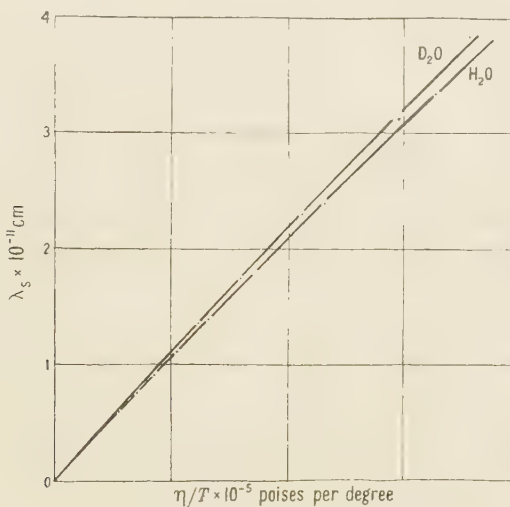


Figure 8. Relation between relaxation time and viscosity.

from unity is obeyed; logarithmic plotting shows it to be a 0.97 law, from which extrapolation will give the real relaxation time at any temperature for which η is shown (e.g. for super-cooled water). Calculation of τ on the accepted basis of $a = 1.38 \text{ \AA}$ gives a value of $\tau = 0.85 \times 10^{-11}$, in good agreement with the experimental value of 0.9×10^{-11} .

Further, the ratio of viscosities and of relaxation wavelengths for water and heavy water show fair agreement over a temperature range, as can be seen from table 6 (viscosities from Lewis 1933).

Table 6

Smoothed values of:

$T(^{\circ}\text{C})$	$\lambda_{s_{D_2O}}$	$\lambda_{s_{H_2O}}$	η_{D_2O}	η_{H_2O}
	$\pm 2\%$			
10	1.30		1.29	
20	1.27		1.25	
30	1.24		1.22	
40	1.21		1.19*	

* Extrapolated

The close numerical agreement between the observed and calculated values of τ is surprising, and probably fortuitous, but the close dependence of τ upon viscosity, both in water and heavy water, seems to us significant. It is evident that viscous flow and dipole orientation are influenced by the same factors, and can thus, in

some ways, be said to favour a hole theory such as that of Eyring (Glasstone, Laidler and Eyring 1941). If one accepts Eyring's result

$$\frac{1}{\tau} = \frac{kT}{h} \cdot e^{\Delta S/R} \cdot e^{-\Delta H/RT},$$

connecting the thermodynamic properties of the activation process involved in re-orientation, one can calculate ΔH from the observed temperature coefficient of τ . The value obtained is about 5 k cal/gm. mol. at 0°C., which is roughly the same as the surface energy. The observed value of ΔH also falls with rising temperature as the surface energy is known to do.

ACKNOWLEDGMENTS

The work described in this paper has been carried out on behalf of the Director of Physical Research, Admiralty, and the authors wish to record their thanks for permission to publish. The authors are grateful to Lord Cherwell for kindly extending to them the facilities of the Clarendon Laboratory. They also wish to thank D.S.I.R. from whom one of them (D.M.R.) has received a grant, and Mr. W. Stonard whose skill in the construction of the absorption cells and other equipment has been of great value.

REFERENCES

- ABADIE, P., and GIRARD, J., 1946, *Trans. Faraday Soc.*, Discussion on Dielectrics.
- BERNAL, J. D., and FOWLER, R. H., 1933, *J. Chem. Phys.*, **1**, 515.
- BÖTTCHER, C. J. F., 1942, *Physica*, **9**, 927.
- CARTWRIGHT, C. HAWLEY, 1936, *J. Chem. Phys.*, **4**, 413.
- CLAYTON, R. J., HOULDIN, J. E., LAMONT, H. R. L., and WILLSHAW, W. E., 1946, *J. Instrn. Elect. Engrs.*, Part III, **93**, 97.
- COLLIE, C. H., HASTED, J. B., and RITSON, D. M., 1948, *Proc. Phys. Soc.*, **60**, 71.
- COLLIE, C. H., RITSON, D. M., and HASTED, J. B., 1946, *Trans. Faraday Soc.*, **42 A**, 129.
- CONNOR, C. P., and SMYTH, W. P., 1943, *J. Amer. Chem. Soc.*, **65**, 382.
- DEBYE, P., 1929, *Polar Molecules* (Chemical Catalogue Co.), p. 92.
- DIVILKOWSKI and MASCH, 1940, *C.R. Acad. Sci., U.S.S.R.*, **27**, 801.
- DORSEY, N. E., 1940, *Properties of the common water-substance* (Reinhold Publishing Co.).
- ESAU, A., and BÄZ, G., 1937, *Phys. Z.*, **38**, 774.
- FOWLER and GUGGENHEIM, 1939, *Statistical Thermodynamics* (Cambridge).
- GLASSTONE, S., LAIDLER, K. J., and EYRING, H., 1941, *Theory of Rate Processes* (McGraw-Hill Co.).
- HACKEL, W., and WIEN, M., 1937, *Phys. Z.*, **38**, 767.
- JACKSON, WILLIS, 1946, *Trans. Faraday Soc.*, Discussion on Dielectrics.
- KEBBEL, W., 1939, *Hochfrequenztech. u. Elektroakust.*, **53**, 81.
- KNERR, H. W., 1937, *Phys. Rev.*, **52**, 1054.
- LEWIS, G. N., 1933, *J. Amer. Chem. Soc.*, **55**, 4730.
- PENROSE, R. P., 1946, *Trans. Faraday Soc.*, Discussion on Dielectrics.
- RUBENS, H., 1915, *Verh. dtsch. phys. Ges.*, **17**, 315.
- SAXTON, J. A., and LANE, J. A., 1947, *Phys. Soc., Meteorological Factors in Radio-Wave Propagation*, p. 278.
- SLEVOGT, 1939, *Ann. Phys., Lpz.*, **36**, 147.

Quantum Mechanical Calculation of the Heat of Solution and Residual Resistance of Gold in Silver

By KUN HUANG

H. H. Wills Physical Laboratory, University of Bristol

MS. received 7 July 1947

ABSTRACT. An attempt is made to calculate the heat of solution of gold in silver on the basis of the quantum theory of metals. These two metals are chosen because they have the same atomic volume, and therefore are the simplest case.

The steps in the argument are as follows : Suppose that a gold atom replaces a silver atom in the lattice. Then, to a certain approximation, one can represent the substitution of the silver ion by a gold ion, in its effect on the electrons, by a " potential hole " of depth ΔE and radius r_0 . This potential hole will alter the energy of the conduction electrons. To a first approximation the change in energy is just ΔE , which would give zero heat of mixing. A second-order term of order $(\Delta E)^2/E_F$ always gives a positive heat of mixing ; E_F is here the Fermi energy. This term is calculated exactly by wave-mechanical methods ; it gives 0.69 ev. per atom. The same calculation shows, however, that there is a concentration of charge in the gold atom in excess of that in the surrounding silver atoms ; this alters the potential in which the electrons move, so that a self-consistent calculation is required to obtain the true energy. For this the labour required would be almost prohibitive ; therefore we use instead the Thomas-Fermi method and obtain 0.45 ev. We thus find 0.15 ev. per atom for the heat of solution, which compares well with the observed value 0.13 ev.

With the help of the potential obtained with the Thomas-Fermi method the residual resistance of gold in silver is found to be 0.16 micro ohm cm. for 1% solution. The considerable discrepancy as compared with the experimental value 0.38 seems closely connected with very similar discrepancies found in other theoretical work on temperature resistance of the noble metals.

§ 1. INTRODUCTION

In many applications of the electron theory of metals to alloys, it has been found possible to treat the different constituent atoms merely as sources supplying different numbers of metallic electrons which belong to the metal as a whole. The irregularities created by the foreign atoms have been entirely ignored and the electronic band structure has been treated in the same way as in pure metals. An exception is the work on residual resistance of alloys, for the residual resistance is a direct result of the local irregularities in the potential field caused by the difference in the nature of the constituent atoms. However, most of this work is essentially formal and succeeds only in correlating certain facts, and leaving the question of the nature of the irregularities untouched. The only attempts at quantitative estimation of absolute magnitudes of residual resistance seem to be those made by Mott (1936). An attempt to obtain some idea of cohesion of alloys with the simple model employed by Mott in his work on resistance has naturally led us to a closer examination of the irregularities in the potential surrounding the foreign atoms. It is the purpose of the present paper to investigate their nature more deeply and give a semi-quantitative discussion of the cohesive energy and resistance. For our actual discussion, the alloy Ag-Au will be used, because the constituent atoms have practically the same radii, so that the effects due to distortion

of the lattice will not be present. Similar effects to those discussed here will occur also in Cu–Ag, Cu–Au, but will be complicated by effects of distortion both in the consideration of resistance and energy.

The sum of the sublimation energy and the ionization energy of the atoms in a metal will be called the *binding energy* of the metal; this is the energy necessary to separate the individual ionic cores and valence electrons into free ions and electrons. Then the binding energy of a monovalent pure metal with “almost-free electrons” can be put rather crudely as

$$W = - \sum_i \left(E^0 + \frac{\hbar^2 \mathbf{k}_i^2}{2m} \right), \quad \dots \dots (1)$$

E^0 is a constant for the metal concerned, and \mathbf{k}_i is the wave number vector of the i th electron, so that the second term alone is just the Fermi energy of the electrons. Formula (1) can be derived theoretically (e.g. Seitz 1940, p. 345) when, owing to correlation, only one electron is in each atomic sphere. $E^0 + \hbar^2 \mathbf{k}_i^2 / 2m$ is thus the eigenvalue of the i th state in the Hartree sense. (By adding these eigenvalues the mutual electronic repulsive energy is counted twice, and this serves very conveniently to take care of the repulsion between the ions). Thus E^0 appears as the constant potential energy of the Sommerfeld model. Mott (1936) has actually shown that to the same approximation this simple interpretation can be extended to alloys. Thus the difference in the ionic field, say, of a gold atom in a silver lattice can be regarded as a change in the potential energy from E_{Ag}^0 to E_{Au}^0 in the atomic sphere surrounding the gold ion. This idea is of importance in making possible at least a semi-quantitative treatment of effects involving such irregularities in the potential field. However, simple consideration will show that it is necessary to elaborate the square-hole potential, before it can be used as the effective field in which the electrons move.

Consider, for instance, an Au atom in an Ag lattice. As the atomic radii are the same, the Fermi energies are the same. From (1) it follows that

$$E_{\text{Ag}}^0 - E_{\text{Au}}^0 = W_{\text{Au}} - W_{\text{Ag}} = 2.60 \text{ ev.}, \quad \dots \dots (2)$$

where the values of the binding energy are obtained from the sublimation energy and the atomic ionization energy (Landolt Börnstein 1936). If the square-hole potential

$$\begin{aligned} U(r) &= E_{\text{Ag}}^0 & r > r_0 (&= 1.59 \times 10^{-8} \text{ cm.}) \\ &= E_{\text{Ag}}^0 - 2.60 & r < r_0 \end{aligned}$$

is taken as the effective field in which the individual electrons move, where the Au atom is supposed to be situated at the origin and r_0 is the atomic radius, the eventual distribution of electrons can be obtained very simply by the Thomas-Fermi method with the particles treated as non-interacting. The number of electrons in any volume element $d\tau$ is given by

$$\rho d\tau = (8\pi/3h^3)[2m(E_m - U(r))]^{3/2} d\tau, \quad \dots \dots (3)$$

where E_m is the energy of the highest level filled. Let ρ_0 be the density of electrons in pure Ag. Then if the metal is taken large enough, obviously

$$\rho_0 = (8\pi/3h^3)[2m(E_m - E_{\text{Ag}}^0)]^{3/2},$$

that is, the constant density outside the potential hole is identical with that of the

pure Ag metal and $E_m - E_{\text{Ag}}^0$ is equal to its maximum Fermi energy: 5.5 ev. From (3) it follows that the ratio of the density for $r < r_0$ in excess of ρ_0 to ρ_0 is given by

$$\frac{(5.5 + 2.6)^{3/2} - (5.5)^{3/2}}{(5.5)^{3/2}} = 0.78,$$

showing a considerable accumulation of charge at the Au atom. The electrostatic potential produced by the excess of charge can be calculated directly. A curve (C) giving the potential energy of an electron caused by this potential together with a curve (A) showing $(\rho - \rho_0)/\rho_0$ is plotted in figure 1. The energy is seen to rise above 10.0 ev. at the centre of the Au atom. The use of the simple square-hole potential alone as the field in which the electrons move, therefore, does not lead to a self-consistent result.

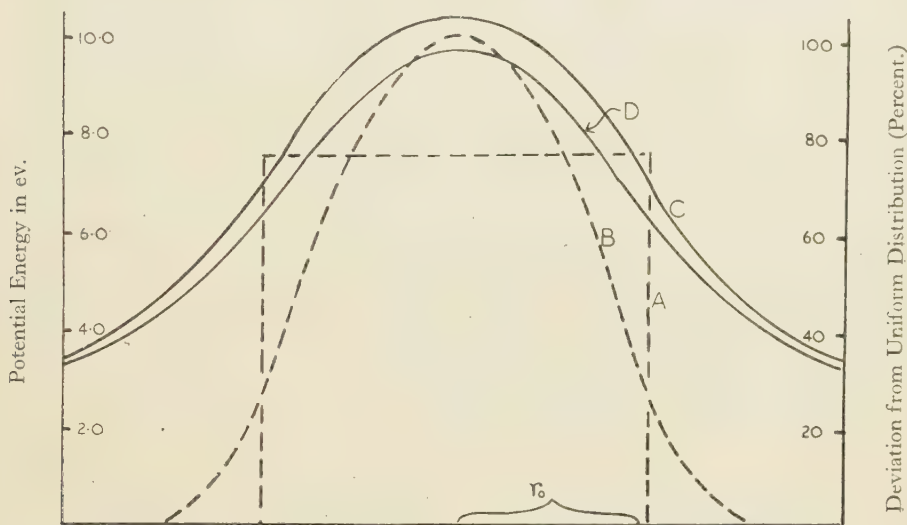


Figure 1.

- A = $\Delta\rho/\rho_0$ by Thomas-Fermi method.
- B = $\Delta\rho/\rho_0$ by wave mechanics.
- C = Potential energy due to $\Delta\rho$ by Thomas-Fermi method.
- D = Potential energy due to $\Delta\rho$ by wave mechanics.

Qualitatively it is clear that when the electronic interaction is properly considered, the potential-hole will be negatively charged due to the preferential accumulation of electrons, and its immediate neighbourhood will be positively charged to screen off the field produced by the negative centre. The rather intricate nature of this charge arrangement suggests the method of Thomas-Fermi (with interacting particles) as the suitable method to treat the problem, at least as a first approximation. To avoid excessive complication the exchange and correlational effects will not be considered, so that the Thomas-Fermi method can be used in its original form. This procedure amounts to ignoring the change in the exchange and correlational effects brought about by the change in electron density.

Since it is difficult to predict the accuracy of the Thomas-Fermi method on *a priori* grounds, the next section will be devoted to finding exact wave functions for electrons in the potential hole, and the results obtained will be compared.

Further developments in §3 concerning energy changes of these cases will be important for later discussions of the energy of cohesion in §5.

§ 2. EXACT WAVE FUNCTIONS AND CHARGE DISTRIBUTION FOR NON-INTERACTING ELECTRONS

For the present purpose it is convenient to suppose the metal to be in the form of a large sphere of silver of radius R with a single gold atom situated at its centre. The normalized wave functions of the electrons have the general form

$$N_{kl} \frac{G_{kl}(r)}{r} \Phi_{lm}(\theta\phi), \quad \dots \dots (4)$$

where $\Phi_{lm}(\theta\phi)$ is the normalized spherical harmonic for a state with orbital quantum number l and azimuthal quantum number m . N_{kl} is the normalization factor for G_{kl} which satisfies the radial wave equation (e.g. Mott and Massey 1933, p. 22)

$$\begin{aligned} \frac{d^2 G_{kl}}{dr^2} + \left(k'^2 - \frac{l(l+1)}{r^2} \right) G_{kl} &= 0 & r < r_0, \\ \frac{d^2 G_{kl}}{dr^2} + \left(k^2 - \frac{l(l+1)}{r^2} \right) G_{kl} &= 0 & r > r_0, \end{aligned} \quad \dots \dots (5)$$

where

$$\frac{\hbar k'^2}{2m} = E - E_1, \quad \frac{\hbar^2 k^2}{2m} = E - E_2$$

denote respectively the kinetic energies in the two regions. Here, for simplicity, E_1, E_2 will be written in place of E_{Au}^0 and E_{Ag}^0 .

The solution of (5) that is regular at the origin is

$$\begin{aligned} G_{kl}(r) &= A \sqrt{r} J_{l+1/2}(k'r) & r < r_0 \\ &= B \sqrt{r} J_{l+1/2}(kr) + C \sqrt{r} J_{-(l+1/2)}(kr) & r > r_0, \end{aligned} \quad \dots \dots (6)$$

$J_{l+1/2}, J_{-(l+1/2)}$ are the Bessel functions of half odd-integer orders. Since G_{kl} and dG_{kl}/dr are continuous at $r=r_0$, the ratio of the constants A, B, C , is fixed so that only a multiplying constant is left arbitrary. To define this, let $G_{kl}(r)$ have the asymptotic form at infinity

$$G_{kl}(r) \sim \left(\frac{2}{\pi k} \right)^{1/2} \sin(kr - \frac{1}{2}l\pi + \eta_{kl}). \quad \dots \dots (7)$$

Then if the radius of the sphere R is taken sufficiently large,

$$\begin{aligned} (N_{kl})^{-2} &\simeq \frac{2}{\pi k} \int_0^R \sin(kr - \frac{1}{2}l\pi + \eta_{kl}) dr \\ &\simeq \frac{R}{\pi k}, \end{aligned} \quad \dots \dots (8)$$

which determines N_{kl} .

For the state represented by (4) to be a stationary state, the condition

$$G_{kl}(R) = 0$$

has to be fulfilled. When R is large (7) may be used. Thus

$$kR = n\pi - \left(\eta_{kl} - \frac{l\pi}{2} \right), \quad \dots \dots (9)$$

where n is an integer. From (9) it follows that the number of states with definite values of l , m , and with k in the interval k to $k+dk$, is given by

$$\frac{2R}{\pi} dk. \quad \dots \dots (10)$$

The factor 2 allows for the two states of spin. With (8) and (10) the electron density can be written down directly in terms of $G_{kl}(r)$. Since the solution corresponding to G_{kl} , where the gold atom is replaced by a silver atom is just $\sqrt{r}J_{l+1/2}(kr)$, which satisfies (7), it is seen that the change in density is given by

$$\begin{aligned}\Delta\rho &= 2 \sum_l \left\{ \sum_{l=-m}^m \Phi_{lm}^*(\theta\phi) \Phi_{lm}(\theta\phi) \right\} \int_0^{k_m} \left(\frac{G_{kl}^2(r)}{r^2} - \frac{J_{l+1/2}^2(kr)}{r} \right) k dk \\ &= \frac{1}{2\pi} \sum_l (2l+1) \int_0^{k_m} \left(\frac{G_{kl}^2(r)}{r^2} - \frac{J_{l+1/2}^2(kr)}{r} \right) k dk,\end{aligned} \quad \dots \dots (11)$$

k_m is the wave number corresponding to the highest filled state. Owing to the complicated natures of the coefficients A , B , C , involved in G_{kl} , the integral can only be evaluated numerically. The result is shown in figure 1, curve B. The Coulomb energy of an electron due to this excess charge density has been worked out from this curve by numerical methods and the result is represented by curve D in the same figure. Owing to the discontinuous nature of the density function as given by the Thomas-Fermi method, the general agreement between A and B is as good as can be expected. The potential is not discontinuous, and the agreement between C and D is remarkably close. Since the case treated actually involves a discontinuous drop in the potential, and since nevertheless the simple Thomas-Fermi method still yields reasonably good results, it seems reasonable to believe that the method will in general lead to fairly reliable conclusions.

§ 3. ENERGY CHANGES IN THE CASE OF HYPOTHETICAL NON-INTERACTING ELECTRONS

It is well known that the Thomas-Fermi method fails generally to take account of the kinetic energy associated with rapid variation in electron density and gives too low a value for the energy when rapid changes in potential are involved. As the square hole potential will still be used in the discussion on cohesive energy, it is important to be able to estimate the inaccuracy caused by its discontinuous change in potential, and to correct for it. The most direct, and probably the best, course is to calculate the energy change caused by the presence of the Au atom in the hypothetical case that has been treated by both methods and use the difference to correct for the inaccuracy in later discussions.

In the Thomas-Fermi method the average energy of an electron in any particular volume element is taken to be the sum of the potential energy at this point and $3/5$ the maximum kinetic energy. As ρ_0 corresponds to just one electron per atom, it follows from § 1 that the number of electrons in the gold sphere is given by $(8.1/5.5)^{3/2}$, and the total energy of these electrons is

$$\left(\frac{8.1}{5.5} \right)^{3/2} \left(\frac{3}{5} \times 8.1 + E_1 \right). \quad \dots \dots (12)$$

Of these, for a pure metal, one electron is normally in the same sphere and the others are to be regarded as drawn from the top of the Fermi distribution of the

whole metal, so that the other electrons might be regarded as not perturbed by the presence of the Au atom. Therefore the energy of the "same" electrons, before the Au atom ion replaces the Ag ion, is

$$\frac{3}{5} \times 5.5 + \left[\left(\frac{8.1}{5.5} \right)^{3/2} - 1 \right] \times 5.5 + \left(\frac{8.1}{5.5} \right)^{3/2} \times E_2. \quad \dots \dots (13)$$

Subtracting (13) from (12), and using the value $E_2 - E_1 = 2.60$ ev. as given by (2), the following value for the energy change is obtained

$$-3.59 \text{ ev.}$$

A more significant quantity is given by

$$-3.59 - (E_1 - E_2) = -0.99 \text{ ev.}, \quad \dots \dots (14)$$

which is the energy change accompanying the transfer of one gold atom from bulk gold to pure silver in this hypothetical case.

The energy change corresponding to the rigorous treatment in §2 can be expressed in terms of the phase shifts η_{kl} introduced in (7). We recall that the solution corresponding to $G_{kl}(r)$, before the Au atom replaces the Ag at the origin is $\sqrt{r} J_{l+1/2}(kr)$, so that the phase shifts are originally zero. It then follows from (9) that if R is taken to be very large, the value of k corresponding to the same quantum number n is altered by the infinitesimal amount

$$dk = -\eta_{kl}/R,$$

when the Au atom is introduced. Accordingly, the change in energy is given by

$$d\left(\frac{\hbar^2 k^2}{2m}\right) = -\frac{\hbar^2 k}{m} \frac{\eta_{kl}}{R},$$

which is independent of the azimuthal quantum number, so that on summing over all the filled states with the help of the density of states given by (10), the total energy change is obtained in the form of a sum of integrals

$$-\left(\frac{\hbar^2}{m\pi}\right) \Sigma 2(2l+1) \int_0^{k_m} k \eta_{kl} dk. \quad \dots \dots (15)$$

In connection with the evaluation of the expression (15), a simple and rather interesting identity may be deduced, which makes it possible to obtain a result of the desired degree of accuracy without numerical work involving terms with $l \geq 2$, so that the necessary values of η_{kl} can be taken directly from results obtained in working out the last section.

It is well known from the theory of collisions that an approximation to η_{kl} is given by (Mott and Massey 1933, p. 28)

$$\eta_{kl} \approx -\frac{\pi m}{\hbar^2} \int_0^{\infty} U(r) (J_{l+1/2}(kr))^2 r dr, \quad \dots \dots (16)$$

where $U(r)$ is the perturbing potential which vanishes at infinity, so that

$$\begin{aligned} U(r) &= -\Delta E = -(E_2 - E_1) & r < r_0 \\ &= 0 & r > r_0 \end{aligned} \quad \dots \dots (17)$$

in the present case. Substituting (16), (17) into (15), the following approximate value for the change of energy is obtained:

$$-\Delta E \Sigma 2(2l+1) \int_0^{k_m} k dk \int_0^{r_0} (J_{l+1/2}(kr))^2 r dr. \quad \dots \dots (18)$$

On the other hand, on using the expansion (Watson 1944)

$$e^{ikr} = \left(\frac{\pi}{2kr}\right)^{1/2} \sum_{l=0}^{\infty} i^l (2l+1) P_l(\cos \theta) J_{l+1/2}(kr),$$

it is easily established after integration over θ that

$$\left. \begin{aligned} \frac{4\pi r_0^3}{3} &= \int_{\text{atomic sphere}} e^{-ikr} \times e^{ikr} dr \\ &= \frac{\pi^2}{k} \sum 2(2l+1) \int_0^{r_0} r (J_{l+1/2}(kr))^2 dr. \end{aligned} \right\} \dots\dots\dots (19)$$

On substituting (19) in (18), the following identity is obtained:

$$\left. \begin{aligned} -\Delta E \sum 2(2l+1) \int_0^{k_m} dk \int_0^{r_0} (J_{l+1/2}(kr))^2 r dr \\ = -\Delta E \left(\frac{4}{9\pi}\right) (k_m r_0)^3 = -\Delta E, \end{aligned} \right\} \dots\dots\dots (20)$$

where use is made of the fact that the distribution corresponds to a density of one electron per atomic sphere. (20) states the fact that when the approximation (16) for η_{kl} is used, the energy change obtained is just $-\Delta E$, the value that would have been obtained if the first-order perturbation theory had been used.

We use this result in the following way. We desire to find the change in energy using exact values of η_{k0} , η_{k1} only. With the help of (20), the change of energy can then be written as

$$\begin{aligned} -\Delta E + \Delta E \left[2 \int_0^{k_m} k dk \int_0^{r_0} (J_{1/2}(kr))^2 r dr + 6 \int_0^{k_m} k dk \int_0^{r_0} (J_{3/2}(kr))^2 r dr \right] \\ - \frac{\hbar^2}{2m} \left[2 \int_0^{k_m} k \eta_{k0} dk + 6 \int_0^{k_m} k \eta_{k1} dk \right], \end{aligned} \dots\dots\dots (21)$$

which corresponds to (15), but with values of η_{kl} given by (16) for $l \geq 0$. The integrals in the second term can be expressed in terms of the Si functions (Jahnke and Emde 1945) and the integrals in the third term are evaluated by numerical integrations. The result is

$$-\Delta E + \Delta E(0.957) - 3.18 = -3.29 \text{ ev.}$$

The first two terms together give the total contribution of all states with $l \geq 2$. It has the very small value 0.11 ev.; the assumption that deviations from (16) could be ignored for states with $l \geq 2$ is therefore justified. The more significant quantity corresponding to (14) of the Thomas-Fermi method (the heat of mixing) is in this case

$$-3.29 + \Delta E = -0.69 \text{ ev.} \dots\dots\dots (22)$$

Comparison of (22) with (14) shows that the energy value given by the Thomas-Fermi method is too low by 0.30 ev. Although the discrepancy is not very great, considering the abrupt change in the potential, it is, however, clear that the conclusions regarding cohesive energy developed in later sections cannot be expected to be more than semi-quantitative. For the ultimate quantity of interest (heat of mixing) corresponding in the real case to (22) and (14) in the above hypothetical case should be of the order 0.1–0.2 ev. So the correction of 0.30 ev. is by comparison very considerable.

§ 4. APPLICATION OF THE THOMAS-FERMI METHOD
TO THE ACTUAL CASE

The considerations of § 1 show that it is necessary to take electronic interaction properly into account to obtain a self-consistent result. The square-hole potential describes the difference of the ionic field within the atomic sphere of the gold atom from that of the rest; so that if the electron cloud were uniform, it would be the effective potential in which the electrons move. Therefore, in order to treat the actual case, a natural procedure would be to take the potential as the superposition of the square-hole potential and that produced by a uniform space distribution of positive charge that would neutralize the electronic charge completely if the latter were uniformly distributed. Let (Ur) be the square hole potential as already given by (17) and $V(r)$, $-e$ be respectively the electrostatic potential and the electronic charge. The density of electrons at any point is then $(8\pi/3h^3)[2m(E_m - U + Ve)]^{3/2}$, which leads to the following Poisson's equation for V :

$$\nabla^2 V = -4\pi\rho = \frac{32\pi^2 e}{3h^3} [2m(E_m - U + eV)]^{3/2} - \frac{3e}{r_0^3}, \quad \dots \dots (23)$$

for the positive charge density is $e(4\pi r_0^3/3)^{-1}$. Equation (23) can be simplified by introducing the dimensionless quantities

$$\left. \begin{aligned} g &= (E_m - U(r) + eV(r))/E_F, \\ \xi &= r/(r_0 E_F / 3e^2)^{1/2} r_0, \end{aligned} \right\} \dots \dots (24)$$

where

$$E_F = \left(\frac{9\pi}{4}\right)^{2/3} \frac{\hbar^2}{2mr_0^2}$$

is the maximum kinetic energy of a free electron gas of the same average density. In terms of (24), (23) becomes

$$\frac{1}{\xi^2} \frac{d}{d\xi} \left(\xi^2 \frac{dg}{d\xi} \right) = g^{3/2} - 1. \quad \dots \dots (25)$$

Introducing f defined by

$$f(\xi) = \xi g(\xi), \quad \dots \dots (26)$$

(25) reduces to

$$\frac{d^2 f}{d\xi^2} = \xi \left[\left(\frac{f}{\xi} \right)^{3/2} - 1 \right]. \quad \dots \dots (27)$$

Since the change in electron density is small compared with the average density, it is advantageous to introduce $\Delta(\xi)$ defined by

$$f(\xi) = \xi + \Delta(\xi). \quad \dots \dots (28)$$

In all cases treated, Δ/ξ can be treated as small and it is sufficient to solve (27) to the second approximation. We thus substitute (28) in (27) and expand $f^{3/2}$ in powers of Δ/ξ to the third term. The result is

$$\frac{d^2 \Delta}{d\xi^2} = \frac{3}{2} \Delta + \frac{3}{8} \frac{\Delta^2}{\xi}. \quad \dots \dots (29)$$

Before solving (29) it is useful first to examine the boundary conditions to be satisfied by Δ . As Δ must tend to zero as ξ tends to infinity, it is clear from (29) that Δ must have the asymptotic form

$$\Delta \sim Ae^{-\sqrt{3/2}\xi}, \quad \dots \dots (30)$$

where A is an arbitrary constant.

At the origin, as the charge density must be finite, it follows directly from Gauss's law that

$$\frac{dV}{dr} \rightarrow 0 \quad \text{as} \quad r \rightarrow 0,$$

and hence that

$$\frac{dg}{dr} \rightarrow 0.$$

Therefore it follows that

$$\Delta \rightarrow \xi \frac{d\Delta}{d\xi} \quad \text{and} \quad \frac{d\Delta}{d\xi} \rightarrow g - 1.$$

Since $g - 1$ must remain finite, it is necessary that

$$\Delta(\xi) \rightarrow 0 \quad \text{as} \quad \xi \rightarrow 0. \quad \dots \dots \dots (31)$$

Therefore in the solution at the origin only one arbitrary constant remains, defined by

$$B = \left(\frac{d\Delta}{d\xi} \right)_{\xi=0},$$

which, together with the arbitrary constant A in the asymptotic solution at infinity, is to be determined by the boundary conditions on the surface of the atomic sphere $\xi = \xi_0$. On this surface the electrostatic potential and field must be continuous. It follows that

$$\begin{aligned} \Delta_2(\xi_0) - \Delta_1(\xi_0) &= \xi_0(g_2(\xi_0) - g_1(\xi_0)) = \xi_0 \frac{(U_1(\xi_0) - U_2(\xi_0))}{E_F} = \xi_0 \frac{E_1 - E_2}{E_F}, \\ \left(\frac{d\Delta_2}{d\xi} \right)_{\xi_0} - \left(\frac{d\Delta_1}{d\xi} \right)_{\xi_0} &= (g_2(\xi_0) - g_1(\xi_0)) + \xi_0 \left(\left(\frac{dg_2}{d\xi} \right)_{\xi_0} - \left(\frac{dg_1}{d\xi} \right)_{\xi_0} \right) \\ &= U_1(\xi_0) - U_2(\xi_0) = \frac{E_1 - E_2}{E_F}, \end{aligned} \quad \dots \dots \dots (32)$$

where the suffixes 1 and 2 indicate the limiting value for $\xi < \xi_0$ and $\xi > \xi_0$ respectively. (32) will determine A and B , which are left arbitrary in (30) and (31).

Let $\phi(\xi)$ be a solution of the homogeneous part of equation (29), so that

$$\frac{d^2\phi}{d\xi^2} = \frac{3}{2}\phi. \quad \dots \dots \dots (33)$$

Construct the integral

$$\int_{\xi_1}^{\xi_2} \left(\phi \frac{d^2\Delta}{d\xi^2} - \Delta \frac{d^2\phi}{d\xi^2} \right) d\xi.$$

A simple application of Green's theorem leads, with the help of (29) and (3), to the following relation:

$$\left(\phi \frac{d\Delta}{d\xi} - \Delta \frac{d\phi}{d\xi} \right) \Big|_{\xi_1}^{\xi_2} = \frac{3}{8} \int_{\xi_1}^{\xi_2} \phi \frac{\Delta^2}{\xi} d\xi, \quad \dots \dots \dots (34)$$

which makes it possible to give explicitly the value of Δ and $d\Delta/d\xi$ at any value of ξ , both for $\xi > \xi_0$ and $\xi < \xi_0$, in terms of the constants A , B in (30) and (31) and the integral involving the small quantity of second order Δ^2/ξ^2 . For the region $\xi > \xi_0$, it is only necessary to take $\xi_2 = \infty$, $\xi_1 = \xi$ and put ϕ equal to $e^{\sqrt{3/2}\xi}$ and $e^{-\sqrt{3/2}\xi}$ successively. The limit on the left-hand side at ξ_2 is determined with the help of (30) and two linear equations are thus obtained with Δ and $d\Delta/d\xi$ as unknown

and may be readily solved. For $\xi < \xi_0$ the procedure is similar, the only difference being that ξ_1 is taken to be at the origin and (31) is used accordingly. A first approximation to Δ involving only the constant A or B may be obtained by leaving out the integral involving Δ^2/ξ . When these first approximations are used for Δ in the integral, Δ and $d\Delta/d\xi$ are obtained in an explicit form to the second approximation. The following are these solutions:

$$\begin{aligned} \xi > \xi_0 \quad \Delta &= \frac{1}{2a} \left\{ 2aAe^{-\alpha\xi} + \frac{3A^2}{8} [e^{\alpha\xi} Ei(-3a\xi) - e^{-\alpha\xi} Ei(-a\xi)] \right\}, \\ \frac{d\Delta}{d\xi} &= \frac{1}{2} \left\{ -2aAe^{-\alpha\xi} + \frac{3A^2}{8} [e^{\alpha\xi} Ei(-3a\xi) + e^{-\alpha\xi} Ei(-a\xi)] \right\}. \end{aligned} \quad \dots \quad (35)$$

$$\begin{aligned} \xi < \xi_0 \quad \Delta &= \frac{1}{2} \left\{ 2B \sinh \gamma \xi + \frac{B^2}{4} \left[e^{\alpha\xi} \int_0^{\alpha\xi} e^{-x} \frac{\sinh^2 x}{x} dx - e^{-\alpha\xi} \int_0^{\alpha\xi} e^x \frac{\sinh^2 x}{x} dx \right] \right\}, \\ \frac{d\Delta}{d\xi} &= \frac{1}{2} \left\{ 2B \cosh \gamma \xi + \frac{B^2}{4} \left[e^{\alpha\xi} \int_0^{\alpha\xi} e^{-x} \frac{\sinh^2 x}{x} dx - e^{-\alpha\xi} \int_0^{\alpha\xi} e^x \frac{\sinh^2 x}{x} dx \right] \right\}, \end{aligned} \quad \dots \quad (36)$$

where for brevity α is used for $\sqrt{3/2}$, and

$$-Ei(-x) = \int_x^\infty \frac{e^{-x}}{x} dx.$$

(35) and (36) are not particularly convenient to give the general form of Δ , but they make it possible to determine directly A , B from the boundary conditions (32). Once they are determined, a single numerical integration of equation (27) provides the complete solution in numerical form and serves furthermore to check the accuracy of (35) and (36). The constants determined are

$$A = -5.50, \quad B = 0.1122.$$

The error in Δ , Δ' is less than 1% and is accordingly smaller in f and g . The total effective electronic potential energy as function of ξ calculated from the numerical solution is represented in figure 2. In the same figure is also shown the corresponding distribution of charge. It is seen that the qualitative feature of the charge distribution is just as expected, a negatively charged core surrounded by an equal amount of positive charge in its immediate neighbourhood. The effect on the potential is to fill up the potential hole to a very considerable extent and should tend to reduce the electrical resistance; this will be discussed quantitatively in § 6.

§ 5. HEAT OF SOLUTION OF A DILUTE SOLUTION OF Au IN Ag

The heat of solution is a convenient measure for the cohesion of an alloy. For a dilute solution of Au in Ag, it is the energy change accompanying the transfer of one gold atom from bulk gold into bulk silver. First consider the energy change in the system, when an Ag ion in pure bulk Ag is replaced by an Au ion. The interaction of positive ions is not altered and may be left out of our consideration. If one adds up the energies of the electrons regarded as moving in the permanent field $U - eV$, one counts the Coulomb energy of the electron cloud twice over, so the energy of the system is obtained by subtracting from the sum of the electron energies the Coulomb energy of the electron cloud. Because of the spherical symmetry, for purpose of calculating change of energy it is only necessary

to consider the electrons in a finite sphere of radius R if R is taken large enough. Therefore the energy change is given by

$$\lim_{R \rightarrow \infty} \int \rho \left\{ \frac{3}{5}(E_m - U + eV) + (U - eV) - \frac{-e}{2} \left[V - \frac{3e}{r_0^3} \left(\frac{R^2}{2} - \frac{r^2}{6} \right) \right] \right\} dr - \int \rho_0 \left\{ \frac{3}{5} E_F + E_1 - \frac{-e}{2} \left[- \frac{3e}{r_0^2} \left(\frac{R^2}{2} - \frac{r^2}{6} \right) \right] \right\} dr. \quad \dots \dots (37)$$

The first integral corresponds to the solution after the Au replaces the Ag ion and the second integral corresponds to the pure Ag. In both integrals, the three terms give respectively the kinetic energy, potential energy and half of the Coulomb energy due to the electron cloud alone. In (37) the Coulomb potential due to the

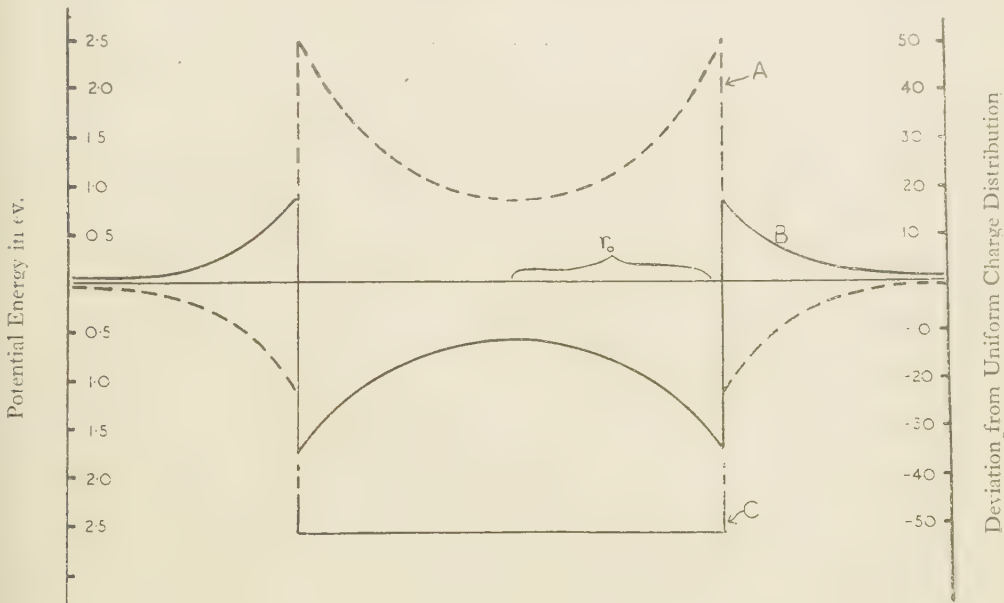


Figure 2.

A = Deviation from uniform charge = $\Delta\rho/\rho_0$.

B = Potential energy curve $U - eV$.

C = Original potential hole.

electron cloud alone has been obtained by subtracting from the total Coulomb potential V , the potential produced by the uniform positive charge, namely

$$\frac{3e}{r_0^3} \left(\frac{R^2}{2} - \frac{r^2}{6} \right).$$

Expressing (37) in terms of the dimensionless quantities g and ξ , and making use of the fact that the solution satisfying (30) corresponds to a neutral distribution

$$\lim_{R \rightarrow \infty} \int_0^R (g^{3/2} - 1) dr = 0, \quad \dots \dots (38)$$

(37) becomes

$$3E_1 \left(\frac{1}{\xi_0} \right)^3 \lim_{R \rightarrow \infty} \int_0^R \xi^2 d\xi \left\{ g^{3/2} \left(\frac{g}{10} + \frac{U - E_1}{2E_1} + \frac{\xi^2}{12} \right) - \left(\frac{1}{10} + \frac{\xi^2}{12} \right) \right\}, \quad \dots \dots (39)$$

which leads to

$$3E_F \left(\frac{1}{\xi_0} \right)^3 \lim_{R \rightarrow \infty} \int_0^R \left\{ \frac{\xi^2}{10} (g-1) + \frac{\xi^2(U-E_1)}{2E_F} + \frac{d}{d\xi} \left(\xi \frac{dg}{d\xi} \right) \left(\frac{g}{10} + \frac{U-E_1}{2E_F} + \frac{\xi^2}{12} \right) \right\} d\xi,$$

on account of (25). The integral can be simplified by integration by parts. It is to be noted that both g and U are discontinuous at ξ_0 , so the integration has to be carried out in two sections. Then after a certain amount of manipulation with the help of the boundary conditions satisfied by g , most particularly those at ξ_0 as given by (32), the following expression is obtained :

$$(E_1 - E_2) - 3\xi_0^{-3} \left\{ \frac{2}{5} (E_2 - E_1) \xi_0^2 \left(\frac{dg}{d\xi} \right)_{\xi_0} + \frac{1}{10} \int_0^\infty \xi^2 \left(\frac{dg}{d\xi} \right)^2 d\xi - \frac{3}{5} \int_0^\infty \xi^2 (g-1) d\xi \right\}. \quad \dots \dots (40)$$

This expression gives the energy change when a gold atom is substituted for a silver atom.

The most important feature of (40) is the fact that $(E_1 - E_2)$ is naturally separated out from the rest. It is the energy change that would be obtained if the electronic wave functions were not distorted by the potential hole; and at the same time, it is, according to (1), the energy difference between a metallic Au atom and a metallic Ag atom (i.e. average energy per atom in bulk material), so it leaves the rest of (40), namely

$$3\xi_0^{-3} \left\{ \frac{2}{5} (E_2 - E_1) \xi_0^2 \left(\frac{dg}{d\xi} \right)_{\xi_0} + \frac{1}{10} \int_0^\infty \xi^2 \left(\frac{dg}{d\xi} \right)^2 d\xi - \frac{3}{5} \int_0^\infty \xi^2 (g-1) d\xi \right\}, \quad \dots \dots (41)$$

as the heat of formation per atom of Au in Ag. This is a very small quantity compared with $(E_1 - E_2)$, so the natural separation of $(E_1 - E_2)$ is of considerable significance in the actual evaluation of the heat of formation. The last integral in (41) contains an integrand which takes on both negative and positive values and nearly cancels out when integrated over the whole range. It is, however, possible to make use of (38) and obtain an approximate but more convenient expression for it of sufficient accuracy. If we write (38) as

$$\begin{aligned} 0 &= \int_0^\infty \xi^2 d\xi (g^{3/2} - 1) \\ &= \int_0^\infty \xi^2 d\xi \left[\left(1 + \frac{\Delta}{\xi} \right)^{3/2} - 1 \right] \simeq \int_0^\infty \left[\frac{3}{2} \frac{\Delta}{\xi} + \frac{3}{8} \left(\frac{\Delta}{\xi} \right)^2 \right] \xi^2 d\xi \end{aligned}$$

or

$$\int_0^\infty (g-1) \xi^2 d\xi = \int_0^\infty \left(\frac{\Delta}{\xi} \right) \xi^2 d\xi \simeq -\frac{1}{4} \int_0^\infty \xi^2 \left(\frac{\Delta}{\xi} \right)^2 d\xi = -\frac{1}{4} \int_0^\infty \xi^2 (g-1)^2 d\xi, \quad \dots \dots (42)$$

we introduce an error less than 1% in (41). Thus (41) becomes

$$-3\xi_0^{-3} \left\{ \frac{2}{5} (E_2 - E_1) \xi_0^2 \left(\frac{dg}{d\xi} \right)_{\xi_0} + \frac{1}{10} \int_0^\infty \xi^2 \left(\frac{dg}{d\xi} \right)^2 d\xi + \frac{3}{2} \int_0^\infty \xi^2 (g-1)^2 d\xi \right\}. \quad \dots \dots (43)$$

The integrand is now always positive and is convenient for evaluation, and furthermore, it shows quite generally that the heat of solution must always be positive. The use of the numerical solution obtained in the last section gives the value 0.45 ev. Applying the correction to take account of the kinetic energy associated

with the rapid change of potential of the potential hole obtained in § 3, the value 0.15 ev. is obtained. The value obtained by extrapolation to infinite dilution of Wachter's data (1932) from measurements made on electrochemical cells is 0.13 ev. The agreement is close. In view of the considerable correction that has to be made, however, the value 0.15 ev. should probably not be taken as more than an indication of the order of magnitude.

§ 6. RESIDUAL RESISTANCE

It is fairly straightforward to work out the residual resistance due to the dissolved Au atoms from the numerical solution of the field obtained in § 4 and represented in figure 2. The residual resistance is determined by the scattering of the electrons on the surface of the Fermi distribution (e.g. Mott and Jones 1936, p. 258). If the wave functions of such electrons are of the form given by (4), the equation satisfied by them is (Mott and Massey 1933, p. 22)

$$\frac{d^2G_l}{d(kr)^2} + \left(1 - \frac{U(r)}{E_F} - \frac{l(l+1)}{(kr)^2}\right) G_l = 0, \quad \dots \dots (44)$$

where $U(r)$ is the potential energy of an electron moving in the effective field, the zero being chosen so that $U(r) \rightarrow 0$ away from the Au ion. As $U(r)$ is only known in numerical form in the present case, it is very much simpler to treat this collision problem by the method of phase shifts (Mott and Massey 1933). If the phase shifts η_l are defined in terms of the asymptotic expression for G_l by (7), the scattering cross-section into a solid angle $d\omega$ is given by

$$I(\theta) d\omega = |f(\theta)|^2 d\omega, \quad \dots \dots (45)$$

where $f(\theta)$ is given by the general expansion

$$f(\theta) = \frac{1}{2ik_m} \sum_{l=0}^{\infty} (2l+1)(e^{2i\eta_l} - 1) P_l(\cos \theta). \quad \dots \dots (46)$$

The resistivity due to Au ions in a dilute solution in which the ions may be regarded as scattering electrons independently of one another, is given in terms of $I(\theta)$ by the formula (Mott 1936)

$$\rho = \frac{\hbar k_m}{e^2} x A, \quad \dots \dots (47)$$

with

$$A = \int_0^\pi (1 - \cos \theta) I(\theta) 2\pi \sin \theta d\theta,$$

where x is the atomic percent. of the Au atoms. Substituting (45), (46) and (47) and integrating over the angle θ with the help of the well known properties of the Legendre polynomials, it is found that

$$\rho = \frac{2h}{e^2 k_m} \sum_{l=0}^{\infty} [(2l+1) \sin^2 \eta_l - 2l \sin \eta_l \sin \eta_{l-1} \cos(\eta_{l-1} - \eta_l)]. \quad \dots \dots (48)$$

Owing to the somewhat larger size of the scattering centre (figure 2) as compared with the potential hole treated in § 2 and § 3, contributions from $l=2$ term are also considered. η_1 and η_2 are obtained with the first approximation given by (16) and η_0 has been obtained with better approximate methods so that the error is of the order of 1%. The values obtained are

$$\eta_0 = 0.189, \quad \eta_1 = 0.005, \quad \eta_2 = -0.025. \quad \dots \dots (49)$$

In this case η_1 is smaller than η_2 for U is partly negative and partly positive and the maximum of G_1 lies somewhere in between, whereas G_2 has its maximum entirely in the region where U is negative. Using (49) in (48) and converting the result into practical units, the following resistivity for 1% of Au atoms is obtained:

$$0.16 \text{ micro ohm cm.}$$

The agreement with the experimental value 0.38 micro ohm cm. is poor. It is particularly to be noticed that the close agreement of the potentials of the hypothetical case treated in § 1 and § 2 calculated with the Thomas-Fermi method and the rigorous method indicate clearly that the application of the statistical method to obtain the field should be almost quantitatively correct. It is, however, believed that this discrepancy does not reflect any particular inadequacy of the model used for the dissolved ion. In the first place the resistance depends on the square of the depth of the potential hole, so it is a very sensitive quantity. Secondly, it only depends on a minute fraction of the bulk of the electrons in the metal which are most likely to be affected by the zone structure. Furthermore, it should be remarked that the only serious attempts at calculating theoretically the temperature dependent part of resistivity of the noble metals by Bardeen (1940) and Peterson and Nordheim (1937) show very similar discrepancies with experimental results (Bardeen's result shows almost exactly the same proportional error as the result just obtained, and Peterson and Nordheim's result is too small by a factor 2). It appears therefore reasonable to suppose that all these discrepancies are due to treating the electrons on the surface of the Fermi distribution as free.

§ 7. CONCLUSION

It is clear from the preceding considerations that when a foreign atom is dissolved in a metal, an appreciable polarization of the electron cloud will in general be caused in its immediate neighbourhood. Either a negatively charged centre is created, surrounded in its immediate neighbourhood by an equal amount of positive charge, or the reverse takes place. Any theory of cohesion must take this fact into account. Owing to the limitation of the method employed, the reasonable agreement of the result obtained in this paper with the observed value could not be looked upon as more than semi-quantitative. It is to be appreciated that the small value of the heat of solution as compared with the primary perturbation in conjunction with the delicate question of polarization makes the problem difficult to treat with great accuracy. Finally, the polarization of the charge tends to fill up irregularities in the potential that would otherwise be there. This reduces the residual resistances caused by the presence of foreign atoms very considerably. In the case treated in the paper, namely, Au in Ag, this leads to a result rather at variance with experiments but at the same time brings it into line with other theoretical works on temperature resistance, indicating therefore a general inaccuracy in treatment rather than particular inadequacy connected with the model employed in this paper to represent a foreign atom.

ACKNOWLEDGMENT

In conclusion, I should like to express my sincere thanks to Professor N. F. Mott, F.R.S., for many discussions and for his kind interest in the work.

REFERENCES

- BARDEEN, J., 1940, *J. Appl. Phys.*, **11**, 88.
 JAHNKE and EMDE, 1945, *Tables of Functions*, 4th edition (New York : Dover Publications).
Landolt-Börnstein Tables, 1936, 5th edition, 3rd supplement.
 MOTT, N. F., 1936, *Proc. Camb. Phil. Soc.*, **32**, 281.
 MOTT, N. F., and JONES, H., 1936, *Theory of Properties of Metals and Alloys* (Oxford).
 MOTT, N. F., and MASSEY, H. S. W., 1933, *Theory of Atomic Collisions* (Oxford).
 PETERSON, E. L., and NORDHEIM, L. W., 1937, *Phys. Rev.*, **51**, 335.
 SEITZ, F., 1940, *Modern Theory of Solids* (McGraw Hill).
 WACHTER, A., 1932, *J. Amer. Chem. Soc.*, **54**, 4609.
 WATSON, G. N., 1944, *Theory of Bessel Functions* (Cambridge : University Press).

Electron Momenta in Atoms

By W. E. DUNCANSON * AND C. A. COULSON †

* University College, London. † Physical Chemistry Laboratory, Oxford,
 now at King's College, London

MS. received 12 June 1947

ABSTRACT. Theoretical expressions are obtained for the momentum distribution of the electrons in atoms of different atomic number. This enables density curves to be drawn for the momentum p . The mean momentum, which is also calculated, shows a steady increase with atomic number. Finally, the new calculations of momentum distribution enable earlier work on the shape of the Compton profile to be extended from sodium to potassium, in monatomic form.

§ 1. INTRODUCTION

THE spatial distribution of electrons in an atom has been fully studied in recent years, and the use of variational methods and self-consistent-field modifications for solving the complete Schrödinger wave equation for an atom have enabled electron density curves to be drawn, in ample and satisfactory agreement with experiments using x-ray scattering. But on the other hand, the velocity distribution is relatively unknown. Yet it is, as Dirac (1947) has shown, equally fundamental. In addition, as Jauncey and DuMond (DuMond 1933) have explained, it is the velocity distribution which determines the shape of the Compton line in x-ray scattering; and, as Hughes has demonstrated both experimentally and theoretically (e.g. Hughes and Mann, 1938) this velocity distribution also describes the inelastic scattering of electrons. It has seemed desirable, therefore, to make explicit calculations of the velocity distribution in simple atoms ($Z < 20$); the results of such calculations are presented in this present paper.

§ 2. METHOD OF CALCULATION

Following the methods developed by the writers in a series of papers since 1941 (see Duncanson 1943 for a complete list of references), we calculate the momentum \mathbf{p} of an electron rather than its velocity. As we use atomic units throughout, the units of momentum and velocity for an electron have the same numerical value, viz. $c/137$. The distribution of \mathbf{p} for a single electron is governed by a momentum wave function $\chi(\mathbf{p})$; there is one $\chi(\mathbf{p})$ for every type of atomic

orbital, and $\chi(\mathbf{p})$ is best found from the normalized space wave function $\psi(\mathbf{r})$ by using a fundamental formula of the Dirac transformation theory:

$$\chi(\mathbf{p}) = (2\pi)^{-3/2} \int \exp(-i\mathbf{p}\cdot\mathbf{r}) \psi(\mathbf{r}) d\mathbf{r}. \quad \dots \dots (1)$$

In this form $\chi(\mathbf{p})$ is already normalized. Associated with $\chi(\mathbf{p})$ is the mean radial distribution function $I(p)$. This function is defined (Duncanson and Coulson 1945, referred to hereafter as D.C.) in such a way that $I(p) dp$ is the probability that the electron has a momentum whose magnitude, independent of direction, lies between p and $p + dp$. Evidently

$$I(p) = \int \chi(\mathbf{p}) \chi^*(\mathbf{p}) p^2 d\omega_p, \quad \dots \dots (2)$$

where the integration is taken over all values of the solid angle ω_p . In this way $I(p)$ is normalized so that

$$\int_0^\infty I(p) dp = 1. \quad \dots \dots (3)$$

The mean momentum \bar{p} for this orbital is given by

$$\bar{p} = \int_0^\infty p I(p) dp. \quad \dots \dots (4)$$

Our present calculations start with a presumed knowledge of $\psi(\mathbf{r})$ for each orbit in the atom: (1)–(3) then allow us to determine $\chi(\mathbf{p})$, $I(p)$ and \bar{p} for the separate orbits. Details of the analysis are given in § 3.

Now, if there are n electrons in an atom with coordinates $\mathbf{r}_1 \dots \mathbf{r}_n$, and momenta $\mathbf{p}_1 \dots \mathbf{p}_n$, the total wave function $\psi(\mathbf{r}_1 \dots \mathbf{r}_n)$ which describes the complete electron configuration is related to the total momentum wave function $X(\mathbf{p}_1 \dots \mathbf{p}_n)$ by a formula similar to (1) for a single electron:

$$X(\mathbf{p}_1 \dots \mathbf{p}_n) = (2\pi)^{-3n/2} \int \exp -i\{\mathbf{p}_1 \cdot \mathbf{r}_1 + \dots + \mathbf{p}_n \cdot \mathbf{r}_n\} \Psi(\mathbf{r}_1 \dots) d\mathbf{r}^n. \quad \dots \dots (5)$$

But $\Psi(\mathbf{r}_1 \dots \mathbf{r}_n)$ is the sum of one or more determinants (Slater 1929), and so, on expansion, it may be regarded as the sum of a large number of distinct terms, each of which is the product of n atomic orbitals. Since the coordinates of each electron appear once and once only in each of these terms, the integration (5) for any one term is immediate; the result is simply that which would be obtained by replacing each space atomic wave function by the corresponding momentum wave function. By addition, therefore, it follows that the complete wave function $X(\mathbf{p}_1 \dots \mathbf{p}_n)$ is formally precisely the same as $\Psi(\mathbf{r}_1 \dots \mathbf{r}_n)$ except that each space orbital is replaced by the corresponding momentum orbital calculated as in § 3.

Knowing $X(\mathbf{p}_1 \dots \mathbf{p}_n)$ the calculation of the generalized mean radial distribution function $I(p_1 \dots p_n)$ follows at once from an integration completely analogous to (2). All the terms are known, so that I is determined for all atoms.

§ 3. WAVE FUNCTIONS AND FORMULAE

For hydrogen, with only one electron, an exact space wave function $\psi(\mathbf{r})$ is known. In atomic units it is simply $(\pi)^{-1/2} e^{-r}$. For atoms in the second row of the periodic table we have used the analytical wave functions originally proposed

by Morse, Young and Haurwitz (1935) and corrected by the present writers (1944). The resulting mean radial distribution functions have been given in D.C. (p. 193) and need not be reproduced here. For the remaining atoms ($11 \leq Z \leq 20$) we have used wave functions suggested by Slater (1930); that is to say, the complete wave function for an atom is made up in the usual way (Slater, 1929) as sums of determinants in each of which the electrons are defined by atomic orbitals of the form

$$\psi_{nlm}(\mathbf{r}) = N_r N_\theta N_\phi r^{n^*-1} e^{-cr} P_l^m(\cos \theta) e^{+im\phi}. \quad \dots \dots (6)$$

The N 's are separate normalizing factors for the radial and the two angular terms in ψ , n^* is the effective principal quantum number whose value is given by Slater in terms of the true quantum number, c is a quantity related to the nuclear charge Z and the screening constant s by the formula

$$c = (Z - s) n^*. \quad \dots \dots (7)$$

In this way all the coefficients in (6) are supposed to be known.

We have also used Slater functions for some of the lighter atoms ($Z \leq 10$). The results, which we do not need to describe in detail, since they are presumably less accurate than the Morse functions, show that for these atoms there is very little difference between the momentum distributions predicted by the two types of wave function. It seems highly probable, therefore, that the same conclusion will hold for the heavier atoms ($11 \leq Z \leq 20$) for which the more detailed wave functions are not known.

The transformation from the complete space wave function for all the electrons in an atom to the complete momentum wave function requires, first of all, that we should be able to transform the individual atomic orbitals $\psi(\mathbf{r})$. This transformation from $\psi(\mathbf{r})$ to $\chi(\mathbf{p})$ proceeds as follows. Using (1) and (6):

$$\chi(\mathbf{p}) = (2\pi)^{-3/2} N_r N_\theta N_\phi \int r^{n^*-1} e^{-cr} P_l^m(\cos \theta) e^{+im\phi} e^{-i\mathbf{p}\cdot\mathbf{r}} d\mathbf{r}. \quad \dots \dots (8)$$

Now Bauer's expansion of $e^{-i\mathbf{p}\cdot\mathbf{r}}$ gives

$$e^{-i\mathbf{p}\cdot\mathbf{r}} = \sum_{j=0}^{\infty} (2j+1)(-i)^j P_j(\cos \vartheta) f_j(pr),$$

where ϑ is the angle between \mathbf{r} and \mathbf{p} , and the functions $f_j(pr)$ are defined by

$$f_0(pr) = \sin pr/pr, \quad f_j(pr) = \sqrt{(\pi/2pr)} J_{j+1/2}(pr). \quad \dots \dots (9)$$

Substitution of these values in (8) allows the integration over the solid angle $d\omega$ [$d\mathbf{r} = d\omega d\mathbf{r}$] to be made at once. And if we write p, θ_p, ϕ_p for the polar co-ordinates of \mathbf{p} , we have

$$\chi(\mathbf{p}) = (-i)^l \sqrt{(2/\pi)} N_r N_\theta N_\phi P_l^m(\cos \theta_p) e^{\pm im\phi_p} R_l(p), \quad \dots \dots (10)$$

where

$$R_l(p) = \int_0^\infty r^{n^*-1} e^{-cr} f_l(pr) r^2 dr. \quad \dots \dots (11)$$

The fact that $\chi(\mathbf{p})$ depends on angle in precisely the same way as $\psi(\mathbf{r})$ has already been noted, for hydrogen-like wave functions, by Pauling and Podolsky (1929): our argument shows it to be true for wave functions in any central field.

Using (10) and the definition (2) of $I(p)$ it follows that

$$I(p) = (2/\pi) N_r^2 p^2 R_l(p)^2, \quad \dots \dots (12)$$

where, by a simple integration it may be shown that

$$N_r^2 = (2c)^{2n^*+1} / \Gamma(2n^* + 1). \quad \dots \dots (13)$$

The calculation of $\chi(\mathbf{p})$ and $I(p)$ for any one electron now depends only on a calculation of $R_l(p)$. This must be made separately for s, p, d, \dots electrons for which $l=0, 1, 2, \dots$. If n^* is integral, as it is for the first three rows of the periodic table, the integration (11) yields algebraic functions. These functions are

$$\begin{aligned} I_{1s}(p) &= \frac{32c^5 p^2}{\pi(p^2 + c^2)^4}, & I_{2s}(p) &= \frac{32c^5 p^2(p^2 - 3c^2)^2}{3\pi(p^2 + c^2)^6}, \\ I_{2p}(p) &= \frac{512c^7 p^4}{3\pi(p^2 + c^2)^6}, & I_{3s}(p) &= \frac{1024c^9 p^2(p^2 - c^2)^2}{5\pi(p^2 + c^2)^8}, \\ I_{3p}(p) &= \frac{1024c^7 p^4(5c^2 - p^2)^2}{45\pi(p^2 + c^2)^8}, & I_{3d}(p) &= \frac{4096c^9 p^6}{5\pi(p^2 + c^2)^8}. \end{aligned} \quad \dots \dots (14)$$

Care must be exercised in this and later formulae to remember, from (7), that c has a different numerical value for each orbit in each atom, and the appropriate value must always be used in any particular case. Different values of c in any single formula, however, merely correspond to changes in scale of p .

For electrons of higher quantum number than those in (14), n^* is not integral, and the evaluation of $R_l(p)$ is more clumsy. It may be systematized most simply in terms of two new sets of functions $C(n)$ and $S(n)$, defined by

$$C(n) = \int_0^\infty r^n e^{-cr} \cos pr dr, \quad S(n) = \int_0^\infty r^n e^{-cr} \sin pr dr. \quad \dots \dots (15)$$

$C(n)$ and $S(n)$ are functions of c and p , as well as of n , and if we put

$$p = c \tan \alpha, \quad (0 \leq \alpha < \pi/2), \quad \dots \dots (16)$$

we may write

$$C(n) = \Gamma(n+1) \cos(n+1)\alpha \cos^{n+1}\alpha,$$

$$S(n) = \Gamma(n+1) \sin(n+1)\alpha \cos^{n-1}\alpha. \quad \dots \dots (17)$$

In terms of these functions it may be shown that

$$\begin{aligned} pR_0(p) &= S(n^*), \\ p^2R_1(p) &= S(n^*-1) - pC(n^*), \\ p^3R_2(p) &= 3S(n^*-2) - 3pC(n^*-1) - p^2S(n^*), \\ p^4R_3(p) &= 15S(n^*-3) - 15pC(n^*-2) - 6p^2S(n^*-1) + p^3C(n^*). \end{aligned} \quad \dots \dots (18)$$

From these relations, with (10) and (12), both $\chi(\mathbf{p})$ and $I(p)$ may be calculated for all electron orbits of s, p, d and f type. The simple results in (14) are, of course, merely particular cases of (18) and (12) in which n^* is integral.

§ 4. THE CALCULATIONS AND RESULTS

As determined above $I(p_1 \dots p_n)$ is a function of the magnitudes $p_1 \dots p_n$. The simplest way of expressing it pictorially is to integrate over all values of $p_2 \dots p_n$ from 0 to ∞ , obtaining a function $I(p_1)$, which we may call the mean

radial momentum density for electron 1. Now, by the very nature of the determinantal wave functions used (which results from the fact that all electrons are identical), $I(p_1) = I(p_2) = \dots = I(p)$, say. So we may regard $I(p)$, which is normalized to unity, as measuring the velocity distribution in the atom, just as the more familiar density $\rho(r)$ measures the space distribution. It is this quantity $I(p)$ which we have calculated.

If all the original atomic orbitals (6) are orthogonal, it follows that $I(p)$ is simply the sum of contributions such as (12) from each electron present. In our calculations for the atoms of the first two rows of the periodic table, this condition is accurately fulfilled. But for the others it is not, and although orbitals with different l values are rigorously orthogonal on account of the surface harmonic terms in (6), there is a small non-orthogonality between $1s$, $2s$, $3s$, $4s$, and between $2p$, $3p$, $4p$ etc. Calculations (D.C., p. 198) for Li and C show that the result of neglecting this non-orthogonality (which is rather clumsy to include) is to change the width of the Compton profile (§ 5) by less than 1%. Now it would be presumptuous to claim an accuracy as good as this for the initial wave functions: accordingly, for the heavier elements for which $11 \leq Z \leq 20$, we have made our calculations of $I(p)$ on the assumption that all the atomic orbitals may be regarded as orthogonal. The curves of $I(p)$, therefore, which we show in figures 1 and 2 are simply sums of curves corresponding to (14) and (18), suitably weighted according to the numbers of each type of electron present. In every case, of course,

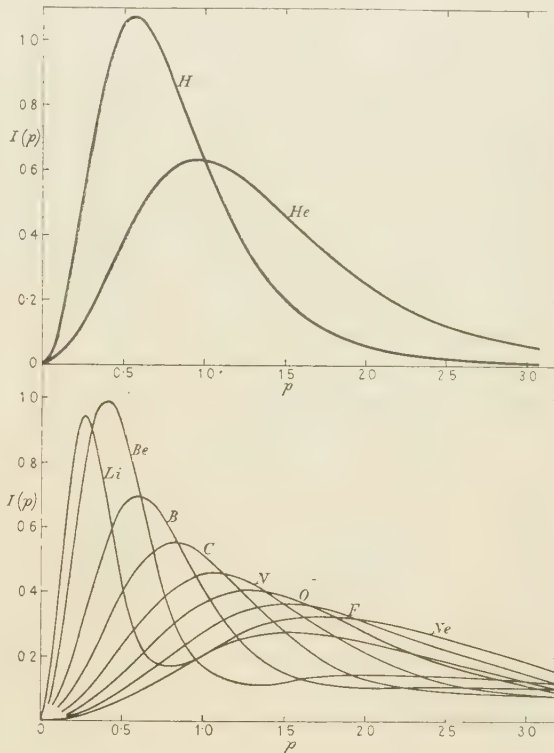


Figure 1.

$$\int_0^\infty I(p) dp = 1.$$

Certain deductions from these curves suggest themselves at once:—

(a) First of all, there is considerable resemblance between the $I(p)$ curves in figures 1 and 2 and corresponding electron density curves. For example, just as in the case of space wave functions, there are momentum shells within an atom. But the behaviour of these shells is exactly opposite to that with space functions. For as we proceed along any row of the periodic table, figures 1 and 2 show that the shells expand (instead of contracting), and when we start a new shell, it appears at the inside (instead of the outside) of the ones already there. The writers have never seen this expressly stated before, but it is implicit in the

Fourier relationship of the two types of wave function; for it is a known result that a function and its transform cannot both be made dense in any given region: and this, of course, is merely the Heisenberg Uncertainty Principle in its fundamental form.

An alternative physically significant interpretation of the behaviour of each new shell is that the electrons in the new shell are at first loosely bound, and therefore have, on the average, small momenta. As the shell is completed, the binding increases, so that the mean momentum increases also.

The steady drift to larger values of momentum with increasing nuclear charge is well illustrated by the behaviour of the $1s$ electrons. According to (14) the peak of the $1s$ curve lies at $p = c/\sqrt{3}$. But c varies from 1 for hydrogen to 18.7 for potassium, so that the peak moves steadily from 0.58 A.U. to 10.8 A.U. At the same time the height of the peak falls, for the height per electron is $27/8\pi c$. When the contributions are weighted according to the number of electrons present, this means that the maximum contribution from the $1s$ electrons falls from 1.05 for hydrogen to 0.01 for potassium. After this stage we may say that the $1s$ electrons are scarcely relevant to the density function except for very large values of p . This is quite different from the behaviour of the space wave functions, where $\psi(1s)$ crowds steadily in towards the nucleus, and may eventually be regarded as completely screening the nucleus.

(b) We also notice that s -electrons give uniformly narrower, or more compact, $I(p)$ curves than the corresponding p -electrons. This means that the alkali atoms for which the outer shell is simply s , and, even more so, the atoms of the next column of the periodic table, for which the outer shell is s^2 , show a pronounced sharp peak in the $I(p)$ curve. But progressive addition of p -electrons smoothes this out so that, for example, whereas in Li there is a very clear separation between the $2s$ and the $1s$ contributions, by the time that we have reached

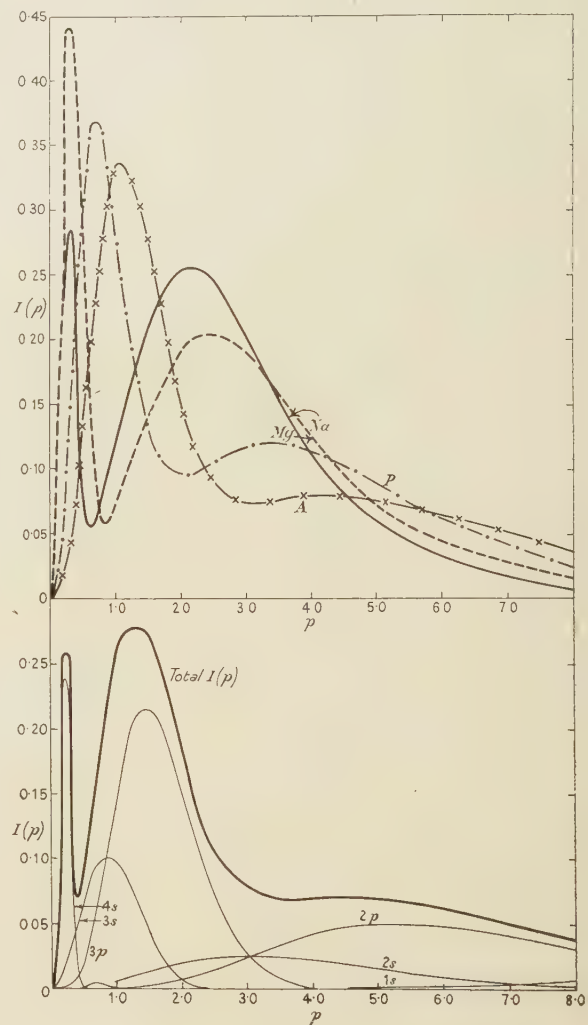


Figure 2.

carbon the distinction is obliterated and one single wider $I(p)$ curve results. There is, in fact, a gradual transition as we proceed along the second row of the periodic table from Li to Ne, and also along the third row from Na to Ar. In each case, at the beginning of the next rows (Na, K) a new inner peak of great sharpness appears.

(c) In the particular case of potassium, shown at the bottom of figure 2, we have drawn both the total $I(p)$ curve and the components, with correct weight, that comprise it. In the total curve, one can clearly distinguish the inner peak due to the $4s$ contribution, followed by a second peak arising from $3s$ and $3p$ electrons; next comes a still wider peak from the $2s$ and $2p$ electrons and there is a very low flat peak at large distances arising from the $1s$ electrons. Similar discussions could be given for the other atoms, but this sufficiently illustrates the way in which the different electrons contribute to $I(p)$.

A quantity of some importance is the mean momentum \bar{p} . According to what we have said about $I(p)$ and the formula (4), this is the sum of suitably weighted contributions $\bar{p}_{1s}, \bar{p}_{2s}, \dots$. Explicit calculation shows that

$$\bar{p}_{1s} = 8c/3\pi, \quad \bar{p}_{2s} = 8c/5\pi, \quad \bar{p}_{3s} = 128c/105\pi, \quad \bar{p}_{2p} = 128c/45\pi, \quad \bar{p}_{3p} = 9472c/4725\pi. \quad \dots \dots (19)$$

Values of \bar{p} for other orbitals may be obtained most easily by numerical integration. Figure 3 shows \bar{p} plotted against the atomic number Z . Along each row of the periodic table the variation of \bar{p} is almost linear, but the slope of each successive shell is less than the one preceding, and there is only a small change in \bar{p} on converting a rare gas to an alkali metal atom. All this is rather as one would have expected because \bar{p} must be related to the total electronic energy E in some such way as $\bar{p} \sim \sqrt{(2E/Z)}$, all in atomic units. Along each row of the periodic table there is a steady increase in E/Z , but on account of the poor binding of the one valence electron in the alkali atom, there is only a small change in E on starting a new shell.

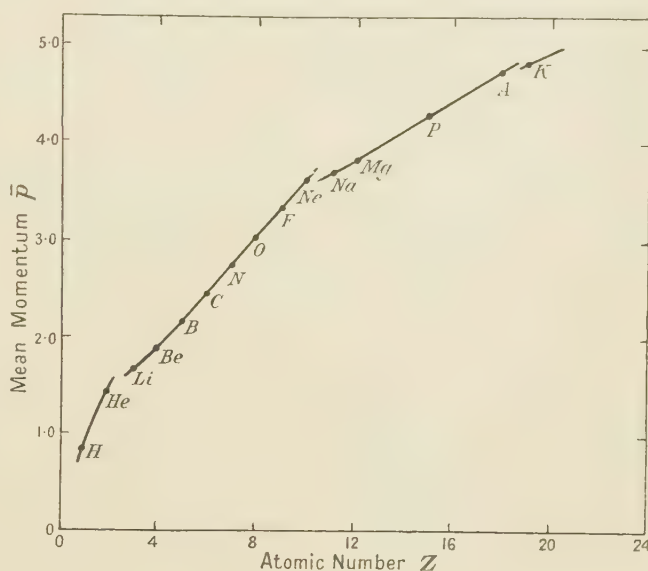


Figure 3.

§ 5. COMPTON PROFILES

It was shown in D.C. § 2 that a knowledge of $I(p)$ enables us to calculate the shape of the Compton profile. All Compton profiles for a given atom (i.e. all incident wavelengths and all angles of scatter) are included, by suitable change

of scale, in a single formula, where the intensity J at "reduced" distance q from the centre of the displaced band, is given by

$$J(q) = \frac{1}{2} \int_q^{\infty} \frac{I(p) dp}{p}. \quad \dots \dots (20)$$

Full particulars are given in D.C. and do not need to be reproduced here. In that paper $J(q)$ curves were plotted for all atoms up to Ne. Our present calculations allow us to extend this work up to K. Five representative examples, each giving one-half of the complete profile, are shown in figure 4. From these the general trend of the curves is apparent. These curves are normalized in each case so that $J(0)=0$. This, while making the areas under the curves different, greatly facilitates comparison of different profiles. In general, the behaviour of these curves agrees closely with that found for the lighter atoms in D.C., that is, s -electrons give narrow profiles and p -electrons wider ones.

Thus the sharpest curve in figure 4 is for Mg, whose outer structure is $(3s)^2$, and the widest is for A, where the outer structure is $(3s)^2(3p)^6$. In the cases of Na and Mg there is an appreciable "lag" at the bottom of the curve, similar to that found before for Li and Be; this might easily cause trouble when separating the contributions to the full experimental profile that arise from satellite lines (e.g. the $K\alpha_1$ and $K\alpha_2$ doublet) in the incident radiation.

Finally, we give below, in tabular form, the theoretical widths Δq at half-maximum value, together with the resulting Δl values, in x-ray units, for back-scattering ($\theta = 180^\circ$) of Mo $K\alpha$ radiation. This table, which may be compared exactly with table 1 in D.C., p. 195, shows again a steady increase, except for Na to Mg, along this, the third row of the periodic table, and the smaller value with which each new row begins.

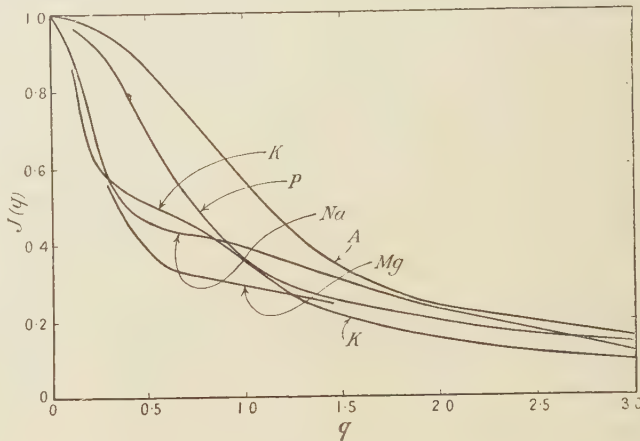


Figure 4.

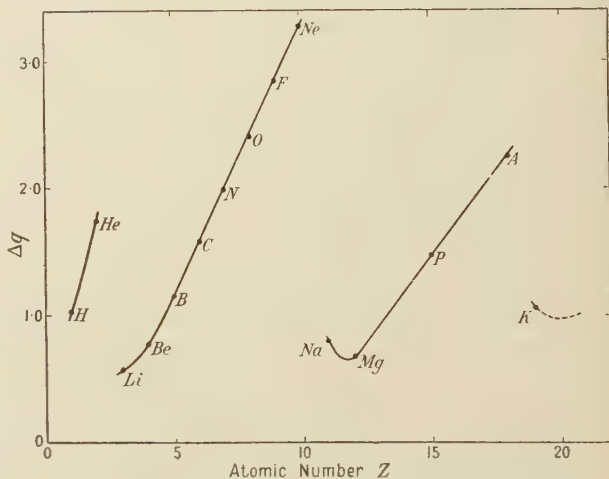


Figure 5.

Atom	Ne	Na	Mg	P	A	K
Δq	3.27	0.80	0.68	1.48	2.24	1.06
$\Delta l(\text{x.u.}) \text{ for MoK}\alpha \left\{ \begin{matrix} \\ \theta = 180^\circ \end{matrix} \right.$	34	8.3	7.1	15	23	11

Thus in the case of the Compton profile, the changes to be expected between one row of the periodic table and the next row are less than between the elements of either row alone. This is shown very clearly in figure 5, which collects together the Δq values for the atoms both of this paper and the preceding one.

REFERENCES

- DIRAC, 1947, *The Principles of Quantum Mechanics*, Chapters 3 and 4 (Oxford : University Press. Third edition).
- DUMOND, 1933, *Rev. Mod. Phys.*, **5**, 1.
- DUNCANSON, 1943, *Proc. Camb. Phil. Soc.*, **39**, 180.
- DUNCANSON and COULSON, 1944, *Proc. Roy. Soc. Edinb.*, A, **62**, 37.
- DUNCANSON and COULSON, 1945, *Proc. Phys. Soc.*, **57**, 190.
- HUGHES and MANN, 1938, *Phys. Rev.*, **53**, 50.
- MORSE, YOUNG, and HAURWITZ, 1935, *Phys. Rev.*, **48**, 948.
- PAULING and PODOLSKY, 1929, *Phys. Rev.*, **34**, 109.
- SLATER, 1929, *Phys. Rev.*, **34**, 1293.
- SLATER, 1930, *Phys. Rev.*, **36**, 57.

Some Experiments with Adjustable Geiger-Müller Counters

By MOHAMMED CHAUDHRI, Ph.D.(Cantab), M.Sc.(Alig.)*

AND A. G. FENTON, B.Sc. †

Physics Department, University, Birmingham

* Of the Muslim University, Aligarh, India. † On leave from the University of Tasmania, Australia.

MS. received 12 June 1947

ABSTRACT. Special counters are described in which it is possible to alter the effective length as well as the material and diameter of the anode without opening them. This is a distinct advantage in that the effects of these factors on the counter characteristics can be studied without complication due to changes in the gas filling and the nature of the cathode surface brought about by opening the counters or by making separate counters with anodes of different diameters.

It was observed that, while in a given counter the anode material and the nature of its surface have little or nothing to do with the characteristics, there is an optimum anode diameter for which the best plateaux are obtained, a factor of obvious practical importance in counter design.

The photosensitivity to visible light and longer wavelengths caused by high counting rates or by "continuous" discharges was shown to be due to some surface phenomenon on the cathode.

It has been shown in a simple manner that the discharge is not localized, but spreads along the length of the counter.

It was observed that the plateau length and slope improve at first, but then deteriorate when the effective length of the counter is reduced by shielding the anode wire at both ends, with glass capillary tubes. With metal capillaries, however, the plateau characteristics are best when the full length of the cathode is used.

§ 1. INTRODUCTION

MUCH work has been done on Geiger counters of the self quenching type (Korff 1946) but very few systematic investigations have been carried out which yield reliable data as to the relative importance of the various components of a counter during its operation. Moreover, there are still a number of factors influencing the plateau characteristics of counters which have not been given due consideration by previous workers.

It is the purpose of the present paper to study the effects of the following factors on the plateau characteristics:—

- (1) The material of the anode wire.
- (2) The diameter of the anode wire.
- (3) The shielding of the anode wire.
- (4) The cathode surface.

It has also been found during the course of these experiments that the cathode surface can be made photosensitive to wavelengths up to about 1 micron, and that the degree of the photosensitivity and its duration can be controlled within limits.

§ 2. APPARATUS

The experiments were performed with four counters having nickel cathodes and one counter with an aluminium cathode. The nickel cathodes were made from sheet nickel 0·1 mm. thick formed into cylinders 2·2 cm. in diameter and 10 cm. long, spot-welded along the seam. The aluminium cathode was a tube 0·1 mm. thick, 10 cm. in length and 2·0 cm. diameter. The cathodes were cleaned with nitric acid and were rinsed thoroughly with water and dried before assembly into the counters.

One of the counters with a nickel cathode has an anode made from a number of wires of different materials and of different gauges spot-welded together end to end. In the discussion which follows we shall refer to this as counter number 1 and we give below a detailed description of it and of the other counters.

The envelope of the counter is a Pyrex glass tube 60 cm. long and 2·5 cm. in diameter. The nickel cathode C, figure 1, is closely fitted into the glass envelope. Electrical connection of C with the external circuit is made by means of a nickel strip spot-welded to the cathode at one end and to the Pyrex-tungsten seal S at the other.

The anode A consists of wires of gold, silver, platinum, copper, molybdenum, tantalum and tungsten, ranging in diameter from 0·065 mm. to 0·25 mm. Any one of these wires may be set within the cathode by rotating the vacuum-tight ground-glass joints E which support the glass tubes F on which the anode is wound. The extreme ends of the anode are spot-welded to 1 mm. nickel wires which run through the glass tubes F and are held in position by the Pyrex-tungsten seals J, so that electrical connection to the anode may be made from outside the tube. The anode passes through the 2 mm. bore Pyrex capillary tubes D, each 15 cm. in length and 5 mm. in external diameter. The outer ends of the capillaries are tightly fitted into the soft iron cylinders B, each 3 cm. long and 2·3 cm. in diameter, which slide smoothly within the outer glass envelope. The weight of the glass capillaries is supported by two glass tubes G with a bore just greater than the external diameter of the capillaries, internally sealed into the envelope. The

ground-glass joints K carry thick leads L through which current may be passed to heat the anode wire when desired. The capillaries may be set in any desired position inside the cathode by moving the soft-iron cylinders from outside with the help of a magnet.

Counter 2 has a nickel cathode similar to that of number 1 but has a fixed anode of 0·2 mm. diameter tungsten wire sealed at the ends of the glass envelope, which is 45 cm. long and 2·5 cm. in diameter. The arrangement of the glass capillaries is the same as in counter 1. Counter 3 has the same construction as 2 but brass capillaries of the same dimensions as in 2 are used instead of glass. In counters 4 and 5 a single adjustable Pyrex glass capillary (15 cm. long and 5 mm. in diameter and 2 mm. bore), sliding over the 0·2 mm. tungsten anode wire is used, the motion of the capillary being controlled mechanically through a ground-glass joint. The cathodes are of the same dimensions but one is of nickel, the other of aluminium.

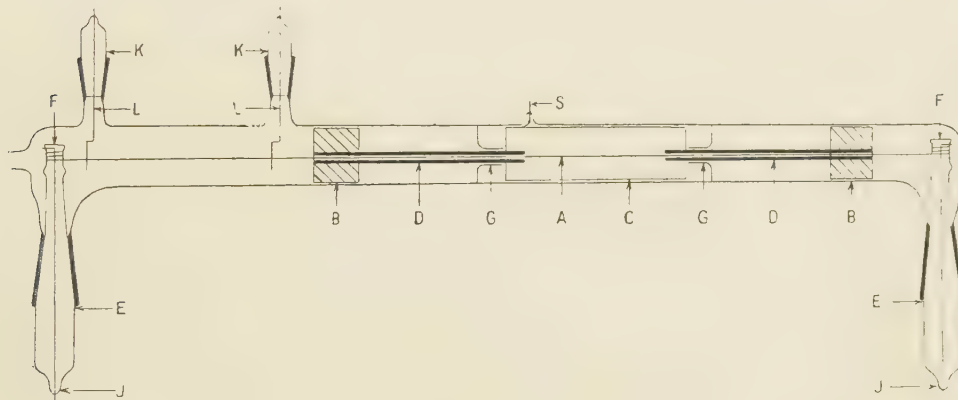


Figure 1.

The counters were evacuated with a mercury diffusion pump and were out-gassed by warming and by letting the pumps run continuously for several hours. The counters were tested for vacuum tightness by allowing them to stand under vacuum for several days.

The gas filling used was an argon-alcohol mixture which was allowed to stand in a flask for over 24 hours to mix thoroughly before being admitted to the counters.

Counters 1, 2 and 3 were filled with the same argon-alcohol mixture containing 23% alcohol, to a pressure of 10 cm. Hg. Counter 2 had been used previously with fillings of different gases but 1 and 3 were new. Counters 4 and 5 were filled with an argon-alcohol mixture containing 10% alcohol, to 10 cm. total pressure. Once filled to the desired pressure the counters were not opened or refilled during the experiments described below.

No wax joint was used in any part of the counters or apparatus and the grease used for the taps and ground-glass joints was apiezon M.

A scale-of-100 recorder was used to record the counts, and the potentials for the counters were obtained from a stabilized H.T. set giving up to 1650 volts.

§ 3. RESULTS

Effective length and plateau characteristics

Preliminary experiments with counters 4 and 5 indicated that the distance between the ends of the capillary tubes within the cathode determines the effective length of the counter. Moreover, it was observed that the plateau slope improved when the effective anode length was reduced by sliding the capillary into the cathode. Detailed measurements were

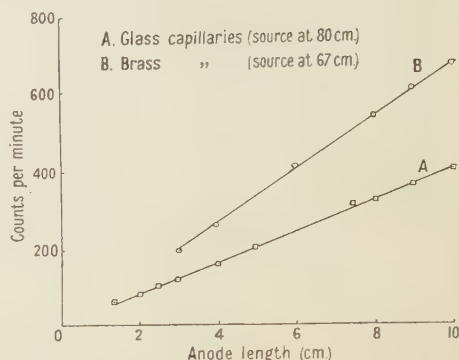


Figure 2.

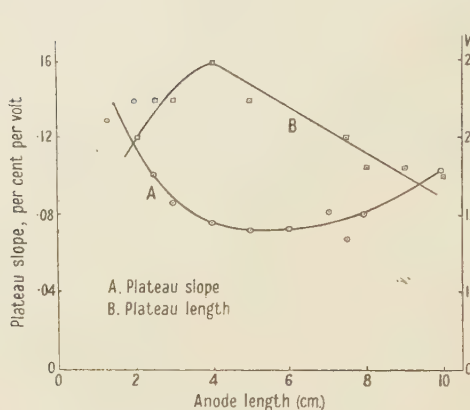


Figure 3.

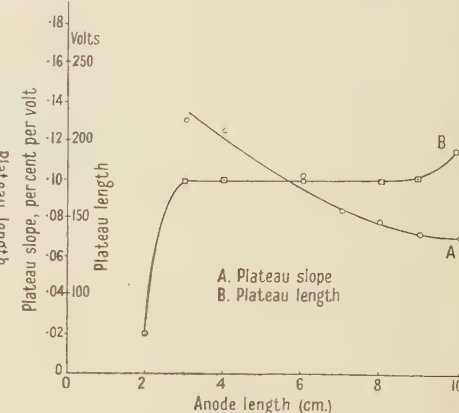


Figure 4.

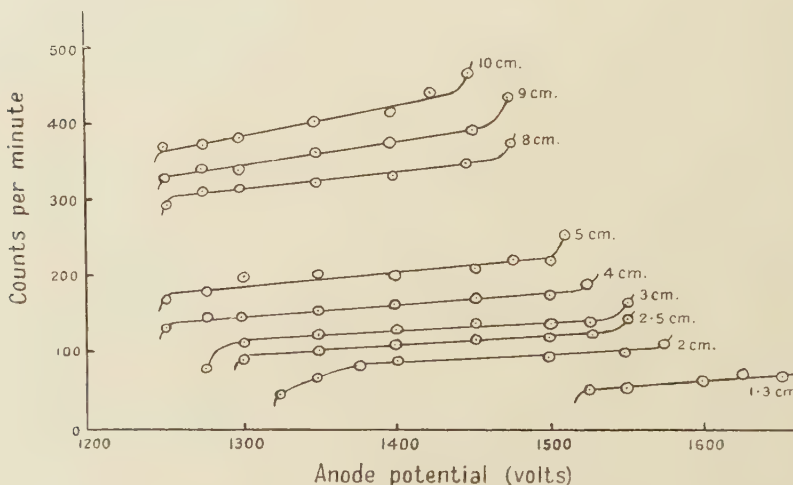


Figure 5.

made with counters 2 and 3, in which both capillaries are adjustable. Figure 2 shows the relation connecting the length of the anode wire exposed to the cathode between the ends of the capillaries and the counting rate at a working potential of 100 volts above the threshold (i.e. about the middle of the plateau) when a gamma-ray source is kept at a fixed distance from each counter. The relation between the effective anode length and the slope of the plateau for counter 2 is shown in figure 3, curve A, while curve B shows

the relation between the effective anode length and the length of the plateau. The curves indicate that as the anode length is reduced from the maximum of 10 cm. the plateau slope and length improve at first but later deteriorate. Similar curves in figure 4 show that for counter 3 the plateau is best at 10 cm. anode length and begins to deteriorate as the metal capillaries are slipped into the cathode. Figure 5 shows the characteristic curves of counter 2 for different lengths of the anode. The variation of the threshold voltage with the effective anode length is shown in curves A and B, figure 6, for counters 2 and 3 respectively. As the effective length is reduced below 2 cm., the threshold voltage increases rapidly until at about 1 cm. there are no counts even at 1600 volts.

§ 4. INFLUENCE OF THE GAUGE AND MATERIAL OF THE ANODE ON PLATEAU CHARACTERISTICS

The plateau characteristics of counter 1 were obtained using anodes of different materials and of different diameters. As the anode could be changed by rotating the ground-glass joints, other conditions could be kept constant during the measurements. A 4 cm. anode length at the centre was used throughout these tests, as earlier work had shown that good plateaux are obtained with this length. Figure 7, curve A, shows the relation between the plateau slope and the wire diameter, while curve B shows how the length of the plateau varies with the wire diameter. It was found that anode wires of a given diameter give the same plateau characteristics although made from different materials.

Figure 7, curve C, shows that the threshold voltage decreases when the diameter of the anode is reduced.

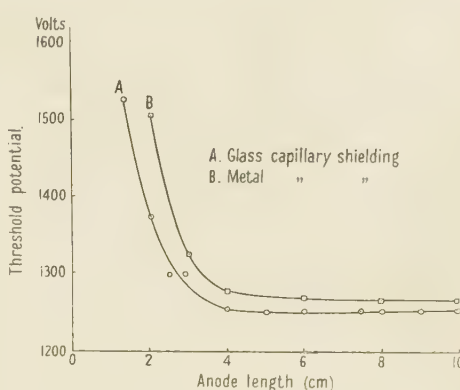


Figure 6.

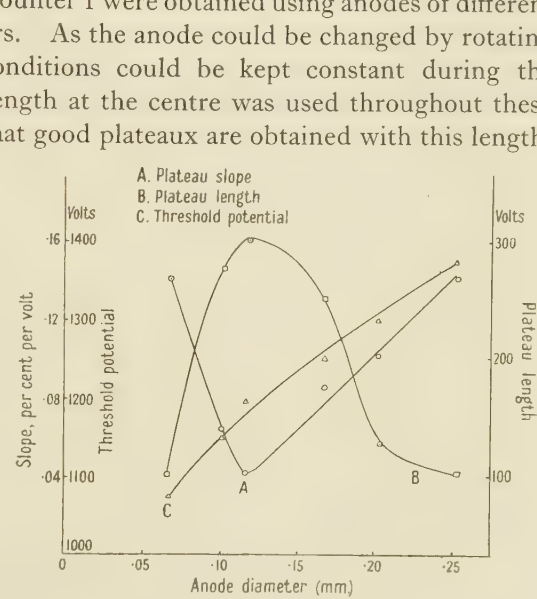


Figure 7.

§ 5. PHOTOSENSITIVITY OF THE COUNTERS

Early experiments with counter 4 showed that after passing a "continuous" discharge * through the counter (by setting the voltage a few hundred volts above the plateau region) the background counting rate immediately afterwards was of the order of 10000 counts per minute, but after 24 hours it had fallen to 200 per minute, the normal background being about 50 counts per minute and the plateau characteristics were slightly better than before the discharge. When counter 5, which has an aluminium cathode, was new, it had plateau characteristics as good as counter 4, but after a continuous discharge it required a considerably longer time to recover and was thereafter unreliable for counting rates of over a few hundred counts per minute. In subsequent measurements, which were carried out in greater detail with other counters, it was found that these effects were primarily due to changes in the behaviour of the cathode surfaces, produced by the discharge.

Counter 2, with which a few million counts had already been recorded over a period of some weeks without making it photosensitive, was run at a high counting rate at an operating voltage about 100 volts above the threshold. In a particular case, an anode length of 3 cm. was used and gamma rays were counted at a rate of about 6000 counts per minute. Background counts taken with the room lights on, following doses of varying duration, showed that a detectable photosensitivity was built up after counting at this rate for 10 minutes. After a few minutes, the background counting rate fell to within probable error of the normal value. The degree of photosensitivity and the period for which it lasts depend upon the dose given.

The photosensitivity caused by passing a continuous discharge was studied in some detail with counter 1 in order to find out what part of the counter becomes photosensitive. The procedure adopted was as follows:

The capillaries in counter 1 were set so that a 3 cm. length of the anode, starting 1 cm. from one end of the cathode, was used during the discharge. Since the cathode is 10 cm. in length, a fresh portion of it is used when the capillaries are adjusted for a similar 3 cm. length at the other end of the counter. After passing a discharge for 5 minutes, the background counting rate with the room lights on was about 20 times the normal value, but the rate on moving the capillaries to the other end of the counter was normal. Thus it appears that this portion of the counter had not been affected at all by the discharge, and that the gas filling retained its quenching characteristics. Next, the portion of the anode which had been used during the discharge, was wound along until it became the anode for the other end of the counter. Again, a normal counting rate was found, while the photosensitivity persisted at the end in which the discharge had been passed. This means that the portion of the cathode which was used during the discharge had become photosensitive. The sensitivity is greater and persists for a longer time when the duration of the discharge is increased.

After a discharge had been passed in this counter for 1 hour, the photosensitivity decayed as shown in figure 8, curve A. The sensitivity decreased rapidly at first and then more slowly. In one counter appreciable photosensitivity remained after it had been standing unused for a period of several months. The data of curve A, figure 8, are shown on a double logarithmic plot in curve B.

* When the potential is set above the Geiger region, the discharge which passes is not really continuous, but consists of discrete pulses in rapid succession.

Two days after a continuous discharge had been passed for 1 hour in counter 1, the spectral sensitivity was tested qualitatively with a set of Wratten filters and a tungsten-filament lamp, as after this time the decay of the photo-sensitivity was too slow to alter appreciably during the counting intervals. It was found that, under these conditions, the maximum sensitivity in the visible region was at the short wavelength end of the spectrum and there was no detectable sensitivity above about 5500 Å. Immediately after a continuous discharge however, the counter was always sensitive to longer wavelengths than this, but measurement was difficult because of the rapid decay rate.

§ 6. EFFECT OF A CONTINUOUS DISCHARGE ON THE PLATEAU CHARACTERISTICS

The plateau characteristics were obtained for two 3 cm. effective lengths of counter 2, each set at a distance of 1 cm. from the ends of the cathode. A discharge was then passed for 1 hour in one of these sections, and immediately afterwards it was observed that the slope and length of the plateau as well as the background in the other section with room lights on, were, within probable error, the same as originally. On the other hand, the background for that section of the counter in which the discharge had been passed was too high for the recording apparatus to follow. In darkness, however, the background for this end of the counter was the same as before the discharge and equal to that of the other end in light. Though the background of this part of the counter was too high in light for several days for the recorder to follow, its plateau characteristics taken with room light off were as good as those obtained in light before the discharge.

§ 7. EFFECT OF A CONTINUOUS DISCHARGE ON THE BACKGROUND IN DARKNESS

During the experiments with counter 1 it was observed that the background counting rate with the tube in darkness was higher than normal immediately after the discharge had been passed in it for an hour, but returned to the normal value within 48 hours. This phenomenon was studied in detail with counter 4, in which the effect was very pronounced. Figure 9, curve A, shows the decay of the background counting rate in

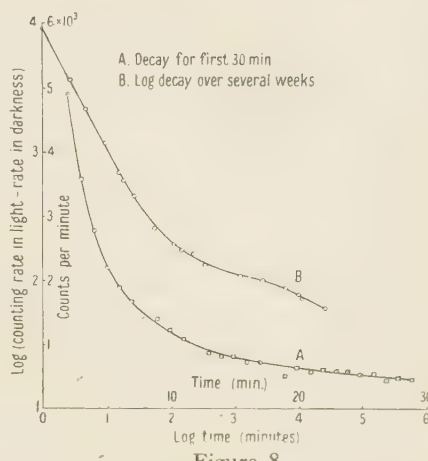


Figure 8.

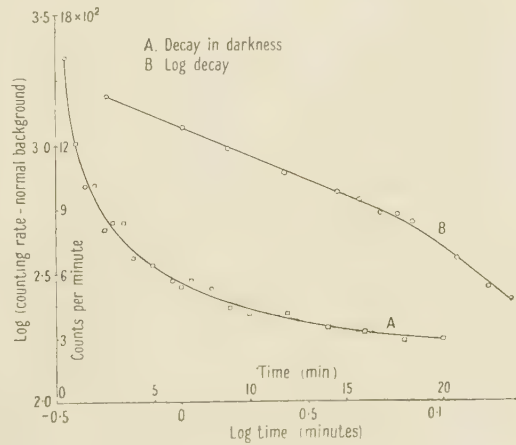


Figure 9.

darkness during the 20 minutes interval immediately after a continuous discharge of 30 minutes. It was found that this effect disappeared altogether after a number of discharges of short duration had been passed in the counter, although it could still be made highly photosensitive. This was found also to be the case with other counters.

§ 8. DISCUSSION OF RESULTS

During the experiments the pulses from counter 2 were examined with a cathode-ray oscilloscope and it was observed that for a given operating potential the pulse amplitude increased almost linearly with the effective anode length, which is consistent with the assumption that the discharge is not localized but spreads along the length of the wire. This demonstrates in a simple way the conclusion arrived at previously by other workers (Wilkening and Kanne 1942, Stever 1942) and studied recently by Hill and Dunworth (1946), Craggs and Jaffe (1947), and Wantuch (1947).

The linear relation (figure 2) between the separation of the ends of the capillaries and the counting rate shows that the efficiency of the counter is unaltered by reducing its length and also that for practical purposes we are justified in referring to the separation of the capillaries as the effective anode length of the counter. At very short lengths, however, the distortion of the fields near the ends of the capillaries would be expected to have a noticeable effect and this appears to be the case, since the counter with glass capillaries was not sensitive to gamma rays at an anode length less than 0.8 cm. with a working potential of 1600 volts; while the metal capillary counter at the same operating voltage would not respond below 1.25 cm. anode length.

The slope of the plateau in self-quenching counters has been attributed by Korff (1944) to the occurrence of multiple pulses which, with a recording circuit of high resolution, give rise to spurious counts. On this view the more ions there are per pulse the greater is the probability of a multiple pulse occurring. Therefore, when the pulse size is reduced by reducing the anode length of a counter, one would expect to obtain a longer and flatter plateau. This would account for the initial improvement in the plateau characteristics for the counter with glass capillaries (figure 3) and for the increase in the upper limit of the plateau as the anode length is reduced (figure 5). Figure 5 shows that as the anode length is reduced below the 4 cm., the threshold moves to higher voltages more rapidly than the upper limit of the plateau, resulting in a reduction of the plateau length. This increase of threshold potential with decreasing anode length (figure 6) may be attributed at least partly to the sensitivity of the recording apparatus which does not respond to pulses of less than a certain minimum amplitude. Observation with a cathode-ray oscilloscope during the experiments showed that this minimum was reached when the anode length was reduced to about 4 cm. with a working potential of 1250 volts. At shorter lengths than 4 cm. the plateau did not begin until the pulse size was increased by using higher operating potentials. The increase in slope of the plateau for short anode lengths suggests that spurious counts due to factors other than the number of positive ions per pulse were recorded. These may be due to point discharges from irregularities on the surfaces of the electrodes or to distortion of the field at the ends of the capillaries,

both of which effects would be more noticeable at the higher potentials used. Furthermore, at higher potentials, the average energy of the positive ions being greater, there is a greater chance for some of them to reach the surface of the cathode and liberate secondary electrons, thus giving rise to spurious counts. In the counter with the brass capillaries, the best plateau was obtained at 10 cm. anode length, suggesting that the expected improvement in the plateau during the initial stages on reducing the anode length was masked by effects caused by the presence of the metal capillaries.

In order to explain the high background in darkness, observed after a continuous discharge (figure 9), one must look for processes occurring on the cathode surface in which electrons or negative ions are emitted. One possibility is that during the discharge active centres are formed on the cathode surface, and these undergo chemical change with the emission of electrons or ions. Also, if during this chemical change, positive ions are formed on an insulating layer, e.g. oxide, on the cathode surface, these may give rise to *field emission* electrons. On the other hand, the photosensitivity which is observed when the cathodes are in an activated condition after a high counting rate or a continuous discharge suggests that centres of low work-function are formed. With a sufficiently low work-function, and under the influence of the electric field at the cathode, an observable number of thermionic electrons would be able to escape at room temperature, thus accounting for the high background in darkness. For example, calculation shows that, if we regard the activated cathode as similar to an oxide coated thermionic emitter for which A in the emission equation $i = AT^2e^{-t/kT}$ is 0.03 amp. per sq. cm. and ϕ is 1.2 volts, the current at 300° K. is about 10 electrons per sq. cm. per second. This view is supported by the observation that the counter was sensitive to wavelengths up to about 10 000 Å. when the high dark background was also present. Furthermore, the counter was sensitive to the long wavelengths only for a short period immediately after a discharge, but sensitivity at the low wavelength end of the visible spectrum remained for a long time, suggesting that the work function of the centres was low at first but increased with time. It is also worth noting that the counting rate in darkness increased when the counter was slightly warmed with hot air from a hair dryer, an effect quite distinct from the photosensitivity at long wavelengths.

High background rates in darkness after high counting rates have been reported by several workers. Lauterjung and Neuert (1944) found the effect most marked for cathodes of low work-function such as Mg (photoelectric work function 2.4 volts), whereas in the present work the effect was observed with nickel cathodes with a work function of about 5 volts. Christoph (1935) reported that in photon counters with Cd or K cathodes the background immediately after a glow discharge was much higher than normal. He also observed an increased photosensitivity after the glow discharge. Lauterjung and Neuert obtained linear decay curves using double logarithmic plots, whereas in our case the curve is linear at first and later changes slope (figure 9, B).

The upper portion of the curve of figure 8, B, representing the first 30 minutes decay in light after a continuous discharge for 1 hour is linear and has a slope of unity which suggests that the natural decay curve follows a rectangular hyperbola law during that period but afterwards the decay becomes more complicated.

After 4 weeks the background in light was about twice the dark background and the decay curve became linear again, indicating that if it were to continue in this way, a measurable sensitivity should remain after 10^6 minutes (i.e. almost 2 years). Actually, one of the counters was found to be photosensitive 4 months after a continuous discharge of 3 hours duration had been passed in it.

Spatz (1943) reported that counters with silver cathodes became photosensitive to visible light after long use, and showed how the plateau was destroyed by running the counters for some time at a high counting rate, but gradually recovered again over a period of several days. In view of the present work, we may suppose that the results obtained by Spatz were probably due to the effects observed by us and discussed in this paper.

Figure 7 shows that for a particular counter there is an optimum anode diameter which results in a long, flat plateau, a point which is of great practical importance.

It was invariably found during the work that the threshold occurred at a slightly lower potential and the plateau was longer when the counters were new or operated after a rest period of a few hours. Some minutes of operation, however, brought the threshold to its higher steady value and the plateau characteristics thereafter were reproducible so long as care was taken not to allow the counter to go into a continuous discharge. Observation with an oscillograph showed that after a rest period the pulses were larger, and this may explain the lower thresholds.

It was also observed that the degree of oxidation of the anode wire does not influence to any appreciable extent the characteristics of a counter, because just as good plateaux were obtained using a heavily oxidized copper anode as with a gold wire of the same diameter. Moreover, no difference was found when the anode wire was slackened so that it was about 2 to 3 mm. off the axis at the centre of the counter.

It is generally believed that after prolonged use the plateau characteristics of a counter deteriorate as a result of the dissociation of the quenching agent. Our results suggest, however, that this may be more closely connected with the changes on the cathode surface than with the breakdown of the filling.

It is hoped to continue the investigation of some of the aspects discussed above.

§ 9. ACKNOWLEDGMENTS

It is a great pleasure to record our sincere thanks to Professor M. L. Oliphant, F.R.S., for providing the facilities for this work, and for his continued interest and guidance during its performance. One of us (R.M.C.) owes thanks to him for the award of a Nuffield Research Fellowship, and the other (A.G.F.) is grateful to Messrs. Cadbury-Fry-Pascall Ltd., Claremont, Tasmania, for the Overseas Fellowship which enabled him to take part in this research. Thanks are due also to our respective Universities for granting us leave of absence.

We wish to thank Mr. H. J. Morris for making the glass parts of the counters and assisting us in their assembly.

REFERENCES

- CHRISTOPH, W., 1935, *Ann. Phys. (Chim.)*, **23**, 747.
 CRAGGS, J. D., and JAFFE, A. A., 1947, *Nature, Lond.*, **159**, 369.
 HILL, J. M., and DUNWORTH, J. V., 1946, *Nature, Lond.*, **158**, 833.
 KORFF, S. A., 1944, *Phys. Rev.*, **65**, 274.
 KORFF, S. A., 1946, *Electron and Nuclear Counters* (Van Nostrand). (The book contains an excellent bibliography on counters.)
 LAUTERJUNG, K., and NEUERT, H., 1944, *Z. Phys.*, **122**, 266.
 STEVER, H. G., 1942, *Phys. Rev.*, **61**, 38.
 WANTUCH, E., 1947, *Phys. Rev.*, **71**, 646.
 WILKENING, M. H., and KANNE, W. R., 1942, *Phys. Rev.*, **62**, 534.

The Calibration of Hydrophones and Crystal Transceivers

BY N. F. ASTBURY

formerly of H.M. Underwater Detection Establishment

MS. received 1 May 1947

ABSTRACT. A scheme of measurements is discussed from which absolute determinations of sound field pressure can be made. The relation between the scheme and the reciprocity method is discussed. It is shown that the measurements also yield the axial pressure and "projection efficiency" of a transceiver, the "projection efficiency" being defined as the ratio of the actual axial intensity to the axial intensity as it would be if the transceiver converted the whole energy absorbed into sound by vibrating as a simple piston. It is suggested, without proof, that the upper limit of the projection efficiency is unity, and the relation between this quantity and the efficiency defined as the ratio of radiated acoustic power to consumed electrical power is shown to depend on a directivity coefficient and on the effective area of the radiator face. It is pointed out that neither of these quantities is readily determinable and that therefore the conversion efficiency of the transceiver, and hence the acoustic power radiated, cannot be obtained.

§ 1. INTRODUCTION

THE determination of the axial pressure, efficiency and directional properties of crystal transceivers used in submarine acoustic work presents many problems which, in the urgency of immediate need, have tended to remain without complete solution. The present paper is a report of a theoretical investigation into the possibilities of making exact measurements on the quantities specified for crystal transceivers.*

An obvious initial requirement is a device for the absolute measurement of sound field pressure. Such devices are provided by the Rayleigh disc and the radiometer disc (which latter measures energy density in the wave) and present considerable technical problems of their own. On the other hand, it is known that by the use of the reciprocity theorem it is possible to measure sound pressures without any "absolute" device. The method described in this paper is closely related to that based on the reciprocity theorem (Foldy and Primakoff 1945) but in its simple form it was developed independently of this result.

* Security reasons still prevent the publication of actual numerical data, but the principles involved are of general interest in acoustical work and it has been thought worth while to prepare the theoretical work for publication.

The reciprocity principle presents the concept that two transceivers placed in a sound-transmitting medium are equivalent to an electric quadripole, and that the transfer impedance is therefore independent of the input direction. In other words, the ratio of open circuit volts on the receiver to driving current in the projector is unique. A concomitant property of the system is that the ratio of the receiving sensitivity of a transceiver, measured in open circuit volts per unit pressure, to its projection sensitivity, measured in pressure units at a given distance per unit driving current, is also unique. This ratio has been called the "reciprocity parameter" and is denoted by J .

The basic principle of the method described in this paper circumvents the reciprocity principle, in effect, by making the analysis rest on voltage measurements together with self impedance measurements on the transceivers. Nevertheless, the full analysis of the method, as we shall see, cannot be carried out without invoking the reciprocity principle.

§ 2. THE BASIC EXPERIMENT

Let us assume that we have a perfect transceiver, T , for which axial pressure is required. We shall require an auxiliary hydrophone, H , and a projector, P , for producing a sound field. The hydrophone may be of any form whatever, provided that it is linear, and it may be supposed to be followed by an amplifier and an output meter. If the output meter records a voltage u when the hydrophone is placed in a field of which the undisturbed pressure is p , then we may write

$$p = hu, \quad \dots \dots (2.1)$$

where h is the calibration constant of the hydrophone.

The transceiver, T , may be represented as in figure 1, in which I is the motional impedance of the device, e is the voltage produced in it by the sound pressure when it is acting as a receiver, and C is a capacitative load. The first part of the basic experiment is to establish a sound field using the projector P , and to determine the voltage developed across C when T is placed in this field. If p_ω be the free field pressure, we have*

$$e = \frac{2A}{k} p_\omega, \quad \dots \dots (2.2)$$

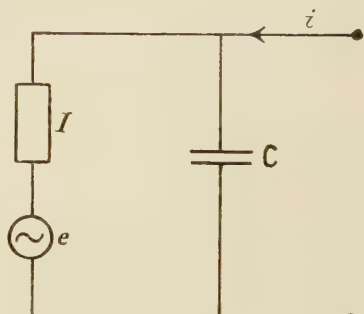


Figure 1.

where A is the effective area of the face of T and k is a constant involving the piezo-electric constant of the crystal and the dimensions of the assembly.

The output voltage, v , developed across C is

$$v = \frac{e}{|1 + KI|} = \frac{2A}{k} \cdot p_\omega \frac{1}{|1 + KI|}, \quad \dots \dots (2.3)$$

where K is the conductance of C .

Since the measured value of v gives no indication of phase, the modulus of the impedance factor $1 + KI$ must be used.

* See (3.1) and (3.2), *infra*.

If, now, T is replaced by H, the output meter of H will record a voltage u_ω given by

$$p_\omega = hu_\omega. \quad \dots \dots \dots (2.4)$$

Let T now be used as a projector, a driving voltage V being applied to its terminals. The power, W , radiated acoustically will be

$$W = \frac{v^2}{|I|^2} S, \quad \dots \dots \dots (2.5)$$

where S is the radiation resistance. If the dimensions of the radiating face of T are not small compared with the wavelength, λ , the axial pressure, p , at a distance $d(\gg\lambda)$ is given by *

$$p = \frac{k}{\lambda d} \sqrt{SW} = \frac{k}{\lambda d} \cdot \frac{VS}{|I|}. \quad \dots \dots \dots (2.6)$$

If this pressure be recorded on H, an output voltage u will be produced, given by

$$p = hu. \quad \dots \dots \dots (2.7)$$

From (2.3) and (2.4) we have

$$\frac{v}{u_\omega} = \frac{2Ah}{|1+KI|k} = m_1. \quad \dots \dots \dots (2.8)$$

From (2.6) and (2.7) we have

$$\frac{u}{V} = \frac{kS}{\lambda d |I| h} = m_2. \quad \dots \dots \dots (2.9)$$

From (2.8) and (2.9) we find

$$m_1 m_2 = \frac{2AS}{\lambda d |I| |1+KI|}, \quad \dots \dots \dots (2.10)$$

$$\frac{m_1}{m_2} = \frac{2A\lambda d}{k^2 S} h^2 \left| \frac{I}{1+KI} \right|. \quad \dots \dots \dots (2.11)$$

For a transceiver with a radiating face of dimensions not small compared with λ , we have (Vigoureux 1947)

$$k^2 S / A = \rho c, \quad \dots \dots \dots (2.12)$$

where ρ is the density of the medium in which T is placed and c is the velocity of sound in the medium.

If we can ensure that $KI \gg 1$, (2.10) and (2.11) become

$$m_1 m_2 = \frac{2AS}{|K| \lambda d |I|^2} = \frac{2k^2}{|K| \lambda d \rho c} \cdot \frac{S^2}{|I|^2}, \quad \dots \dots \dots (2.13)$$

$$m_1/m_2 = \frac{2\lambda d}{\rho c |K|} h^2. \quad \dots \dots \dots (2.14)$$

The former relation depends only on the properties of T but not of H, and the latter on the properties of H but not of T. In particular, (2.14) allows us to determine h , the hydrophone constant, directly in terms of voltage ratios, impedance and frequency. From (2.6) and (2.13) we have, further,

$$\begin{aligned} \frac{p}{V} &= \frac{k}{\lambda d} \cdot \frac{S}{|I|} = \frac{k}{\lambda d} \sqrt{\frac{m_1 m_2 \lambda d \rho c |K|}{2k^2}} \\ &= \sqrt{\frac{m_1 m_2 f \rho |K|}{2d}}, \end{aligned} \quad \dots \dots \dots (2.15)$$

where $f = c/\lambda$ is the frequency of the sound. Thus the axial pressure is determined in terms of directly measurable quantities.

* See (3.1) and (3.2), *infra*.

Finally, if we make the measurements at the resonant frequency of T , I becomes identical with S for our assumed perfect transceiver, so that (2.13) becomes

$$m_1 m_2 = \frac{2A}{|K|\lambda d S}, \quad \dots \dots \dots (2.16)$$

which suggests that by working at the resonant frequency of T we might determine its radiation resistance.

We have shown then, in principle, that the system of measurements outlined above (to describe which the adjective "trimetric" is proposed) permits the absolute measurement of free field pressure and of certain constants of transceivers without invoking the reciprocity principle explicitly, provided certain conditions are fulfilled. The most important assumption made in the analysis has been that the transceiver has been vibrating as a perfect piston and has therefore possessed directional characteristics in accord with the geometry of the system. The implications of this will be discussed more fully in the following paragraph.

§ 3. EFFECT OF DIRECTIONALITY

The sound power, W , radiated by a perfect piston of effective area A_1 in an infinite baffle is

$$W = \rho c A_1 \dot{\xi}^2, \quad \dots \dots \dots (3.1)$$

where $\dot{\xi}^2$ is the mean square velocity of the radiating face (Rayleigh 1929). The axial pressure, p_0 , at a distance d from this source is

$$p_0 = \frac{\rho c A}{d\lambda} \dot{\xi}, \quad \dots \dots \dots (3.2)$$

where A is the geometrical area of the radiating face (Vigoureux 1947).

It is implicit in (3.1) and (3.2) that $d > \sqrt{A} > \lambda$. Thus

$$W = \frac{\lambda^2 d^2 p_0^2 A_1}{\rho c A^2}. \quad \dots \dots \dots (3.3)$$

Consider now a radiator which is not a perfect piston and let its axial pressure at a distance d be p_1 when it is radiating a total power W . Then the pressure at some point on the surface of a sphere of radius a centred on the piston can be written as

$$\hat{p}(\theta, \phi) = p_1 f(\theta, \phi), \quad \dots \dots \dots (3.4)$$

where θ and ϕ are the angular coordinates of the point considered and f is some unknown function. Then the rate of flow of energy radially through an element ds of the surface at this point will be

$$\frac{\{p(\theta, \phi)\}^2 ds}{\rho c} = \frac{p_1^2}{\rho c} \{f(\theta, \phi)\}^2 ds,$$

so that we have

$$\begin{aligned} W &= \frac{p_1^2}{\rho c} \int_s \{f(\theta, \phi)\}^2 ds, \\ &= \frac{p_1^2}{\rho c} \Delta, \end{aligned} \quad \dots \dots \dots (3.5)$$

where

$$\Delta = \int_s \{f(\theta, \phi)\}^2 ds.$$

For the perfect oscillator the relation between radiated power and axial pressure is given by (3.3), so that from (3.3) and (3.5) we have

$$p_1^2 = p_0^2 \frac{\lambda^2 d^2 A_1}{A^2 \Delta}, \quad \dots \dots (3.6)$$

or

$$p_1 = \beta p_0, \quad \dots \dots (3.7)$$

where

$$\beta = \lambda d / \sqrt{A^2 \Delta / A_1}.$$

The factor β may be called the "directivity coefficient" for the radiator. (It differs from the "directivity index" which has been used by other writers in that we have taken as a reference standard a perfect radiator of the same form as our imperfect one, instead of a spherical radiator.)

It is worth while digressing for a moment to consider the form of Δ for the particular case of a circular radiator of radius a . This system possesses axial symmetry and

$$f(\theta, \phi) = \frac{2J_1(b \sin \theta)}{b \sin \theta}, \quad \dots \dots (3.8)$$

where J_1 is the Bessel function of order one and $b = 2\pi a / \lambda$ (Morse 1936). Then

$$\begin{aligned} \Delta &= 8\pi d^2 \int_0^{\pi/2} [J_1(b \sin \theta)/b \sin \theta]^2 \sin \theta d\theta, \\ &= \frac{d^2 \lambda^2}{\pi a^2} \left[1 - \frac{J_1(2b)}{b} \right]. \end{aligned} \quad \dots \dots (3.9)$$

Since for a perfect piston we must have $\beta = 1$, it follows that

$$\frac{A^2 \Delta}{A_1} = \frac{A^2}{A_1} \frac{d^2 \lambda^2}{\pi a^2} \left[1 - \frac{J_1(2b)}{b} \right] = \lambda^2 d^2,$$

whence, since

$$A = \pi a^2,$$

$$A_1 = A \left[1 - \frac{J_1(2b)}{b} \right]. \quad \dots \dots (3.10)$$

This is the result given by Rayleigh (1929) for a circular piston. In most of the transceivers used the value of b was such that $\{J_1(2b)\}/b$ was generally very small compared with unity, and we can take $A_1 = A$.

This, then, has given some idea of the part played by the directivity coefficient in the behaviour of the transceiver as a projector. We have now to decide what part β plays in the behaviour of a receiver. It is arguable physically that the generated voltage e (figure 1) for a "piston" of directivity coefficient β must be β times that for a perfect piston of the same materials and dimensions, since β implicitly describes the mode of vibration of the radiating face however excited. It is, however, interesting to give a formal demonstration of this by invoking the reciprocity principle.

Referring to the crystal transceiver represented diagrammatically in figure 1, let the axial pressure ϖ_1 produced by a driving current i be given by

$$\varpi_1 = \mu i, \quad \dots \dots (3.11)$$

and let the open circuit voltage v produced by a free field pressure ϖ_2 be given by

$$v = \nu \varpi_2. \quad \dots \dots (3.12)$$

Then the reciprocity theorem states that

$$\frac{\nu}{\mu} = J = \frac{2d\lambda}{\rho c}. \quad \dots \dots (3.13)$$

In figure 1 the actual current entering I is

$$i_1 = \frac{1}{1 + KI} i,$$

and the power radiated acoustically is

$$\begin{aligned} W &= S |i_1|^2 = \frac{S}{|1 + KI|^2} i^2, \\ &= \rho c A_1 \dot{\xi}^2. \end{aligned}$$

The axial pressure for an ideal radiator is

$$\begin{aligned} p_0 &= \frac{\rho c A}{\lambda d} \dot{\xi}, \\ &= \frac{\rho f i}{d} \cdot \frac{1}{|1 + KI|} \sqrt{\frac{SA^2}{\rho c A_1}}. \end{aligned} \quad \dots \dots (3.14)$$

The actual axial pressure p_1 is

$$p_1 = \beta p_0 = \frac{\beta \rho f i}{d} \cdot \frac{1}{|1 + KI|} \sqrt{\frac{SA^2}{\rho c A_1}}. \quad \dots \dots (3.15)$$

$$\text{Thus } \mu = \frac{\beta \rho f}{d} \cdot \frac{1}{|1 + KI|} \sqrt{\frac{SA^2}{\rho c A_1}}, \quad \dots \dots (3.16)$$

$$\text{and } \nu = \frac{2d\lambda}{\rho c} \cdot \mu = 2\beta \frac{1}{|1 + KI|} \sqrt{\frac{SA^2}{\rho c A_1}}. \quad \dots \dots (3.17)$$

Thus, in a free field p ,

$$\begin{aligned} v &= \nu p, \\ &= 2\beta p \frac{1}{|1 + KI|} \sqrt{\frac{SA^2}{\rho c A_1}}. \end{aligned} \quad \dots \dots (3.18)$$

If e be the generated voltage

$$v = \frac{1}{|1 + KI|} e,$$

$$\text{so that } e = 2\beta p \sqrt{\frac{SA^2}{\rho c A_1}}. \quad \dots \dots (3.19)$$

For an ideal piston the generated voltage is given by

$$e_0 = 2p \sqrt{\frac{SA^2}{\rho c A_1}} = e/\beta, \quad \dots \dots (3.20)$$

so that the generated voltage for an imperfect receiver is equal to its directivity coefficient multiplied by the generated voltage for an ideal receiver of the same materials and dimensions.

§ 4. THE TRIMETRIC SCHEME: HYDROPHONE CALIBRATION

We can now develop more fully the analysis given in § 2 for an ideal piston. We have, in fact, to rewrite the equations of that section in the light of the discussion given in § 3.

We have instead of (2.3)

$$v = \frac{2\beta A}{k} p_\omega \frac{1}{|1+KI|}, \quad \dots \dots (4.1)$$

and instead of (2.6)

$$p = \frac{\beta k}{\lambda d} \frac{VS}{|I|} \frac{A}{A_1}. \quad \dots \dots (4.2)$$

Combining these with (2.4) and (2.7) we have

$$m_1 = \frac{v}{u_\omega} = \frac{2\beta Ah}{|1+KI|k}, \quad \dots \dots (4.3)$$

$$m_2 = \frac{u}{V} = \frac{\beta k S}{\lambda d |I| h} \frac{A}{A_1}, \quad \dots \dots (4.4)$$

whence

$$m_1 m_2 = \frac{2\beta^2 A^2 S}{\lambda d A_1 |I| |1+KI| k}, \quad \dots \dots (4.5)$$

$$\frac{m_1}{m_2} = \frac{2A_1 \lambda d}{k^2 S} \left| \frac{I}{1+KI} \right| h^2. \quad \dots \dots (4.6)$$

Instead of (2.12) we must use the more precise form

$$k^2 S / A_1 = \rho c, \quad \dots \dots (4.7)$$

so that

$$h^2 = \frac{m_1}{m_2} \left| \frac{1+KI}{I} \right| \cdot \frac{\rho f}{2d}, \quad \dots \dots (4.8)$$

which we may write as

$$h^2 = \frac{m_1 |K| \rho f}{m_2 2d} \left| 1 + \frac{1}{KI} \right|. \quad \dots \dots (4.9)$$

Thus the calibration of the hydrophone does not depend on the directivity coefficient of T nor on the relation between its effective and geometrical areas, nor does it depend on measurements being made at or near the resonant frequency of T. If the load on T is a capacitance C, as in figure 1, having a power factor δ , then $|K|$ can be written as ωC to an accuracy of $0.5\delta^2$, and since δ is never likely to exceed 5%, we can in general ignore this correction.

The correction $1/KI$ will be small even if we work at the resonant frequency of T, for then I will approximate to the radiation resistance. This suggests that if the correction be not very large, use can be made of the ideal equation (2.16), which gives,

$$|K| S = \frac{2A}{\lambda d m_1 m_2},$$

so that, bearing in mind that we are dealing with r.m.s. quantities throughout, we have

$$h^2 = \frac{m_1 \pi C \rho f^2}{d} \left(1 + \frac{m_1^2 m_2^2 \lambda^2 d^2}{8A^2} \right). \quad \dots \dots (4.10)$$

We shall see, however, in general that $[1/KI]^2$ is in fact negligible compared with unity.

§ 5. THE TRIMETRIC SCHEME: TRANSCEIVER CALIBRATION

To determine the axial pressure of T we combine (4.2), (4.5) and (4.7), and obtain

$$p = V \sqrt{\frac{m_1 m_2 \rho f |K|}{2d}} \left[1 + \frac{1}{KI} \right]. \quad \dots \dots (5.1)$$

This again does not depend on β , since the product $m_1 m_2$ is experimentally determined, nor on the ratio of effective and geometric areas.

Disregarding the corrections for $1/KI$ and δ , in the light of what has already been discussed, we have

$$p = Vf \sqrt{\frac{\pi m_1 m_2 \rho C}{d}}. \quad \dots \dots (5.2)$$

Both this result and (4.10) are independent of any resonance conditions, and therefore we can measure absolutely the axial pressure at any frequency and so plot the true acoustic projector response curve.

We saw in § 2 that the possibility of determining radiation resistance arises from the present series of measurements (equation (2.16)). Actually, it appears from the more complete expression given in (4.5) that the particular property of the transceiver which does exist and which is directly determinable from this trimetric series of measurements is the quantity $\beta^2 A^2 S / A_1 |I|^2$.

In order to find what significance can be attached to this quantity, suppose that measurements are made at the resonant frequency of T—that is, at the frequency at which p/V , defined by (5.2), is a maximum. At this frequency $|I|$ becomes a pure resistance, the value of which may be denoted by S_1 . This will in general be greater than the radiation resistance S , because it will include internal losses arising from mechanical and other causes. Any electrical method which determines total power loss in the transceiver can be used to determine S_1 for, clearly, at a known r.m.s. driving voltage V the total power consumed will be V^2/S_1 . At resonance, therefore, we can determine a quantity R given by

$$R = \frac{A_1 S_1^2}{A \beta^2 S} = \frac{A}{m_1 m_2 \lambda d \pi f C}. \quad \dots \dots (5.3)$$

If the whole power consumed were radiated acoustically by an ideal piston of effective area A , identical with its geometrical area, the axial pressure p_0 at distance d would be given by

$$p_0^2 = \frac{\rho c A}{\lambda^2 d^2} \cdot \frac{V^2}{S_1}. \quad \dots \dots (5.4)$$

The actual axial pressure, p , is, however, given by (5.2)

$$\begin{aligned} p^2 &= V^2 f^2 \frac{\pi m_1 m_2 \rho C}{d}, \\ &= \frac{V^2 f \rho A}{\lambda d^2 R} = \frac{V^2 \rho c A}{\lambda^2 d^2 R}. \end{aligned} \quad \dots \dots (5.5)$$

Thus

$$\frac{p^2}{p_0^2} = \frac{S_1}{R}. \quad \dots \dots (5.6)$$

Thus with a knowledge of R and S_1 , we can determine the ratio of the actual axial intensity to that which would be given by an ideal piston radiating the whole

of the power as sound. This ratio may be called the "projection efficiency", and we can denote it by η_p .* Thus

$$\eta_p = \frac{S_1}{R} = \frac{\pi d C c S_1 m_1 m_2}{A}. \quad \dots \dots (5.7)$$

It is obvious that the efficiency with which T converts electrical power into sound power is given by the ratio S/S_1 . This may be called the "conversion efficiency", η_c , and we have

$$\eta_c = \frac{S}{S_1} = \eta_p \frac{A_1}{\beta^2 A}. \quad \dots \dots (5.8)$$

Thus the actual conversion efficiency, or the actual sound energy radiated, cannot be determined from this scheme of measurements unless β and A_1/A are known. There is no accurate method of determining β : for axially symmetrical systems an estimate can be made from directional curves, but the method is unsatisfactory. Again, theoretical estimates of A_1/A rest on the assumption that β is unity, so that it appears that η_c is a somewhat inaccessible quantity.

This, however, need not concern us unduly, for the projection efficiency is an equally useful practical concept for asdic applications. While it is obvious that $\eta_c \geq 1$, yet it is not immediately clear that $\eta_p \geq 1$. This has led to the enunciation of the following proposition:—

"A plane radiator consuming, and radiating the whole of a given amount of power produces a maximum axial intensity at a given distance when it is vibrating as an ideal piston."

No formal proof has been evolved, but there is a strong supposition that the proposition is true. If it is true, then of course the upper limit of η_p would be unity.

§ 6. CONCLUSION

It has been shown that the scheme of measurements discussed in this paper can be made to yield the following results:—

- (i) The calibration constant for a hydrophone in "absolute" units.
- (ii) The axial pressure, at any frequency, of a transceiver, in "absolute" units.

These results depend only on directly measurable quantities such as voltage, capacitance, frequency and range. If measurements are made at the resonant frequency of a transceiver, then there is determined also:

- (iii) The projection efficiency.

It is hoped that it may be possible later to publish practical details of the technique developed from this paper. The following results indicate the order

* The choice of an ideal piston without edge-correction as a norm is arbitrary, and it is arguable that it would be better to take a simple piston with appropriate edge-correction as a reference standard. If this is done, we find that $p^2/p_0^2 = (S_1/R)(A_1/A)$, which is in general smaller than the quantity η_p as defined in (5.7). A third possibility is to take a small spherical radiator as a standard, but then the ratio of p^2/p_0^2 would depend on A/λ^2 , and no convenient physical interpretation can be placed on the result. The present suggestion for the definition of η_p is tentative, and may require revision as experience is acquired.

of magnitude of the quantities involved in the calibration of a small tourmaline hydrophone:—

$$\begin{aligned} m_1 &= 9.33 \times 10^1, & f &= 3.06 \times 10^4 \text{ c/s.}, \\ m_2 &= 1.08 \times 10^{-4}, & \rho &= 1.02 \text{ gr./cc.}, \\ C &= 4.01 \times 10^{-9} \text{ farad}, & S_1 &= 3.31 \times 10^4 \text{ ohms}, \\ d &= 6.10 \times 10^2 \text{ cm.} \end{aligned}$$

We note first that $1/KI = -j/2\pi \times 3.06 \times 4.01 \times 13.31 \times 10^{-1} = -0.04j$ so that $|1+1/KI|$ differs from unity by less than 1 %. To this accuracy then we have, from (4.10)

$$h^2 = \frac{m_1}{m_2} \cdot \frac{\pi C \rho f^2}{d},$$

$$\text{or } h = 5.70f \sqrt{\frac{m_1}{m_2} \cdot \frac{C}{d}} \text{ dynes/cm}^2 \text{ per volt,}$$

where C is in $\mu\mu F.$, f is in kc/sec., d is in cm. and $\pi\rho$ is embodied in the constant. Thus

$$\begin{aligned} h &= 5.70 \times 30.6 \sqrt{\left(\frac{9.33 \times 4.10}{1.08 \times 6.10} \times 10^6 \right)}, \\ &= 4.20 \times 10^5 \text{ dynes/cm}^2 \text{ per volt.} \end{aligned}$$

This gives the hydrophone constant as already defined. Alternatively, the sensitivity can be expressed as $1/h$, i.e. as 2.38 $\mu V.$ per dyne/cm².

It can be further shown that the quantity R (equation (5.3)) is, for the present cases, 6.15×10^4 ohms, and $S\beta^2 A/A_1 = S_1^2/R = 18000$ ohms. Approximately, $A \approx A_1$, so that $S\beta^2 \approx 18000$ ohms, which means that the actual radiation resistance is of this order, although nothing is known of β except what might be inferred roughly from directional curves. Nevertheless, the example does serve to bring out the significance of the three "resistances" associated with a transceiver. The true radiation resistance, S , is that arising from the damping due to the medium (in our case, water), the dissipation resistance S_1 is the equivalent shunt resistance responsible for the absorption of electrical power, while the third quantity, which we have denoted by R , can be regarded as the radiation resistance of the equivalent perfect piston. The magnitudes will be in the order $R > S_1 > S$.

ACKNOWLEDGMENTS

The work described in this paper was carried out while the author was serving in the Royal Naval Scientific Service under Sir Charles Wright, to whom thanks are due for permission to publish it. It is a pleasure for the writer to record his indebtedness to Mr. J. Anderson, O.B.E., Chief Scientist at H.M. Underwater Detection Establishment and to Dr. Paul Vigoureux, Superintending Scientist at H.M. Torpedo Experimental Establishment, for the benefit of many stimulating discussions.

REFERENCES

- FOLDY, L., and PRIMAKOFF, H., 1945, *J. Acoust. Soc. Amer.*, **17**, 109.
- MCLACHLAN, N. W., 1934, *Loud Speakers*, p. 96 (Oxford : Clarendon Press).
- MCLACHLAN, N. W., 1941, *Bessel Functions for Engineers*, p. 98 (Oxford : University Press).
- MORSE, P. M., 1936, *Vibration and Sound*, p. 256 (New York : McGraw-Hill).
- PRIMAKOFF, H., and FOLDY, L., 1947, *Ibid.*, **19**, 50.
- RAYLEIGH, Lord, 1929, *Theory of Sound*, vol. 2, para. 302; p. 164 (London : Macmillan).
- VIGOUREUX, P., 1947, *Proc. Phys. Soc.*, **59**, 19.

A Method of Computing a Vertical Section of the Combined Polar Diagram of a Radio Aerial, a Flat Earth and a Vertical Screen

By N. CORCORAN * AND J. M. HOUGH †

Malvern

* Now Senior Assistant, Stockport College for Further Education

† Now at University College, Hull

M.S. received 7 March 1947

ABSTRACT. The method described is based on the Sommerfeld formula for diffraction at an edge, combined with the effect of reflection at the earth. A table is given which reduces the amount of numerical work involved.

§ 1. INTRODUCTION

IN the winter of 1944–45 it was found necessary to use narrow-beam radar equipments at wavelengths of the order of 10 centimetres for locating targets at small angles of elevation. As the edge of the beam struck the ground near the equipment, there was a considerable amount of "ground-clutter" which greatly increased the background of noise as seen on the display, thus swamping the echo from the target. With a view to reducing this clutter, calculations and experiments were carried out on the use of opaque vertical screens placed in front of the equipment, providing an artificial horizon slightly above the true horizon. The experiments were carried out by Army personnel in the campaign in Holland, and by Hey, Parsons and Jackson of Army Operational Research Group in this country.

By a well-known theorem, the polar diagram of an aerial system is the same for transmitting as for receiving; it is more convenient to consider the equipment as a receiver. The treatment adopted is to sum with respect to phase and amplitude all the rays which reach the aerial, deducing the relative phases from the path differences, and the relative amplitudes from the Sommerfeld expression for the amplitude diffracted through a given angle.

§ 2. THEORY

The arrangement of screen SS' and receiver or transmitter T considered is shown in figure 1. The calculations are simplified by considering T to be a receiver and by considering plane waves coming from the right at an angle θ . In all there are ten rays to consider, which can be put into four groups. Group 1 consists of rays which have suffered no reflection; Group 2 consists of rays which have been reflected before reaching the screen; Group 3 consists of rays which have been reflected after reaching the screen; and Group 4 consists of rays which have been reflected both before and after reaching the screen.

The component rays in each group are:

- Group 1. Direct ray TN_1 if $\theta > A$;
Diffracted rays TSN_2 and $TS'N_3$.
- Group 2. Reflected ray TQ_1N_4 if $D > \theta > B$;
Diffracted rays TSQ_3N_6 and $TS'Q_2N_5$.
- Group 3. Reflected ray TQ_1N_4 if $\theta > C$;
Diffracted rays TQ_4SN_2 and $TQ_5S'N_3$.
- Group 4. Diffracted rays $TQ_4SQ_3N_6$ and $TQ_5S'Q_2N_5$.

All rays in a given group arrive at the equipment in phase except for the phase changes on diffraction.* If the resulting complex amplitude is A_1 for Group 1, A_2 for Group 2, etc., and the reflection coefficient is R , we have:

$$\text{Resultant field} = A_1 + A_4 R^2 + (A_2 + A_3) Re \frac{-i4\pi h_T \sin \theta}{\lambda}.$$

The reflection coefficient R is in general a complex quantity which varies with the angle of incidence. For horizontal polarization R does not differ greatly

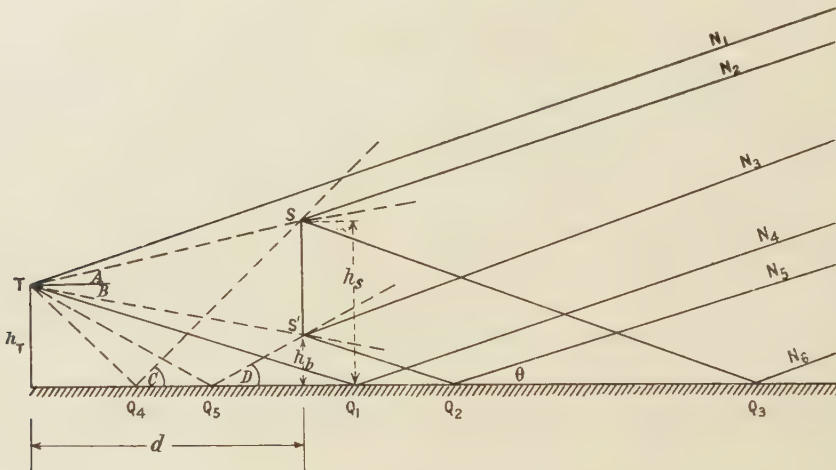


Figure 1.

from -1, and for vertical polarization and small values of θ this is also approximately true. In this problem the angles are always small, and so R is taken to be -1.

$$\therefore \text{Resultant field is } A_1 + A_4 - (A_2 + A_3) e \frac{-i4\pi h_T \sin \theta}{\lambda}.$$

If the free-space polar diagram of the equipment over the range of angles concerned is appreciably different from that of an isotropic source, the rays should be multiplied by a correcting factor $F(\theta)$ for the direct ray, $F(-\theta)$ for the reflected ray, and $F(A)$, $F(-B)$, $F(-C)$ and $F(-D)$ for the diffracted rays, where $F(\theta)$ is the amplitude of the voltage polar diagram in the direction θ .

* The phase is calculated on the basis of the path-length of the geometrical-optics ray (real or virtual) for the given group, and not that of the ray which travels via the diffracting edge; this is not of course the actual phase of the diffracted ray, or of the resultant of the group, because of the phase change due to diffraction.

To calculate the diffracted rays, use is made of Sommerfeld's solution of the half-plane. In his solution there are two terms, one of which corresponds to simple diffraction and the other to diffraction and reflection. This second term is always small and is ignored. Figure 2 is a simplified part of figure 1, and the diffracted ray TSN_2 is given by Sommerfeld as

$$\pm \left[\frac{1}{2} + \frac{(1+i)}{2} (C - iS) \right],$$

where $(C - iS)$ is the Fresnel integral function for

$$u = 2 \left(\frac{2d}{\lambda} \right)^{\frac{1}{2}} \sin \frac{A - \theta}{2}.$$

The expression is taken positive when the diffracted ray is in the shadow region and negative when in the illuminated region, i.e. the sign of the function is the same as the sign of u .

Similar expressions are found for the other rays. The values of u for the rays are

Ray	$u / 2 \left(\frac{2d}{\lambda} \right)^{1/2}$
Group 1	$\sin \frac{A - \theta}{2}$
	$\sin \frac{B + \theta}{2}$
Group 2	$\sin \frac{A + \theta}{2}$
	$\sin \frac{B - \theta}{2}$
Group 3	$\sin \frac{C - \theta}{2}$
	$\sin \frac{D - \theta}{2}$
Group 4	$\sin \frac{C + \theta}{2}$
	$\sin \frac{D + \theta}{2}$

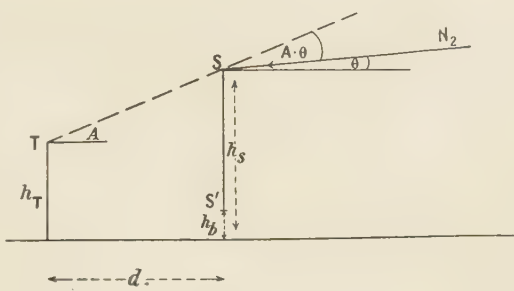


Figure 2.

§ 3. METHOD OF COMPUTATION

For simplicity of computation the Sommerfeld formula is split into real and imaginary parts:

$$\begin{aligned} \frac{1}{2} + \frac{(1+C)}{2} (C - iS) &= \frac{1}{2}[(1+C+S) + i(C-iS)] \\ &= M + iN \text{ say.} \end{aligned}$$

C and S can be found in tables as functions of u , and table 1 gives M and N as functions of u . As the angles are small, we have approximately:

$$u = \frac{\pi}{180} \sqrt{\frac{2d}{\lambda}} F,$$

where F is the angle of diffraction and is given in degrees, or

$$u = 0.0247 \sqrt{\frac{d}{\lambda}} F;$$

$$\begin{aligned} \text{also } A &= \tan^{-1} \frac{h_s - h_T}{d}, & B &= \tan^{-1} \frac{h_T - h_b}{d}, \\ C &= \tan^{-1} \frac{h_s + h_T}{d}, & D &= \tan^{-1} \frac{h_T + h_b}{d}. \end{aligned}$$

Thus the method of computing consists of choosing a value of θ , finding the corresponding values of u , and then adding real and imaginary parts of the five rays in Group 1 and Group 4 and also the five rays in Groups 2 and 3. If θ is chosen in such a way that

$$\frac{4\pi h_T \sin \theta}{\lambda} = \frac{n\pi}{2},$$

then the phase difference between the two sets of rays is a multiple of 90° . This simplifies the addition, as it only involves multiplying the resultant real and imaginary parts of Groups 2 and 3 by ± 1 or $\pm i$. The resultant intensity in the direction θ is then the sum of the squares of the real and imaginary parts. This process is repeated for different values of θ , thus giving the polar diagram. In practice some of the above rays give a negligible contribution to the total amplitude. An example is given in the Appendix.

§ 4. COMPARISON WITH EXPERIMENT

Figure 3 gives a set of readings taken for a GL3 with a screen 9 ft. from top to bottom, placed 35 yards from the set, the angle of elevation of the set being 2° and the top of the screen 15 ft. above ground. For the purpose of the calculations λ was taken as 10 cm. and the height of the transmitter as 12 ft. above ground. The calculated curve is shown in figure 14. It will be seen that the calculated points agree reasonably well with the observed curve, and it therefore appears that the approximate method outlined above gives a sufficiently good approximation for practical purposes in the field. The experimental curve was obtained by Mr. J. T. G. Milne, of the Army Operational Research Group, while temporarily attached to 21 Army Group.

It is important to note that the observations were made in Holland, where the ground is exceptionally flat over large areas, and that such agreement may not be found on more undulating country.

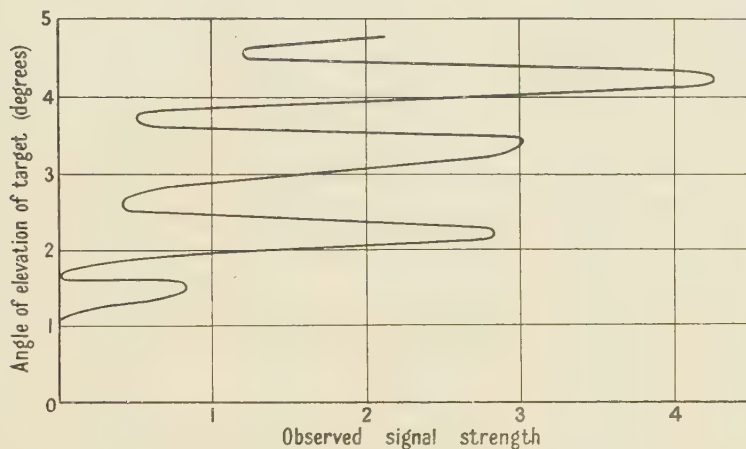


Figure 3. Signal strength of target echo above a wire screen (observed).

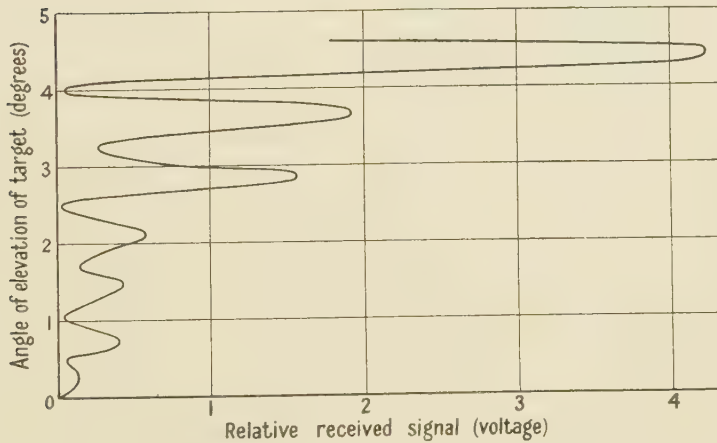


Figure 4. Signal strength of target echo above a wire screen (theoretical).

§ 5. ACKNOWLEDGMENTS

The above work was carried out while the authors were on the staff of the Radar Research and Development Establishment of the Ministry of Supply, and the authors wish to thank the Chief Scientist, Ministry of Supply, for permission to publish this paper. They also wish to thank Mr. J. M. C. Scott for his help and advice.

Table 1

<i>u</i>	<i>M</i>	<i>N</i>	<i>u</i>	<i>M</i>	<i>N</i>
0.000	0.500	0.000	1.300	-0.163	-0.023
0.025	0.488	0.012	1.325	-0.156	-0.039
0.050	0.475	0.025	1.350	-0.148	-0.055
0.075	0.462	0.037	1.375	-0.139	-0.070
0.100	0.450	0.050	1.400	-0.128	-0.083
0.125	0.437	0.062	1.425	-0.114	-0.095
0.150	0.424	0.074	1.450	-0.100	-0.106
0.175	0.411	0.086	1.475	-0.086	-0.116
0.200	0.399	0.098	1.500	-0.071	-0.124
0.225	0.385	0.109	1.525	-0.054	-0.131
0.250	0.371	0.120	1.550	-0.037	-0.134
0.275	0.357	0.131	1.575	-0.020	-0.136
0.300	0.343	0.142	1.600	-0.003	-0.137
0.325	0.329	0.152	1.625	0.014	-0.136
0.350	0.314	0.162	1.650	0.031	-0.133
0.375	0.299	0.172	1.675	0.047	-0.125
0.400	0.284	0.181	1.700	0.061	-0.113
0.425	0.269	0.190	1.725	0.074	-0.099
0.450	0.253	0.198	1.750	0.086	-0.086
0.475	0.237	0.205	1.775	0.097	-0.072
0.500	0.221	0.212	1.800	0.105	-0.057
0.525	0.205	0.219	1.825	0.111	-0.041
0.550	0.188	0.225	1.850	0.115	-0.024
0.575	0.171	0.230	1.875	0.117	-0.007
0.600	0.154	0.236	1.900	0.116	0.011
0.625	0.137	0.240	1.925	0.114	0.026
0.650	0.119	0.242	1.950	0.109	0.042
0.675	0.102	0.243	1.975	0.100	0.057
0.700	0.084	0.244	2.000	0.084	0.072
0.725	0.067	0.244	2.025	0.069	0.084
0.750	0.049	0.243	2.050	0.053	0.093
0.775	0.032	0.240	2.075	0.038	0.100
0.800	0.014	0.236	2.100	0.022	0.104
0.825	-0.003	0.231	2.125	0.005	0.104
0.850	-0.019	0.225	2.150	-0.012	0.102
0.875	-0.037	0.219	2.175	-0.029	0.100
0.900	-0.052	0.211			
0.925	-0.067	0.202	2.200	-0.048	0.090
0.950	-0.081	0.192	2.225	-0.057	0.077
0.975	-0.095	0.181	2.250	-0.068	0.064
1.000	-0.109	0.169	2.275	-0.079	0.050
1.025	-0.121	0.157	2.300	-0.092	0.037
1.050	-0.132	0.143	2.325	-0.094	0.020
1.075	-0.142	0.128	2.350	-0.095	0.002
1.100	-0.151	0.113	2.375	-0.093	-0.015
1.125	-0.156	0.097	2.400	-0.087	-0.032
1.150	-0.161	0.080	2.425	-0.075	-0.045
1.175	-0.165	0.063	2.450	-0.063	-0.057
1.200	-0.168	0.046	2.475	-0.051	-0.069
1.225	-0.170	0.029	2.500	-0.038	-0.081
1.250	-0.169	0.011	2.525	-0.021	-0.086
1.275	-0.167	-0.006	2.550	-0.004	-0.086
			2.575	0.013	-0.084

Table 1 (contd.)

<i>u</i>	<i>M</i>	<i>N</i>	<i>u</i>	<i>M</i>	<i>N</i>
2.600	0.030	-0.081	3.900	0.051	-0.027
2.625	0.042	-0.068	3.925	0.056	-0.010
2.650	0.054	-0.055	3.950	0.058	0.006
2.675	0.066	-0.043	3.975	0.058	0.023
2.700	0.075	-0.030	4.000	0.041	0.039
2.725	0.079	-0.013	4.025	0.023	0.050
2.750	0.080	-0.004	4.050	0.005	0.054
2.775	0.078	0.021	4.075	-0.012	0.054
2.800	0.071	0.038	4.100	-0.030	0.049
2.825	0.056	0.056	4.125	-0.044	0.034
2.850	0.042	0.066	4.150	-0.054	0.019
2.875	0.028	0.073	4.175	-0.054	0.004
2.900	0.013	0.076	4.200	-0.053	-0.011
2.925	-0.003	0.076	4.225	-0.048	-0.030
2.950	-0.019	0.072	4.250	-0.038	-0.046
2.975	-0.035	0.063	4.275	-0.024	0.052
3.000	-0.051	0.055	4.300	-0.002	-0.052
3.025	-0.061	0.039	4.325	0.020	-0.051
3.050	-0.069	0.022	4.350	0.038	-0.040
3.075	-0.073	0.006	4.375	0.048	-0.026
3.100	-0.072	-0.010	4.400	0.050	-0.012
3.125	-0.068	-0.023	4.425	0.047	0.002
3.150	-0.058	-0.037	4.450	0.040	0.017
3.175	-0.044	-0.050	4.475	0.030	0.031
3.200	-0.030	-0.064	4.500	0.020	0.046
3.225	-0.013	-0.067	4.525	0.005	0.049
3.250	0.004	-0.068	4.550	-0.011	0.048
3.275	0.021	-0.067	4.575	-0.028	0.036
3.300	0.038	-0.057	4.600	-0.042	0.025
3.325	0.054	-0.042	4.625	-0.047	0.010
3.350	0.062	-0.026	4.650	-0.047	-0.006
3.375	0.065	-0.011	4.675	-0.045	-0.022
3.400	0.066	0.004	4.700	-0.029	-0.038
3.425	0.066	0.018	4.725	-0.013	-0.045
3.450	0.058	0.032	4.750	0.003	-0.047
3.475	0.042	0.045	4.775	0.019	-0.042
3.500	0.026	0.059	4.800	0.035	-0.032
3.525	0.010	0.062	4.825	0.045	-0.015
3.550	-0.007	0.062	4.850	0.046	0.001
3.575	-0.024	0.060	4.875	0.045	0.017
3.600	-0.040	0.048	4.900	0.032	0.033
3.625	-0.052	0.032	4.925	0.017	0.045
3.650	-0.060	0.016	4.950	0.001	0.045
3.675	-0.063	-0.001	4.975	-0.016	0.042
3.700	-0.057	-0.017	5.000	-0.032	0.032
3.725	-0.046	-0.032			
3.750	-0.033	-0.046			
3.775	-0.020	-0.058			
3.800	-0.007	-0.059			
3.825	0.008	-0.058			
3.850	0.022	-0.050			
3.875	0.037	-0.038			

APPENDIX

Computation of one point

To illustrate the method of computation, the intensity for one angle of elevation is calculated in detail below. The following values of the relevant lengths are used:—

Transmitter height	12 ft.
Distance from screen to transmitter ..	100 ft.
Height of bottom of screen	6 ft.
Height of top of screen	15 ft.
Wavelength	4 in.

The four fixed angles are, therefore,

$$A = \tan^{-1} \frac{15 - 12}{100} = 1^\circ 7,$$

$$B = \tan^{-1} \frac{12 - 6}{100} = 3^\circ 45,$$

$$C = \tan^{-1} \frac{15 + 12}{100} = 15^\circ 1,$$

$$D = \tan^{-1} \frac{12 + 6}{100} = 9^\circ 65,$$

and the parameter $n = 0.0247 \sqrt{\frac{d}{\lambda}} F = 0.428F$,

F being the angle of diffraction measured in degrees. For convenience we choose our steps of θ such that $\frac{4\pi \cdot 12 \cdot \theta}{\frac{1}{3}} = \frac{n\pi}{2}$,

i.e., θ increases in steps of $0^\circ 2$. This interval is sufficiently small for the resulting points to give a good indication of the curve.

As an example, the calculation for $\theta = 2^\circ 8$ is given. For this angle there is only one geometrical-optics ray, TN, and so we have the following table.

Group	Ray	F	u	M (from table 1)	N (from table 1)
1	TN ₁	0	0	1.000	0
	TSN ₂	-1.1	0.0471	-0.240	-0.204
	TS'N ₃	6.25	2.674	0.066	-0.043
2	TSQ ₃ N ₆	4.5	1.925	0.114	0.026
	TS'Q ₂ N ₅	0.65	0.278	0.355	0.132
3	TQ ₄ SN ₂	12.3	5.262*		
	TQ ₅ S'N ₃	6.85	2.931	-0.007	0.075
4	TQ ₄ SQ ₃ N ₆	17.9	7.658*		
	TQ ₅ S'Q ₂ N ₅	12.45	5.326*		
				1.288	-0.014

* The table of M and N is only given for $0 \leq u \leq 5$. For larger u the diffracted ray is negligible owing to the narrow polar curve of the equipment.

The geometrical path of Group-2 rays is 3.5λ greater than that of Group 1. As these rays undergo a phase reversal on reflection, all groups arrive in phase and the summation above is correct. Had we taken $\theta = 2^\circ 4$, rays in Groups 2 and 3 would arrive in opposite phase to those in Groups 1 and 4, and would, therefore, be multiplied by -1 before being added.

LETTERS TO THE EDITOR

An Isotopic Abundance Rule and its Bearing on the Origin of the Nuclei

The natural abundances of all stable isotopes of any element of higher atomic number than 43 are of similar magnitude, except when there exist natural isobars of lower atomic number ; those that have isobars of lower charge are comparatively rare.

The limit at $Z=43$ is rather arbitrary ; indications of the same type of abundance pattern persist down to ^{34}Se but are not present among light nuclei. "Of similar magnitude" means, commonly, within a factor of 2 ; at the worst, within a factor of 11 ($^{138}_{56}\text{Ba} : ^{135}_{56}\text{Ba}$). "Comparatively rare" means, generally, between 10 times and 100 times rarer. There are only four actual exceptions, i.e. nuclei which, possessing lower charge isobars, are more abundant than one or more of their isotopes which possess none. These are $^{110}_{48}\text{Cd}$, $^{116}_{59}\text{Sn}$, $^{142}_{60}\text{Nd}$, $^{198}_{80}\text{Hg}$. Of those isotopes which do not possess lower charge isobars, the heaviest is occasionally rather less abundant than the rest ; in all such cases it possesses a higher charge isobar, which is less rare than usual (the four exceptions mentioned are such cases).

The isotopic abundance pattern of ^{54}Xe (table 1) is particularly interesting, since, in obeying the above rule, it breaks the usual rule that every odd isotope of even atomic number has at least one more abundant adjacent even isotope.

The only other exceptions to the latter rule, beyond boron, are $^{147}_{62}\text{Sm}$, $^{149}_{62}\text{Sm}$, $^{196}_{78}\text{Pt}$ and $^{235}_{92}\text{U}$.

Table 1. (From Mattauch, *Kemphysikalische Tabellen* (Berlin : Springer))

^{54}Xe Mass No.	124	126	128	129	130	131	132	134	136
Abundance %	0.094	0.088	1.91	26.23	4.06	21.18	26.98	10.55	8.95
Lower charge isobar	Yes	Yes	Yes	No	Yes	No	No	No	No

In conjunction with Goldschmidt's (1937) estimates of the cosmic abundances of the elements, the first rule may be generalized to the form :

The total cosmic nuclear abundance at each mass number (above 60) is of the same order of magnitude ; where there is more than one stable nucleus of a given mass, the predominantly abundant nucleus at this mass is that of lowest charge, and the others may be much rarer.

The only grave exception to the rule in this form is the relative rarity of mass number 185 ($^{185}_{75}\text{Re}$, possessing no isobar), by a factor between 100 and 1000. It is suggested that new determinations of the abundance of rhenium, particularly in meteorites, are called for.

The rule in this latter form gives evidence in support of the hypothesis that in the origin of the nuclei, the heavier ones (as distinct from the lighter nuclei whose abundance is known to correspond approximately to a thermodynamic equilibrium (von Weizsäcker 1938; Chandrasekhar and Henrich 1942)) have been built up by a sequence of neutron capture processes. Since the nuclei then assume their final charge chiefly by β -decay, the predominance of the lowest charge isobars is a natural consequence. Detailed considerations of the neutron condensation process (to be published elsewhere) account also for the general form of the abundance curve for the heavier nuclei, and show that this process is the natural sequel to the thermodynamic equilibrium state indicated by the cosmic abundances of light nuclei.

F. C. FRANK.

H. H. Wills Physical Laboratory,
University of Bristol.

CHANDRASEKHAR and HENRICH, 1942, *Astrophys. J.*, **95**, 288.

GOLDSCHMIDT, 1937, *Skrifter Norske Videnskapsakad.*, iv.

VON WEIZSÄCKER, 1938, *Phys. Z.*, **38**, 641.

REVIEWS OF BOOKS

Achievements in Optics, by A. BOUWERS. Pp. viii + 125. (Brit. Emp. Distr.: Cleaver Hume Press, 1947.) 12s. net.

This book, one of a series of monographs dealing with progress of research in Holland, was prepared for the press before the liberation of the Low Countries, and deals almost exclusively with work done—often under conditions of secrecy—during the occupation.

The first chapter deals with "New Optical Systems". A clear and simple account is given of the advantages possessed by the concave spherical mirror, viz. small spherical aberration, complete absence of chromatic aberration, negative Petzval sum and absence of all orders of oblique aberrations when used with a stop at the centre of curvature. A series of systems is then described, comprising the Schmidt camera, the Maksutov telescope, and derivatives of these two. Very notable results seem to have been achieved. It is interesting to note that yet another claimant to priority for the use of weak negative meniscus lens for correcting the aberrations of a concave spherical mirror has appeared. This device has been generally attributed, so far, both in America and in this country, to Maksutov.

Chapter II deals with applications of mirror systems to microscopes, telescopes and cameras, and contains little that will be unfamiliar to the informed reader.

Chapter III deals with geometrical aberration theory. An interesting discussion of purely geometrical constructions for ray-paths and image points shows that even this somewhat dated approach can yet yield useful results. It is followed by a summary of the work of Korringa (Thesis, Delft, 1942) and Stephan, and Nijboer (Thesis, Groningen, 1942), all of which starts from the analytical standpoint introduced by Hamilton and developed in England, in particular by T. Smith. The chapter concludes with a description of a method of dealing with the light distributions in images in the presence of larger amounts of spherical aberration. As with so many of the methods of applied mathematics, one can but say that the grave suspicions provoked by the analytical procedure are allayed by the apparent success of the method.

Chapter IV, "Physical Optics", summarizes the elegant treatment of aberrational diffraction theory given by Nijboer (*ibid.*) dealing with cases in which aberrational asphericities are small; and finally, Zernike's remarkable analysis of the theory of the microscope is given, with particular reference to the phase-contrast method.

The English used is but rarely foreign to a native ear. The only serious ambiguity arises when a full-circular aperture is described as ring-shaped. This would easily be taken to mean an annular aperture, and in the context the two have to be carefully distinguished. Apart from this, and the use of "feeded" and "grinded" for the past participles of "to feed" and "to grind" respectively, a very fluent and natural style is maintained.

In sum, this book offers little really new information, but a wealth of scattered and useful material has been compressed into it. It can be wholeheartedly recommended to specialists and non-specialists alike. Finally, it is no mere courtesy to congratulate the Dutch workers who have contributed to optical research with such enviable enthusiasm and pronounced success under very unfavourable conditions.

H. H. H.

Microtecnic. International review for measuring and gauging technique, optics and precision mechanics. (Published in Lausanne, Switzerland.) Price 52s. 6d. per annum. British agents: Bailey Bros and Swinfen, London.

A bi-monthly journal with text in both English and French. A specimen issue includes articles on:—Documentation and International Decimal Classification; Some Applications of Optics to Metrology; The Hairspring; Equipment of a Laboratory for Precision Instruments; Beryllium and Beryllium Bronze; Rotating substandard Meters and their Uses.

A. C. S.

REPORT OF AN INTERNATIONAL CONFERENCE
ON
FUNDAMENTAL PARTICLES
AND
LOW TEMPERATURES

HELD AT

*The Cavendish Laboratory, Cambridge,
on 22-27 July 1946*

Volume I 200 pages
FUNDAMENTAL PARTICLES

Volume II 148 pages
LOW TEMPERATURES

Price of each volume (in paper covers) 15s., inclusive of postage

*Orders, with remittances, should be sent to
THE PHYSICAL SOCIETY,
1 Lowther Gardens, Prince Consort Road, London S.W.7*

**METEOROLOGICAL
FACTORS IN RADIO-WAVE
PROPAGATION**

*Report of a Conference held
in London in April 1946 by*

THE PHYSICAL SOCIETY
AND
THE ROYAL
METEOROLOGICAL SOCIETY

Opening paper by Sir Edward Appleton, G.B.E.,
K.C.B., F.R.S., and twenty papers by other
contributors. The first comprehensive account
of this entirely new field of investigation.

iv+325 pages. 24s. inclusive of postage.

*Orders, with remittances, should be sent to the publishers
THE PHYSICAL SOCIETY
1 Lowther Gardens, Prince Consort Road,
London S.W.7*

**CATALOGUES
OF THE
PHYSICAL SOCIETY'S
EXHIBITIONS
OF
SCIENTIFIC INSTRUMENTS
AND APPARATUS**

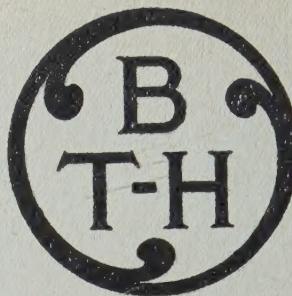
The two post-war Catalogues are widely acknowledged
as very useful records and valuable books of reference.

30th (1946) CATALOGUE (reprinted):
288+lxix pages; 176 illustrations.
1s.; by post 2s.

31st (1947) CATALOGUE:
298+lxvii pages; 106 illustrations.
2s. 6d.; by post 3s. 6d.

(The two Catalogues together, 4s. 6d. inclusive
of postage)

*Orders, with remittances, should be sent to
THE PHYSICAL SOCIETY
1 Lowther Gardens, Prince Consort Road,
London S.W.7*



RESEARCH & ENGINEERING

BTH Products are available
as instruments and apparatus
for research, development, and
engineering, including all branches
of electronic control.

• • •

THYRATRONS MAGNETRONS
CRYSTAL RECTIFIERS
SPECIAL VACUUM ELECTRONIC DEVICES
GLASS, AND GLASS METAL SEALS
RECTIFIERS
FRACTIONAL HORSEPOWER MOTORS
ETC.

BTH

RUGBY

THE BRITISH THOMSON-HOUSTON COMPANY LIMITED, RUGBY, ENGLAND.



A3595N